# DEVELOPMENT OF A DUAL HYDRAULIC MANIPULATORS SIMULATOR and ANALYSIS of MANIPULABILITY

**BY**

**JUNGTAEK LIM**

**A Thesis**
**Submitted to the Faculty of Graduate Studies**
**In Partial Fulfillment of Requirements**
**For the Degree of**

**MASTER OF SCIENCE**

**Department of Mechanical and Manufacturing Engineering**
**The University of Manitoba**
**Winnipeg, Manitoba, Canada**

THE UNIVERSITY OF MANITOBA

FACULTY OF GRADUATE STUDIES

*****

COPYRIGHT PERMISSION

**"Development of a Dual Hydraulic Manipulators Simulator and Analysis of Manipulability"**

**BY**

Jungtaek Lim

**A Thesis/Practicum submitted to the Faculty of Graduate Studies of The University of Manitoba in partial fulfillment of the requirement of the degree**

**Of**

**MASTER OF SCIENCE**

## Abstract

Virtual Reality simulators have the potential to offer a new training paradigm for improving the practical skills of robot operators. They provide a training environment where robot operators can make mistakes and learn from these mistakes without any risks and cost. This thesis follows through the design and evaluation of a robotic simulator for 7 functions Magnum subsea dual arms. The simulator of Magnum subsea dual arms is developed using OpenGL and Microsoft Visual C++. The program offers the capability in carrying out a number of different commands. The inverse kinematics allows the user to specify a desired end-effector's position in the workspace and again see the arm move accordingly. As well, the robot may operate in a complete dynamic simulation mode. Hydraulic functions are also presented in the dynamic simulator.

The main purpose of this simulator is to train a robot operator. In order to take advantage of the capabilities offered by robots, operators must learn a completely new set of skills. These skills include understanding the robots condition by interpreting sensor data, adapting to the view provided by an operated robot, and recognizing the capabilities and limitations of the robot they are operating. To give operators understanding of the robots kinematics abilities, manipulability is employed in this thesis. When the operators use this simulator, they can see manipulability ellipsoids and measure, which indicate the ability of the robot arm from the viewpoints of kinematics. This thesis analyzes manipulability for the Magnum subsea dual arms as well. The analysis of manipulability can be used for optimal posture of the manipulators in the workspace for performing a given task during training. Especially, the trainer can know immediately not only the manipulability of Magnum subsea dual arms but also the desirable direction for good performance through the ellipsoid shown in the graphic user interface. This thesis analyzes robot arms dynamics through case studies of dynamics. The case studies show dynamic conditions of Magnum subsea dual arms and capabilities from the viewpoints of dynamics.

## Acknowledgements

I would like to express my deep gratitude to Dr. Nariman Sepehri for his support, supervision, and advice throughout my research.

I would also like to thank Hairong Zeng for offering useful suggestions and providing the dynamic model of the dual arms.

I would like to thank my parents for always believing in me and for always giving me full moral support no matter the situation.

Last but certainly not least, my special thanks go to my wife for her understanding and always being there for me.

The numbers of those to whom I owe gratitude are too great to be listed here. I can only honor them appropriately by giving thanks to God for bringing them into my life.

## Dedication

I dedicate this work to my wife, Hyojeong Kim, and my family

# Contents

# List of Figures

## List of Tables

# 1 Introduction

Nowadays, graphic simulators for robotic systems are indispensable in most of the robot design, learning, and exploitation steps. The technological advances and improvements in computing engineering allow them to be applied to any field in robotics. In addition, they have become significantly more powerful and flexible. In this thesis an application of a simulator is presented. This simulator uses the dynamics of the real robot. The simulator provides several advantages, like being able to train robot operators without the cost, nor the risk of manipulating a real robot. Many problems associated with robot operator training can be reduced or eliminated using a virtual approach. While they may never fully replace real life training, it is believed that simulating robotic use can become an important tool for training robot operators.

## *1.1 Motivation and General Overview*

Simulators are often described as a risk free method of allowing novices to practice their skills. They also have the potential to improve safety during training in a safety critical task as demonstrated by the success and widespread adoption of flight simulators. The use of robot simulators can achieve the same level of success. Moreover, recent advances in virtual reality technology including haptic interfaces and significant reduction in the cost to performance ratio of computers have enabled researchers to perform real-time interactive simulations on desktop computer stations. This thesis is to develop a training system for a robot operator. This work presents development of a simulator for a class of cooperating Magnum manipulators in response to a need to develop training systems for robot operators, especially those operating in unstructured environments. The simulator must include dynamic interactions. The ability of analyzing the arms' dynamics will be used to evaluate the performance of Magnum subsea dual arms from viewpoints of dynamics.

This thesis presents manipulability also. Manipulability is defined as the measure of the flexibility of the manipulator to transmit the end-effector motion in response to a unit norm motion of the rates of active joints in the system. Manipulability indices have been

widely used in robotics analysis, task specification, and mechanism design. The basic idea of manipulability analysis consists of describing directions in the task or joint space that extremize the ratio between some measure of effort in joint space and a measure of performance in task space. The concept of the manipulability ellipsoid of robotic mechanism is extended to two cooperating robots. Yoshikawa [23, 24] is credited with first introducing the concept of manipulability. Since then, various alternative formulations with different aspects of manipulability have been investigated and proposed by a number of other authors in different applications, including robot control, fault diagnostic, robot design and optimization. The measure of manipulability is further utilized in this thesis to help finding optimal posture of Magnum subsea dual arms from the viewpoints of kinematics through various case studies.

## 1.2 Magnum Subsea Manipulators

Magnum subsea manipulators (Figure1-1) are developed by International Submarine Engineering Ltd. (ISE) in B.C. Canada [26]. They have discovered that there is no universal manipulator for submersible applications. Thus 3, 4, 5, 6, and 7 functions Magnum master/slave and force reflecting manipulators have been produced. Manipulator requirements, including size, envelopes, lift capacity, joint mobility, kinematics, and actuators, differ between applications. Figure 1-1 shows the 7 functions Magnum subsea manipulator.

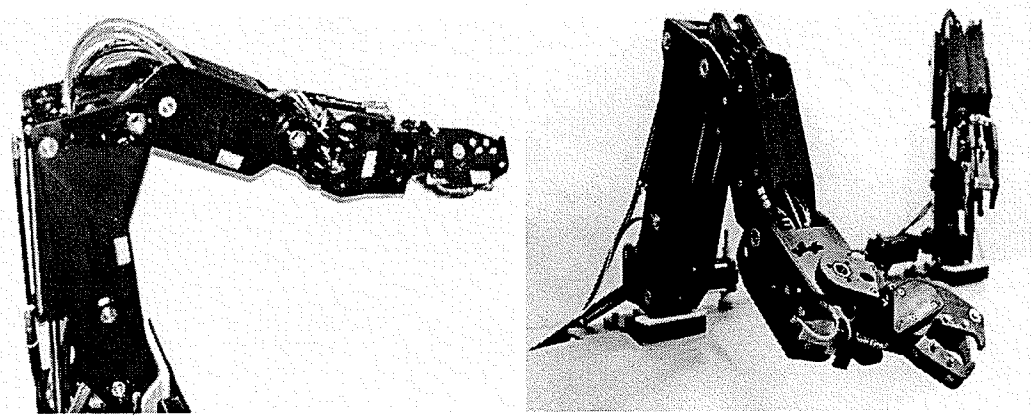

**Figure 1-1 7 functions Magnum subsea manipulator [26].**

Typical tasks for which Magnum is used include: i) cleaning sand, mud cutting build up and debris clearance; ii) jetting and brushing operations; iii) wall thickness measurements in flow line; iv) valve turning and bolt torquing and cable cutting; v) hot line stabbing for hydraulic overrides; vi) accident investigation; vii)biological and geological sampling. ISE offers a number of standard Magnum manipulators. However, these manipulators are often customized to perform some of the more specialized aforementioned tasks. Table 1-1 shows specifications of the 7 functions Magnum subsea manipulator.

**Table 1-1 7 functions Magnum subsea manipulator specifications.**

| Term | description |
|---|---|
| Lift | 295 kg at full extension |
| Reach | 1.5 m |
| Weight in Air | 71 kg (nominal) |
| Operating Pressure | 6,890 kPa (nominal) |
| Accuracy | Better than +/- 12.7 mm |
| Swing Joint | 50 degrees; 20 degrees per second (nominal) |
| Shoulder Joint | 90 degrees; 20 degrees per second (nominal) |
| Elbow Joint | 130 degrees; 30 degrees per second (nominal) |
| Pitch Joint | 115 degrees; 30 degrees per second (nominal) |
| Yaw Joint | 120 degrees; 30 degrees per second (nominal) |
| Rotate Joint | Continuous and servo (360 degrees);<br>150 degrees per second (nominal) |
| Jaw Open/Close | 7.5 cm opening ; 10.2 cm per second (nominal);<br>Clamp force 150 kg |

## *1.3 Scope and Objects of the Thesis*

The objectives of this research are to develop and implement a simulator for the 7 functions Magnum subsea dual manipulators and to analyze its manipulability that may be

applied to improved training. This work began with the investigation of various mathematical abstractions relating to robotics and the study of Visual C++ and OpenGL. In this thesis, it first shows that creating an application, the Magnum subsea dual arms simulator, using Visual C++ and OpenGL. Second, the thesis explains the equations for the robot arms. Finally, the simulator is tested and the manipulability of robot arms is analyzed. The development of a simulator can essentially be divided into two parts: modeling, and verification/investigation the simulator. Modeling can be into three parts: 3D graphic modeling, kinematics, and dynamics. Aspects of game technologies are used for 3D graphic modeling and programming parts such as collision detection. The required mathematical model is obtained from the literature, and is kept simple yet accurate. The dynamic model developed is expected to describe fully the nonlinear dynamical behavior of the Magnum's hydraulic actuators and rigid body system. This thesis presents robot arms manipulability and analyzes the manipulability of Magnum subsea dual arms. The analysis can be used for understanding robot operator actions during the training and to find optimal posture of Magnum subsea dual arms.

# 2 Literature Review

## *2.1 Overview of OpenGL*

Standard three-dimensional graphics application programming interfaces (API), such as OpenGL which is employed for this project, are software interfaces to graphics hardware that allow developers to create interactive 3D applications. They usually provide a complete set of functions to build these applications. This section details the origin, the benefits, the functionality and the applications of one of the most used graphics application programming interface (API): the OpenGL API.

### 2.1.1 A Brief History of OpenGL

The OpenGL API began as an initiative of Silicon Graphics Incorporated (SGI) to create a single, vendor-independent API for the development of 2D and 3D graphics applications. In the late 80's it was established that almost each hardware vendor made use of its own graphics libraries. This made it very difficult, time-consuming and expensive for software developers to implement versions of their products for each hardware platform. Aware of this lack of uniformity in graphics software devices and convinced that this was a real inhibitor to the expansion of the 3D market, SGI decided in 1990 to start a project intending to create a standard graphics application programming interface. The first version of the OpenGL API (currently version 1.5) was released two years later. It was for the most part the descendant of a previous graphics library known as IRIS GL, developed by SGI in the 80's, which lacked general functionality and was suffering from problems of platform independence. But SGI preserved the assets of their previous API, which is its ability to render 3D objects quickly and efficiently [22]. OpenGL first was just a specification but then SGI licensed the use of the name, a set of conformance tests, and a sample implementation that hardware vendors had to buy to develop official OpenGL-compliant drivers for their hardware. A consortium, the OpenGL Architecture Review board (ARB), was formed in 1992, originally to license OpenGL and to direct further developments. However, as the

sample implementation was recently released under an open source license, the ARB is now responsible of changes in the specification and of proposal of new releases only. The ARB is independent and composed of a set of major graphics vendors like SGI itself, IBM, Microsoft or 3Dlabs, which ensures that SGI has not an absolute power on the standard. Currently, OpenGL counts Development of an object-oriented API for particle simulation – Anthony Bridon 5 over 70 licensees among the industry's leading companies involved with the computing industry such as Sun Microsystems, Compaq or Apple. Software developers are free to use the OpenGL API in their applications with no need to license. As for hardware developers, they can get the sample implementation for free but need an additional license to be proclaimed OpenGL conform and to use the OpenGL trademark [17].

### 2.1.2 Benefits for Hardware and Software developers

This section lists briefly the advantages offered by OpenGL to developers: i)Industry standard: the OpenGL API is the only open, vendor and platform independent graphics standard and it has been available for over ten years so that it is now very well-documented, either in literature or on the internet . Numerous websites offer tutorials and sample code to easily get started with the API. Since its creation, the OpenGL API has also proven its stability and reliability on a large number of platforms, which make it the graphics standard used in every technologic sector. Additions and modifications to the specification are controlled by the ARB and announced in time to allow developers to take them into account. Updates are moreover made in order to ensure backward compatibility with existing applications; ii) Portability: OpenGL applications can be developed regardless of operating system; iii) Evolving: the OpenGL API extension feature allows staying current with new hardware features; iv) Scalable: OpenGL applications can run on a wide range of systems including PCs, workstations, supercomputers and consumer electronics. This way, the developer does not need to worry about the type of machine its application is going to run on; v) Easy to use: OpenGL drivers hide low-layer information, making programming easier for the developer and freeing him from having to design for specific hardware features [4, 17].

## 2.2 Kinematics

In the kinematics analysis of manipulator position, there are two separate problems to solve: forward kinematics, and inverse kinematics. Forward kinematics involves solving the forward transformation equation to find the location of the hand in terms of the angles and displacements between the links. The angles and displacements between the links are called joint coordinates and are described with link variables, while the location of the hand in space is described with Cartesian coordinates. Inverse kinematics involves solving the inverse transformation equation to find the relationships between the links of the manipulator from the location of the hand in space.

Forward kinematics is the problem of locating the position and orientation of the end link, given the joint angles. This computation is straightforward for serial-link manipulators, but difficult for parallel-link manipulators. The Magnum is a serial-link manipulator. This thesis begins by discussing the setting up of coordinate systems in the links and transformations between them, through the use of the named Denavit-Hartenberg representation.

### 2.2.1 Denavit-Hartenberg Coordinates

The standard way for setting up coordinate systems in links is the Denavit-Hartenberg representation. The Denavit-Hartenberg Coordinate system works by defining an orthonormal coordinate system for each robot joint. After these are defined, then each joint is related to the next through a transformation. This is the information stored in the representation. Figure 2-1 shows two joints in a complex robotic system, and the involved parameters. Four parameters are involved between each pair of joints. In Figure 2-1, the origins of the coordinate frames at link $n+1$ and link $n+2$ are marked with a black dot in the figure. Four transformations in a specific order will bring these frames coincident with each other. By definition, coordinate axis $Z_n$ passes though link $n+1$.

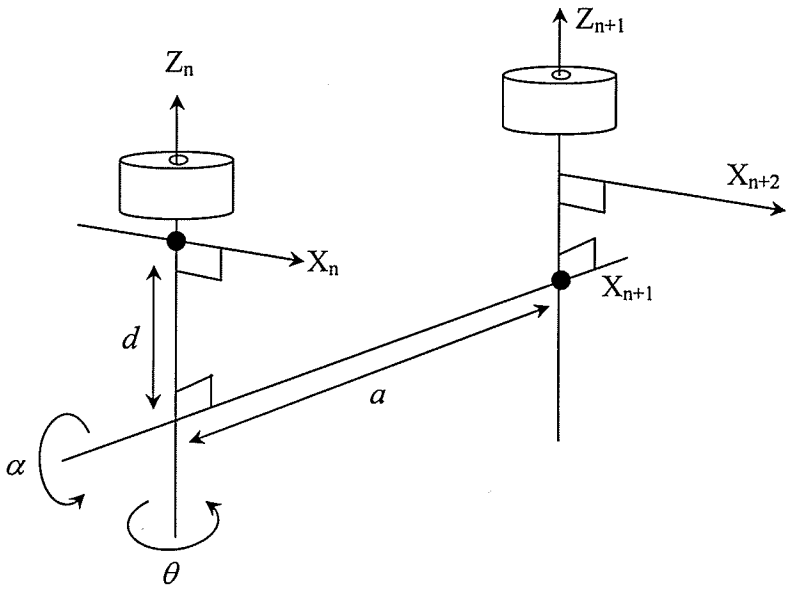


**Figure 2-1 Parameters in Denavit-Hartenberg representation.**

The four transformations are as follows:

1. A rotation $\theta_{n+1}$ about the $Z_n$ axis to bring $X_n$ parallel with $X_{n+1}$
2. A translation $d_{n+1}$ along the $Z_n$ axis, to make the X axes collinear
3. A translation $a_{n+1}$ along the $X_n$ axis to make the Z axes coincide
4. A rotation $a_{n+1}$ about the $X_n$ axis to bring $Z_n$ parallel with $Z_{n+1}$

Quite often, several of the four transformations are zero.

## 2.2.2 Link Coordinate Transformation

A commonly used convention for selecting frames of reference in robotic applications is the Denavit-Hartenberg convention. In this convention, each homogeneous transformation $A_i$ is represented as a product of four basic transformations [13]:

$$A_i = R_z(\theta_i)Trans_z(d_i)Trans_x(a_i)R_x(\alpha_i)$$

$$= \begin{bmatrix} \cos\theta_i & -\sin\theta_i & 0 & 0 \\ \sin\theta_i & \cos\theta_i & 0 & 0 \\ 0 & 0 & 1 & 0 \\ 0 & 0 & 0 & 1 \end{bmatrix} \begin{bmatrix} 1 & 0 & 0 & 0 \\ 0 & 1 & 0 & 0 \\ 0 & 0 & 1 & d_i \\ 0 & 0 & 0 & 1 \end{bmatrix} \begin{bmatrix} 1 & 0 & 0 & \alpha_i \\ 0 & 1 & 0 & 0 \\ 0 & 0 & 1 & 0 \\ 0 & 0 & 0 & 1 \end{bmatrix} \begin{bmatrix} 1 & 0 & 0 & 0 \\ 0 & \cos\alpha_i & -\sin\alpha_i & 0 \\ 0 & \sin\alpha_i & \cos\alpha_i & 0 \\ 0 & 0 & 0 & 1 \end{bmatrix}$$

$$= \begin{bmatrix} \cos\theta_i & -\sin\theta_i\cos\alpha_i & \sin\theta_i\sin\alpha_i & a_i\cos\theta_i \\ \sin\theta_i & \cos\theta\cos\alpha_i & -\cos\theta_i\sin\alpha_i & a_i\sin\theta_i \\ 0 & \sin\alpha_i & \cos\alpha_i & d_i \\ 0 & 0 & 0 & 1 \end{bmatrix} \tag{2.1}$$

## 2.3 Jacobian

The Jacobian is a multidimensional form of the derivative and is useful in robotics because it relates the joint velocities to the velocities for a given manipulator. The Jacobian can be found by calculating the derivative of the kinematics equations described earlier.

The derivative of a transformation $dT$, representing rotation and translation, can be expressed in terms of a matrix product

$$dT = \Delta T \tag{2.2}$$

where the differential change is expressed with respect to base coordinates, and

$$dT = T^T \Delta \tag{2.3}$$

where the differential change is expressed with respect to coordinate frame $T$ coordinates. The differential rotation and translation transformation $\Delta$ is composed from the elements of two vectors: $d$, the differential translation vector, and $\delta$, the differential rotation vector

$$\Delta = \begin{bmatrix} 0 & -\delta_z & \delta_y & d_x \\ \delta_z & 0 & -\delta_x & d_y \\ -\delta_y & \delta_x & 0 & d_z \\ 0 & 0 & 0 & 0 \end{bmatrix} \tag{2.4}$$

The elements of $\delta$ represent differential rotations about the X, Y, and Z axes. In the case of differential rotations it will be shown that the result is independent of the order of rotation and that differential rotations $\delta_x$, $\delta_y$, and $\delta_z$ made about the X, Y, and Z axes, respectively, are equivalent to a differential rotation $d\theta$ made about a unit magnitude vector $k$ if

$$\begin{aligned} \delta_x &= k_x d\theta \\ \delta_y &= k_y d\theta \\ \delta_z &= k_z d\theta \end{aligned} \tag{2.5}$$

The relationship between ${}^T\Delta$ and $\Delta$ was is shown to be

$${}^T\Delta = T^{-1}\Delta T \tag{2.6}$$

where the transformation $T$, composed of column $n$, $o$, $a$, and $p$, is known as the differential coordinate transformation. The elements of ${}^T\Delta$, in terms of the elements of $\Delta$, are shown to be

$$\begin{aligned} {}^T d_x &= n \cdot ((\delta \times p) + d) \\ {}^T d_y &= o \cdot ((\delta \times p) + d) \\ {}^T d_z &= a \cdot ((\delta \times p) + d) \end{aligned} \tag{2.7}$$

$$\begin{aligned} {}^T\delta_x &= n \cdot \delta \\ {}^T\delta_y &= o \cdot \delta \\ {}^T\delta_z &= a \cdot \delta \end{aligned} \tag{2.8}$$

Given any transformation expression represented by a transformation graph, the differential coordinate transformation $T$, which relates differential changes between coordinate frames, is the path traced from the head of the link representing the transform in which the change occurred to the head of the transform in which the equivalent change is desired.

These methods will be applied to develop the manipulator Jacobian, in which case the differential coordinate transformation for a differential change in coordinate frame $T_6$ caused

by a differential change in joint coordinate $i$ is ${}^{i-1}T_6$. The differential translation and rotation vectors representing the column of the Jacobian for a revolute joint can be simplified to

$$ {}^{T6}d_i = (-n_x p_y + n_y p_x)\mathrm{i}(-o_x p_y + o_y p_x)\mathrm{j}(-a_x p_y + a_y p_x)\mathrm{k} \tag{2.9} $$

$$ {}^{T6}\delta_i = n_z\mathrm{i} + o_z\mathrm{j} + a_z\mathrm{k} \tag{2.10} $$

and where the joint is prismatic the differential translation and rotation vectors become

$$ {}^{T6}d_i = n_z\mathrm{i} + o_z\mathrm{j} + a_z\mathrm{k} \tag{2.11} $$

$$ {}^{T6}\delta_i = 0\mathrm{i} + 0\mathrm{j} + 0\mathrm{k} \tag{2.12} $$

## *2.4 Manipulability*

Various factors should be taken into account when the mechanism and the size of a robot manipulator are chosen at the design stage, or when the posture of the manipulator is determined in the workspace for performing a given task during operation. An important factor among these is the ease of arbitrarily changing the position and orientation of the end-effector at the tip of the manipulator. In this chapter an approach will be presented for evaluating quantitatively this ability of manipulators from the viewpoint of kinematics. From the kinematics aspect, the concepts of the manipulability ellipsoid and the manipulability measure will be introduced.

### 2.4.1 Single Arm Manipulability Ellipsoid and Manipulability Measure

#### 2.4.1.1 Manipulability Ellipsoid

The unit sphere defined at the origin of the joint velocity space can be mapped to the ellipsoid in the Cartesian velocity space by Jacobian transformation. This ellipsoid is called the manipulability ellipsoid. The manipulability ellipsoid describes the characteristics of the feasible motion in the Cartesian space corresponding to unit norm joint velocities. The manipulability ellipsoid is mathematically defined as follows. Assuming that an $n$ degree of freedom robot arm is working in an $m$ dimensional task space, where $m \leq n$,

$$\dot{x} = J(q)\dot{q} \tag{2.13}$$

$\dot{x}$ and $\dot{q}$ indicate the Cartesian and joint velocity vectors defined in the task space $R^m$ and the joint space $R^n$ respectively. $J$ represents the $m \times n$ Jacobian matrix. The Jacobian $J$ defines the mapping from $R^n$ to $R^m$. The unit sphere in $R^n$ described by $\|\dot{q}\|^2 = 1$ can be mapped into an ellipsoid in $R^m$ through $J$ [8, 9].

$$\begin{aligned} \|\dot{q}\|^2 &= \dot{q}^T \dot{q} \\ &= \dot{x}^T (J^+)^T J^+ \dot{x} \\ &= \dot{x}^T (JJ^T)^+ \dot{x} \\ &= \dot{x}^T (JJ^T)^{-1} \dot{x} = 1 \end{aligned} \tag{2.14}$$

where the superscript "+" indicates the pseudo-inverse(see Appendix 1) of the matrix , $J^+ = J^T (JJ^T)^{-1}$ . Equation (2.14) represents an ellipsoid in $R^m$. This ellipsoid is called the manipulability ellipsoid.

Now the principal axes of the manipulability ellipsoid can be found by making use of the singular-value decomposition (see Appendix 2) of $J$ . Let the singular-value decomposition of $J$ be [18, 19]

$$J = U \Sigma V^T \tag{2.15}$$

where $U$ and $V$ are, respectively, $m \times m$ and $n \times n$ orthogonal matrices, and where $\Sigma$ is an $m \times n$ matrix defined by

$$\Sigma = \left[\begin{array}{ccc:c} \sigma_1 & & 0 & \\ & \ddots & & 0 \\ 0 & & \sigma_m & \end{array}\right], \quad \sigma_1 \geq \sigma_2 \geq \cdots \geq \sigma_m \geq 0. \tag{2.16}$$

The scalars $\sigma_1, \sigma_2, \ldots, \sigma_m$ are called singular value of $J$, and they are equal to the $m$ larger values of the $n$ root $\left\{\sqrt{\lambda_i}, i = 1, 2, \ldots, n\right\}$, where $\lambda_i$ $i^{th}$ column vector of $U$ [23, 24]. Then the

principal axes of the manipulability ellipsoid are $\sigma_1 u_1, \sigma_2 u_2, ..., \sigma_m u_m$. The major axis of the ellipsoid $\sigma_1 u_1$ corresponds to the direction of the end-effector that can move the most easily and the least easily at $\sigma_m u_m$ direction. When this ellipsoid becomes a sphere, the end-effector can move with uniform ease in all directions. Also, the larger the ellipsoid is, the faster the end-effector can move. Hence, such singular-value decomposition and the subsequent geometric interpretation as the manipulability ellipsoid permits a very useful tool in development of various performance measures and metrics, which will be summarized briefly next.

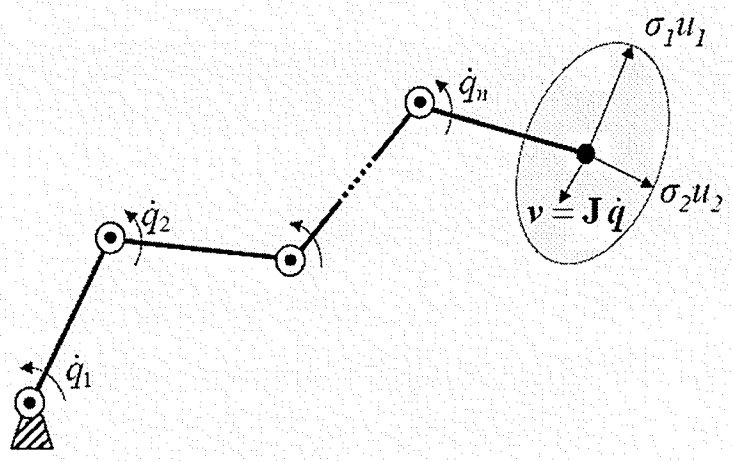


Figure 2-2 Manipulability ellipsoid I [24].

### 2.4.1.2 Yoshikawa's Measure of Manipulability

The following is the method of manipulability measure, introduced by Yoshikawa [23, 24]. One of the representative measures for the ability of manipulation derived from the manipulability ellipsoid is the volume of the ellipsoid. This is given by $c_m w$, where

$$w = \sigma_1 \sigma_2 ... \sigma_m, \tag{2.17}$$

$$c_m = \begin{cases} (2\pi)^{m/2} / [2 \cdot 4 \cdot 6 .... (m-2) \cdot m] & if \ \ m \ \ is \ \ even \\ 2(2\pi)^{(m-)/2} / [1 \cdot 3 \cdot 5 .... (m-2) \cdot m] & if \ \ m \ \ is \ \ odd \end{cases} \tag{2.18}$$

Since the coefficient $c_m$ is constant when $m$ is fixed, the volume is proportional to $w$. Hence, $w$ as a representative measure can be regarded. $w$ is defined as the manipulability measure for manipulator configuration $q$.

The manipulability measure $w$ has the following properties:

(i) $w = \sqrt{\det J(q) J^T(q)}$. (2.19)

(ii) When $m \times n$ (that is, non-redundant manipulators), the measure $w$ reduces to

$$w = |\det J(q)|. \tag{2.20}$$

(iii) Generally $w \geq 0$ holds, and $w = 0$ if and only if

$$rank J(q) < m \tag{2.21}$$

(in other words, if and only if the manipulator is in a singular configuration). From this fact the manipulability measure is to be regarded as a kind of distance of the manipulator configuration from singular ones.

(iv) When $m \times n$, the set of all $v$ which is realizable by a joint velocity $\dot{q}$ such that

$$|\dot{q}_i| \leq 1, \qquad i = 1, 2, ..., m \tag{2.22}$$

is a parallelepiped in $m$-dimensional space, with a volume of $2^m w$. In other words, the measure $w$ is proportional to the volume of the parallel-piped. This gives another physical interpretation of $w$, different from the volume of the manipulability ellipsoid, although this is valid only for the case of $m \times n$ [23, 24].

### 2.4.1.3 Condition Number

Salisbury and Craig [14] defined the manipulability to evaluate the workspace quality by utilizing the condition number of $J$, which is given by

$$\Gamma_C(J) = \frac{\sigma_1}{\sigma_m} \tag{2.23}$$

where $\sigma_1$ and $\sigma_m$ are the minimum and maximum singular values of $J$, and

$$\sigma_1 = \sqrt{\lambda_1}, \quad \sigma_m = \sqrt{\lambda_m} \tag{2.24}$$

and $\lambda_1$ and $\lambda_m$ are the minimum and maximum of the eigenvalues of $JJ^T$, respectively. Geometrically, it is the ratio of the length of the major semiaxis to the length of the minor semiaxis of the manipulability ellipsoid. Such measure has a lower bound of 1, but it grows out of bound and tends to infinity when the manipulator is near the singular configuration.

#### 2.4.1.4 Isotropy Index

Isotropy Index is defined by the reciprocal of the condition number of $J$, which is given by

$$\Gamma_I(J) = \frac{\sigma_m}{\sigma_1} \tag{2.25}$$

Geometrically, it is the ratio of the length of the minor axis to the length of the major axis of the manipulability ellipsoid. Such a measure is better behaved compared with the condition number, since the values remain bounded between the values of 0 and 1. When this value is close to 1, the end-effector can move with uniform ease in all directions [9].

### 2.4.2 Example of Planar Serial RR Manipulator

A two-link manipulator is shown in Figure 2-3. The hand position is $[x, y]^T$, and the Jacobian matrix is

$$J = \begin{bmatrix} -l_1 S_1 - l_2 S_{12} & -l_2 S_{12} \\ l_1 C_1 + l_2 C_{12} & l_2 C_{12} \end{bmatrix} \tag{2.26}$$

and the manipulability measure $w$ is

$$w = |\det J| = l_1 l_2 |S_2| . \tag{2.27}$$

Thus, the manipulator tasks its optimal configuration when $q_2 = \pm 90°$, for any given values of $l_1, l_2$, and $\theta_1$. If the lengths $l_1$ and $l_2$ can be specified under the condition of constant total length (that is, $l_1 + l_2 = \text{constant}$), then the manipulability measure attains its maximum when $l_1 = l_2$ for any given $\theta_1$ and $\theta_2$. When the human arm is regarded as a two-link mechanism by neglecting the degree of freedom of sideward direction at the shoulder and the degree of freedom at the wrist, it approximately satisfies the relation $l_1 = l_2$. Moreover, when humans use their hands to perform some task such as writing letters, the angle of the elbow is usually in the neighborhood of 90°. Thus, it could be said that humans unconsciously use the arm postures that are best from the viewpoint of manipulability [24].

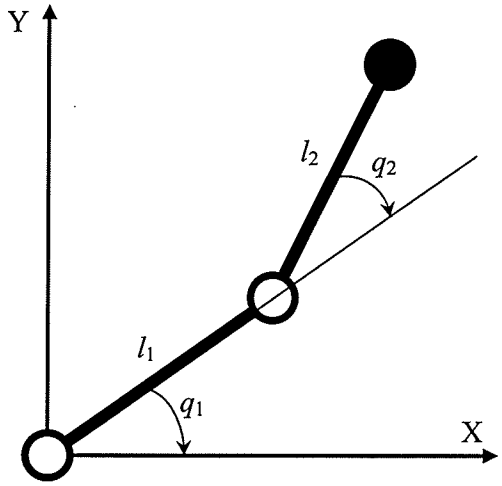


**Figure 2-3 Two-link manipulator.**

The two principal axes of the manipulability ellipsoid of the case of $l_1 = l_2 = 1$, are specified by $\sigma_1$, $\sigma_2$, $u_1$, and $u_2$, and can be derived as follows using the method described in Appendix 2. First, is given by

$$JJ^T = \begin{bmatrix} (S_1 + S_{12})^2 + {S_{12}}^2 & -(S_1 + S_{12})(C_1 + C_{12}) - S_{12}C_{12} \\ -(S_1 + S_{12})(C_1 + C_{12}) - S_{12}C_{12} & (C_1 + C_{12})^2 + {C_{12}}^2 \end{bmatrix},$$

and its eigenvalues are

$$\lambda_1 = \left[3 + 2C_2 + \sqrt{5 + 12C_2 + 8C_2^{\,2}}\right]/2\,,$$
$$\lambda_2 = \left[3 + 2C_2 - \sqrt{5 + 12C_2 + 8C_2^{\,2}}\right]/2\,.$$

Thus, the singular values are given by $\sigma_i = \sqrt{\lambda_i}$, where $i = 1, 2$. Next, from equation (A 2.8'),

$$u_i = \left[\left\{(S_1 + S_{12})(C_1 + C_{12}) + S_{12}C_{12}\right\}/k_i, \left\{(S_1 + S_{12})^2 + S_{12} - \lambda_i\right\}/k_i\right]^T,$$

where

$$k_i = \left\{\left[(S_1 + S_{12})(C_1 + C_{12}) + S_{12}C_{12}\right]^2 + \left[(S_1 + S_{12})^2 + S_{12} - \lambda_i\right]^2\right\}^{1/2}.$$

Figure 2.4 shows the manipulability ellipsoid and the manipulability measure for $l_1 = l_2 = 1$. obtained by use of the above expression. Figure 2.4 states clearly the direction in which it is easy to manipulate the end-effector [24].

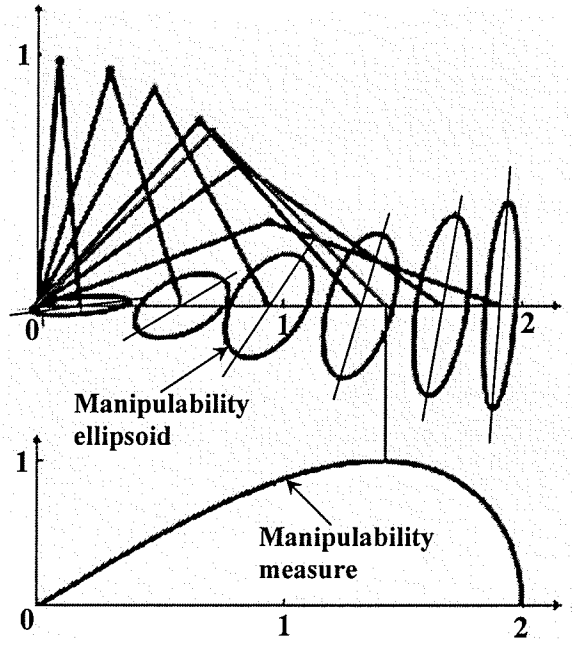


**Figure 2-4 Manipulability ellipsoid and manipulability measure of a RR manipulator [24]**

# 3 Modeling

3D visualization of the manipulator model is an important component of this project. The related work in this area is quite advanced and a number of excellent commercial products are available to perform robot visualization.

## *3.1 3D Graphic Modeling*

The simulator was developed by using OpenGL and Microsoft Visual C++. But, OpenGL doesn't provide high-level commands for describing models of three-dimensional objects. Such commands might not allow specifying relatively complicated shapes such as automobiles, parts of the body, airplanes, or molecules. So, AutoCAD 2004, 3D Max 5.0, and 3D Exploration were employed for 3D graphic modeling in this project.

### 3.1.1 Schematic Drawing

To create 3D graphic modeling, AutoCAD was employed. AutoCAD is a general purpose computer aided drafting application program designed for use on single-user, desktop personal computers and graphic workstations. It was initially developed in the early 1980's by Autodesk Inc. Up until Release10; AutoCAD was essentially a two-dimensional drawing system. Following that release, it now supports a full three-dimensional database. This has had the effect that the features of AutoCAD that support two-dimensional drawing are fully self-contained and can still be used as a 2D system without being concerned with its 3D features. AutoCAD 2004 was employed for this project. Figure 3-1 shows a schematic drawing of 7 functions Magnum subsea manipulator and represents its dimensions. The 3D model of Magnum was created by and based on these dimensions. These dimensions were provided by International Submarine Engineering Ltd. It was not difficult to build a 3D model by using AutoCAD 2004. According to the dimensions, the 3D model was created by using several solid commands, such as extrude, union, and intersection in AutoCAD 2004. The shape of the arm was modified slightly but the dimensions were exactly the same. However, it was the first step to convert the 3D model to OpenGL code.

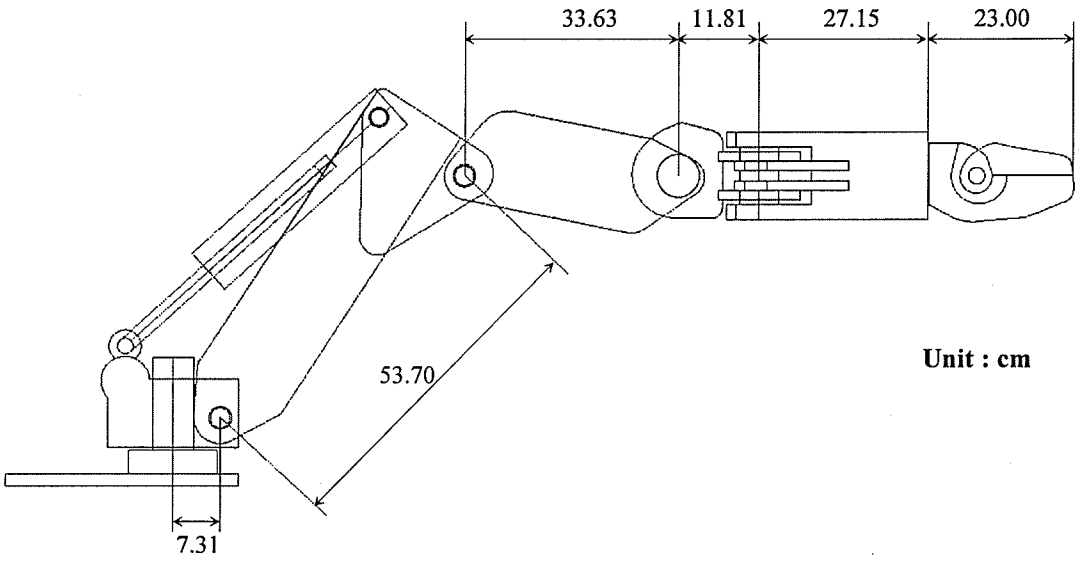


**Figure 3-1 Schematic drawing of 7 functions Magnum subsea manipulator.**

Figure 3-2 is a captured image while the 3D graphic model was being created by AutoCAD 2004.

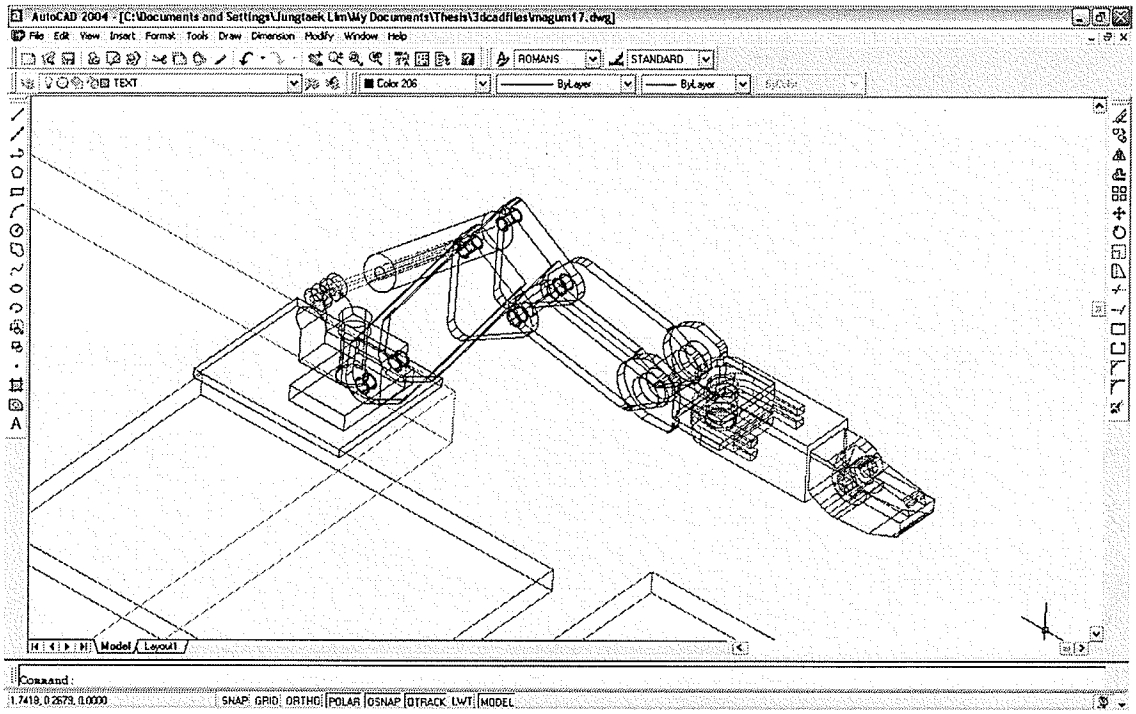


**Figure 3-2 3D modeling with AutoCAD.**

### 3.1.2 Converting 3ds file

3D Studio Max was also developed by Autodesk Inc. This 3D modeling software was used to import the 3ds files which were exported from AutoCAD and to export those files to the ASE (ASCII Scene Export) files in this project. It was also used for converting the coordinates of each of the links because each link needed the pivot points for OpenGL code. After this processing, the 3D Exploration was used for converting ASE (ASCII Scene Export) files to OpenGL files. 3D Exploration can convert 3D models into OpenGL code (polygons). Steps for converting 3ds file into OpenGL code include: i) 3D Modeling using AutoCAD; ii) Export to a 3ds (3D Studio) using AutoCAD; iii) Import to a 3ds (3D Studio) File using 3D Studio Max; iv) Export to ASE Files using 3D Studio Max; v) Convert ASE Files to C++ code using 3D Exploration.

## *3.2 Kinematics of Magnum*

### 3.2.1 Forward Kinematics of Magnum

Forward kinematics is the problem of locating the position and orientation of the end link, given the joint angles. This computation is straightforward for the Magnum subsea dual arms. This thesis begins by discussing the transformations between them, through the use of the named Denavit-Hartenberg representation.

#### 3.2.1.1 Link Coordinate Transformation

A commonly used convention for selecting frames of reference in robotic applications is the Denavit-Hartenberg convention. In this convention, each homogeneous transformation $A_i$ is represented as a product of four basic transformations. $A_i$ is already defined in chapter 2. According to Figure 3-3, the $5^{th}$ link frame is rotated about Y axis, so $A_i$ can be represented as following:

$$A_i = R_z(\theta_i)Trans_z(d_i)Trans_x(a_i)R_y(\alpha_i)$$

$$
= \begin{bmatrix} \cos\theta_i & -\sin\theta_i & 0 & 0 \\ \sin\theta_i & \cos\theta_i & 0 & 0 \\ 0 & 0 & 1 & 0 \\ 0 & 0 & 0 & 1 \end{bmatrix} \begin{bmatrix} 1 & 0 & 0 & 0 \\ 0 & 1 & 0 & 0 \\ 0 & 0 & 1 & d_i \\ 0 & 0 & 0 & 1 \end{bmatrix} \begin{bmatrix} 1 & 0 & 0 & \alpha_i \\ 0 & 1 & 0 & 0 \\ 0 & 0 & 1 & 0 \\ 0 & 0 & 0 & 1 \end{bmatrix} \begin{bmatrix} \cos\alpha_i & 0 & \sin\alpha_i & 0 \\ 0 & 1 & 0 & 0 \\ -\sin\alpha_i & 0 & \cos\alpha_i & 0 \\ 0 & 0 & 0 & 1 \end{bmatrix}
$$

$$
= \begin{bmatrix} \cos\theta_i\cos\alpha_i & -\sin\theta_i & \cos\theta_i\sin\alpha_i & a_i\cos\theta_i \\ \sin\theta_i\cos\alpha_i & \cos\alpha_i & \sin\theta_i\sin\alpha_i & a_i\sin\theta_i \\ -\sin\alpha_i & 0 & \cos\alpha_i & d_i \\ 0 & 0 & 0 & 1 \end{bmatrix} \tag{3.1}
$$

So, (2.1) and (3.1) are used to solve the forward kinematics of Magnum subsea dual arms in this thesis. Figure 3-3 shows the coordinate frames of 7 functions Magnum subsea manipulator.

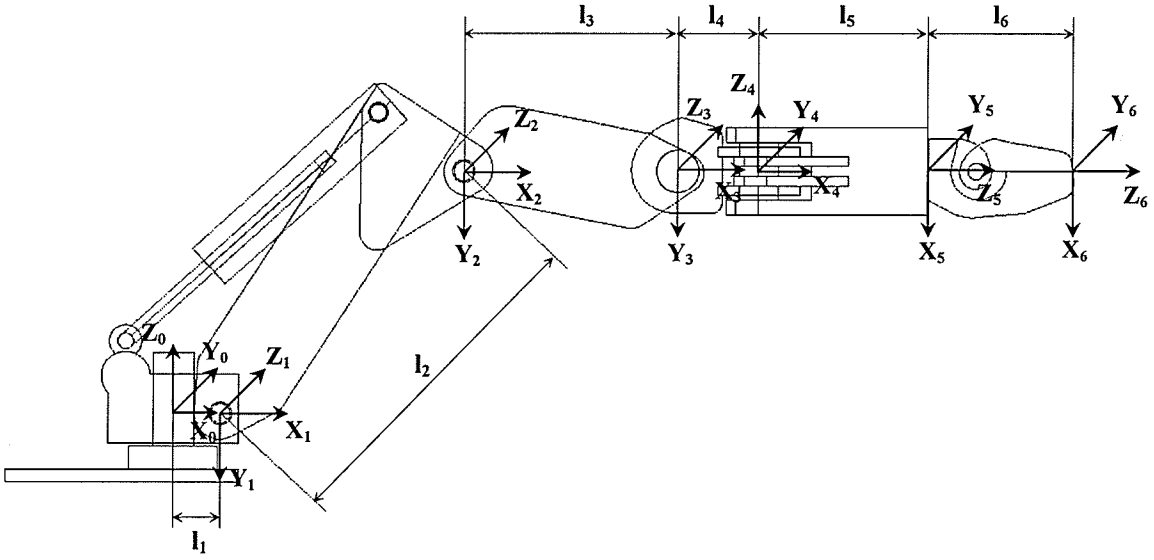


**Figure 3-3 Coordinate frames of 7 functions Magnum subsea manipulator.**

Table 2-1 lists the Denavit-Hartenberg coordinates for Magnum subsea manipulator.

**Table 3-1 Denavit-Hartenberg parameters**

| link | variable | $\alpha$ | a | d |
|---|---|---|---|---|
| 1 | $\theta_1$ | 90° | $l_1$ | 0 |
| 2 | $\theta_2$ | 0 | $l_2$ | 0 |
| 3 | $\theta_3$ | 0 | $l_3$ | 0 |
| 4 | $\theta_4$ | –90° | $l_4$ | 0 |
| 5 | $\theta_5$ | 90° | $l_5$ | 0 |
| 6 | $\theta_6$ | 0 | 0 | $l_6$ |

According to equation (2.1) and (3.1), $A_i$ matrix will be defined by following.

$$A_1 = \begin{bmatrix} \cos\theta_1 & 0 & \sin\theta_1 & l_1\cos\theta_1 \\ \sin\theta_1 & 0 & -\cos\theta_1 & l_1\sin\theta_1 \\ 0 & 1 & 0 & 0 \\ 0 & 0 & 0 & 1 \end{bmatrix} \tag{3.2}$$

$$A_2 = \begin{bmatrix} \cos\theta_2 & -\sin\theta_2 & 0 & l_2\cos\theta_2 \\ \sin\theta_2 & \cos\theta_2 & 0 & l_2\sin\theta_2 \\ 0 & 0 & 1 & 0 \\ 0 & 0 & 0 & 1 \end{bmatrix} \tag{3.3}$$

$$A_3 = \begin{bmatrix} \cos\theta_3 & -\sin\theta_3 & 0 & l_3\cos\theta_3 \\ \sin\theta_3 & \cos\theta_3 & 0 & l_3\sin\theta_3 \\ 0 & 0 & 1 & 0 \\ 0 & 0 & 0 & 1 \end{bmatrix} \tag{3.4}$$

$$A_4 = \begin{bmatrix} \cos\theta_4 & 0 & -\sin\theta_4 & l_4\cos\theta_4 \\ \sin\theta_4 & 0 & \cos\theta_4 & l_4\sin\theta_4 \\ 0 & -1 & 0 & 0 \\ 0 & 0 & 0 & 1 \end{bmatrix} \tag{3.5}$$

$$A_5 = \begin{bmatrix} 0 & -\sin\theta_5 & \cos\theta_5 & l_5\cos\theta_5 \\ 0 & \cos\theta_5 & \sin\theta_5 & l_5\sin\theta_5 \\ -1 & 0 & 0 & 0 \\ 0 & 0 & 0 & 1 \end{bmatrix} \tag{3.6}$$

$$A_6 = \begin{bmatrix} \cos\theta_6 & -\sin\theta_6 & 0 & 0 \\ \sin\theta_6 & \cos\theta_6 & 0 & 0 \\ 0 & 0 & 1 & l_6 \\ 0 & 0 & 0 & 1 \end{bmatrix} \tag{3.7}$$

$$A_1A_2A_3A_4A_5A_6 = T_6 = \begin{bmatrix} n_x & o_x & a_x & p_x \\ n_y & o_y & a_y & p_y \\ n_z & o_z & a_z & p_z \\ 0 & 0 & 0 & 1 \end{bmatrix} \tag{3.8}$$

$$\begin{aligned}
n_x &= c_1(s_{234}c_6 - c_{234}s_5s_6) - s_1(c_5s_6) \\
n_y &= s_1(s_{234}c_6 - c_{234}s_5s_6) + c_1(c_5s_6) \\
n_z &= -c_{234}c_6 - s_{234}s_5s_6 \\
o_x &= c_1(-s_{234}s_6 - c_{234}s_5c_6) - s_1(s_5c_6) \\
o_y &= s_1(-s_{234}s_6 - c_{234}s_5c_6) + c_1(s_5c_6) \\
o_z &= c_{234}s_6 - s_{234}s_5c_6 \\
a_x &= c_1(c_{234}c_5) - s_1s_5 \\
a_y &= s_1(c_{234}c_5) + c_1s_5 \\
a_z &= s_{234}c_5 \\
p_x &= c_1[(l_5 + l_6)c_{234}c_5 + l_4c_{234} + l_3c_{23} + l_2c_2] - s_1(l_5 + l_6)s_5 + l_1c_1 \\
p_y &= s_1[(l_5 + l_6)c_{234}c_5 + l_4c_{234} + l_3c_{23} + l_2c_2] + c_1(l_5 + l_6)s_5 + l_1s_1 \\
p_z &= (l_5 + l_6)s_{234}c_5 + l_4s_{234} + l_3s_{23} + l_2s_2
\end{aligned} \tag{3.9}$$

### 3.2.2 Inverse Kinematics of Magnum

Forward kinematics can only indirectly control the position of each segment by specifying rotation angles at the joints between the root and the end-effector. This may result

in unpredictable behavior during interpolation. In contrast, inverse kinematics provides direct control over the placement of the end-effector by solving for the joint angles that can place it at the desired location.

### 3.2.2.1 Magnum Manipulator Solution

For Magnum, $T_6$ is calculated through the position and Euler angles of Magnum end-effector. It is equal to the product of the six $A$ matrices (See Figure 3-4).

$$A_1A_2A_3A_4A_5A_6 = T_6 \tag{3.10}$$

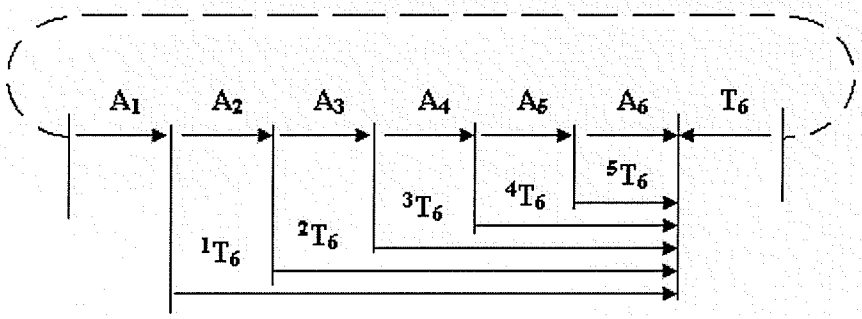


**Figure 3-4 The manipulator transform graph [13]**

The equation (3.10) is premultiplied by $A_1^{-1}$ and the equation (3.11) is obtained.

$$A_2A_3A_4A_5A_6 = A_1^{-1}T_6 \tag{3.11}$$

The left side of equation (3.11) is obtained through calculating with equations (2.1) and (3.1) and is given by

$$A_2A_3A_4A_5A_6 = \begin{bmatrix} s_{234}c_6 - c_{234}s_5s_6 & -s_{234}s_6 - c_{234}s_5c_6 & c_{234}c_5 & (l_5+l_6)c_{234}c_5 + l_4c_{234} + l_3c_{23} + l_2c_2 \\ -c_{234}c_6 - s_{234}s_5s_6 & c_{234}s_6 - s_{234}s_5c_6 & s_{234}c_5 & (l_5+l_6)s_{234}c_5 + l_4s_{234} + l_3s_{23} + l_2s_2 \\ -c_5s_6 & -s_5c_6 & -s_5 & -(l_5+l_6)s_5 \\ 0 & 0 & 0 & 1 \end{bmatrix} \tag{3.12}$$

The right side of equation (3.11) is given by

$$A_1^{-1}T_6 = \begin{bmatrix} c_1 & s_1 & 0 & -l_1 \\ 0 & 0 & 1 & 0 \\ s_1 & -c_1 & 0 & 0 \\ 0 & 0 & 0 & 1 \end{bmatrix} \begin{bmatrix} n_x & o_x & a_x & p_x \\ n_y & o_y & a_y & p_y \\ n_z & o_z & a_z & p_z \\ 0 & 0 & 0 & 1 \end{bmatrix}$$

$$= \begin{bmatrix} n_x c_1 + n_y s_1 & o_x c_1 + o_y s_1 & a_x c_1 + a_y s_1 & p_x c_1 + p_y s_1 - l_1 \\ n_z & o_z & a_z & p_z \\ n_x s_1 - n_y c_1 & o_x s_1 - o_y c_1 & a_x s_1 - a_y c_1 & p_x s_1 - p_y c_1 \\ 0 & 0 & 0 & 1 \end{bmatrix} \tag{3.13}$$

Now, in order to get the each link angle, the following steps are shown

## Step 1

To get link1 angle $\theta_1$ first of all the row 3 column 3 element of equations (3.12) and (3.13) are taken.

$$a_x s_1 - a_y c_1 = -s_5 \tag{3.14}$$

The row 3 column 4 element of equations (3.12) and (3.13) are obtained also.

$$p_x s_1 - p_y c_1 = -(l_5 + l_6) s_5 \tag{3.15}$$

Finally the $\theta_1$ is defined by equation (3.16).

$$p_x s_1 - p_y c_1 = (l_5 + l_6)(a_x s_1 - a_y c_1)$$

$$[(l_5 + l_6)a_y - p_y]c_1 = [(l_5 + l_6)a_x - p_x]s_1$$

$$\tan(\theta_1) = \frac{s_1}{c_1} = \frac{[(l_5 + l_6)a_y - p_y]}{[(l_5 + l_6)a_x - p_x]}$$

$$\theta_1 = a\tan 2([(l_5 + l_6)a_y - p_y],\ [(l_5 + l_6)a_x - p_x]) \tag{3.16}$$

$$\left( \theta_1 \in (-\frac{\pi}{2}, \frac{\pi}{2}) \right)$$

## Step 2

The row 3 column 3 element of equations (3.12) and (3.13) are taken and the $\theta_5$ is defined by equation (3.17).

$$s_5 = a_y c_1 - a_x s_1$$

$$\theta_5 = \text{asin}(a_y c_1 - a_x s_1) \tag{3.17}$$

$$\left( \theta_5 \in (-\frac{\pi}{2}, \frac{\pi}{2}) \right)$$

## Step 3

The row 3 column 1 element of equations (3.12) and (3.13) are taken and the $\theta_6$ is defined by equation (3.18).

$$-c_5 s_6 = n_x s_1 - n_y c_1$$

$$s_6 = (n_y c_1 - n_x s_1)/c_5$$

$$\theta_6 = \text{asin}((n_y c_1 - n_x s_1)/c_5) \tag{3.18}$$

$$\left( c_5 \neq 0 \ , \ \theta_6 \in (-\frac{\pi}{2}, \frac{\pi}{2}) \right)$$

## Step 4

The row 2 column 3 and the row 1 column 3 element of equations (3.12) and (3.13) are taken and the $\theta_{234}$ is defined equation (3.19).

$$s_{234} c_5 = a_z$$

$$c_{234} c_5 = a_x c_1 + a_y s_1$$

$$\theta_{234} = \text{atan}(a_z / c_5, (a_x c_1 + a_y s_1)/c_5) \tag{3.19}$$

$$\left( c_5 \neq 0 \ , \ \theta_{234} \in (-\frac{\pi}{2}, \frac{\pi}{2}) \right)$$

## 3.3 Jacobian of Magnum

The Magnum was defined by the $A$ transformations (equations (3.2) to (3.7)). In order to compute the columns of the Jacobian, it will be needed the differential coordinate transformations corresponding to all six differential changes $d\theta_1, d\theta_2, d\theta_3, d\theta_4, d\theta_5, d\theta_6$; these are $T_6$, ${}^1T_6$, ${}^2T_6$, ${}^3T_6$, ${}^4T_6$, ${}^5T_6$, respectively. The first column of the Jacobian corresponds to $\partial T_6 / \partial \theta_1$; the differential coordinate transform is $T_6$, given by equations (3.8) and (3.9). Equations (2.9) and (2.10) will be taken to compute the differential translation and rotation vectors whose elements make up the first column.

$$
\begin{aligned}
{}^{T6}d_{1x} = \{&-[c_1(s_{234}c_6 - c_{234}s_5s_6) - s_1(c_5s_6)][s_1((l_5+l_6)c_{234}c_5 + l_4c_{234} + l_3c_{23} + l_2c_2) + c_1(l_5+l_6)s_5 + l_1s_1] \\
&+[s_1(s_{234}c_6 - c_{234}s_5s_6) + c_1(c_5s_6)][c_1((l_5+l_6)c_{234}c_5 + l_4c_{234} + l_3c_{23} + l_2c_2) - s_1(l_5+l_6)s_5 + l_1c_1]\}
\end{aligned}
\tag{3.20}
$$

$$
\begin{aligned}
{}^{T6}d_{1y} = \{&-[c_1(-s_{234}s_6 - c_{234}s_5c_6) - s_1(s_5c_6)][s_1((l_5+l_6)c_{234}c_5 + l_4c_{234} + l_3c_{23} + l_2c_2) + c_1(l_5+l_6)s_5 + l_1s_1] \\
&+[s_1(-s_{234}s_6 - c_{234}s_5c_6) + c_1(s_5c_6)][c_1((l_5+l_6)c_{234}c_5 + l_4c_{234} + l_3c_{23} + l_2c_2) - s_1(l_5+l_6)s_5 + l_1c_1]\}
\end{aligned}
\tag{3.21}
$$

$$
\begin{aligned}
{}^{T6}d_{1z} = \{&-[c_1(c_{234}c_5) - s_1s_5][s_1((l_5+l_6)c_{234}c_5 + l_4c_{234} + l_3c_{23} + l_2c_2) + c_1(l_5+l_6)s_5 + l_1s_1] \\
&+[s_1(c_{234}c_5) + c_1s_5][c_1((l_5+l_6)c_{234}c_5 + l_4c_{234} + l_3c_{23} + l_2c_2) - s_1(l_5+l_6)s_5 + l_1c_1]\}
\end{aligned}
\tag{3.22}
$$

$$
{}^{T6}\delta_{1x} = -c_{234}c_6 - s_{234}s_5s_6 \tag{3.23}
$$

$$
{}^{T6}\delta_{1y} = c_{234}s_6 - s_{234}s_5c_6 \tag{3.24}
$$

$$
{}^{T6}\delta_{1z} = s_{234}c_5 \tag{3.25}
$$

On simplification, the first column is obtained as

$$\partial T_6/\partial\theta_1 = \begin{bmatrix} -(s_{234}c_6 - c_{234}s_5s_6)(l_5+l_6)s_5 + (c_5s_6)[(l_5+l_6)c_{234}c_5 + l_4c_{234} + l_3c_{23} + l_2c_2 + l_1] \\ -(-s_{234}s_6 - c_{234}s_5c_6)(l_5+l_6)s_5 + (s_5c_6)[(l_5+l_6)c_{234}c_5 + l_4c_{234} + l_3c_{23} + l_2c_2 + l_1] \\ -(c_{234}c_5)(l_5+l_6)s_5 + s_5[(l_5+l_6)c_{234}c_5 + l_4c_{234} + l_3c_{23} + l_2c_2 + l_1] \\ -c_{234}c_6 - s_{234}s_5s_6 \\ c_{234}s_6 - s_{234}s_5c_6 \\ s_{234}c_5 \end{bmatrix} \tag{3.26}$$

The second column of the Jacobian corresponds to $\partial T_6/\partial\theta_2$; the differential coordinate transform is ${}^1T_6$,

$$\begin{aligned} {}^{T6}d_{2x} &= \{-[s_{234}c_6 - c_{234}s_5s_6][(l_5+l_6)s_{234}c_5 + l_4s_{234} + l_3s_{23} + l_2s_2]\} \\ &\quad + \{[-c_{234}c_6 - s_{234}s_5s_6][(l_5+l_6)c_{234}c_5 + l_4c_{234} + l_3c_{23} + l_2c_2]\} \end{aligned} \tag{3.27}$$

$$\begin{aligned} {}^{T6}d_{2y} &= \{-[-s_{234}s_6 - c_{234}s_5c_6][(l_5+l_6)s_{234}c_5 + l_4s_{234} + l_3s_{23} + l_2s_2]\} \\ &\quad + \{[c_{234}s_6 - s_{234}s_5c_6][(l_5+l_6)c_{234}c_5 + l_4c_{234} + l_3c_{23} + l_2c_2]\} \end{aligned} \tag{3.28}$$

$$\begin{aligned} {}^{T6}d_{2z} &= \{-[c_{234}c_5][(l_5+l_6)s_{234}c_5 + l_4s_{234} + l_3s_{23} + l_2s_2]\} \\ &\quad + \{[s_{234}c_5][(l_5+l_6)c_{234}c_5 + l_4c_{234} + l_3c_{23} + l_2c_2]\} \end{aligned} \tag{3.29}$$

$${}^{T6}\delta_{2x} = -c_5s_6 \tag{3.30}$$

$${}^{T6}\delta_{2y} = -s_5c_6 \tag{3.31}$$

$${}^{T6}\delta_{2z} = -s_5 \tag{3.32}$$

Upon simplification, the second column of the Jacobian becomes

$$\partial T_6/\partial\theta_2 = \begin{bmatrix} -[s_{34}c_6 - c_{34}s_5s_6][(l_5+l_6)s_{34}c_5 + l_4s_{34}] + [-c_{34}c_6 - s_{34}s_5s_6][(l_5+l_6)c_{34}c_5 + l_4c_{34} + l_3c_3 + l_2] \\ -[-s_{34}s_6 - c_{34}s_5c_6][(l_5+l_6)s_{34}c_5 + l_4s_{34}] + [c_{34}s_6 - s_{34}s_5c_6][(l_5+l_6)c_{34}c_5 + l_4c_{34} + l_3c_3 + l_2] \\ -[c_{34}c_5][(l_5+l_6)s_{34}c_5 + l_4s_{34} + l_3s_3] + [s_{34}c_5][(l_5+l_6)c_{34}c_5 + l_4c_{34} + l_3c_3 + l_2] \\ -c_5s_6 \\ -s_5c_6 \\ -s_5 \end{bmatrix} \tag{3.33}$$

The coordinate transformation for the third column is ${}^{2}T_{6}$ whose elements make up the third column, which may be written directly as

$$\partial T_6 / \partial \theta_3 = \begin{bmatrix} -[-c_4 s_5 s_6 - s_4 c_6][(l_6 + l_5) s_4 c_5 + l_4 c_4 + l_3] + [-s_4 s_5 s_6 + c_4 c_6][(l_6 + l_5) c_4 c_5 + l_4 c_4 + l_3] \\ -[-c_4 s_5 s_6 + s_4 s_6][(l_6 + l_5) s_4 c_5 + l_4 c_4 + l_3] + [-s_4 s_5 s_6 - c_4 s_6][(l_6 + l_5) c_4 c_5 + l_4 c_4 + l_3] \\ -[c_4 c_5][(l_6 + l_5) s_4 c_5 + l_4 c_4 + l_3] + [s_4 s_5][(l_6 + l_5) c_4 c_5 + l_4 c_4 + l_3] \\ -c_5 s_6 \\ -s_5 c_6 \\ -s_5 \end{bmatrix} \tag{3.34}$$

The differential coordinate transformation for the joint 4, 5, and 6 of results are

$$\partial T_6 / \partial \theta_4 = \begin{bmatrix} s_5 s_6 l_4 + c_6[(l_6 + l_5) c_4 c_5 + l_4] \\ -s_5 c_6 l_4 + s_6[(l_6 + l_5) c_4 c_5 + l_4] \\ c_5 l_4 \\ -c_5 s_6 \\ -s_5 c_6 \\ -s_5 \end{bmatrix} \tag{3.35}$$

$$\partial T_6 / \partial \theta_5 = \begin{bmatrix} s_6(l_5 + l_6) \\ 0 \\ 0 \\ c_6 \\ -s_6 \\ 0 \end{bmatrix} \tag{3.36}$$

$$\partial T_6 / \partial \theta_6 = \begin{bmatrix} 0 \\ 0 \\ 0 \\ 0 \\ 0 \\ 1 \end{bmatrix} \tag{3.37}$$

## 3.4 Dynamics of Dual Arms

The dynamic model is obtained from the kinematics model by adding dynamics properties to the robot model such as mass, inertia moments, joint torques as well as by extending the virtual environment. The dynamic models can be used in torque analysis and stability analysis. This simulator is for dual manipulators. So, in this thesis, a nonlinear control scheme is developed to perform a cooperative task by hydraulic manipulators. It is going to focus on a cooperative manner. The following concept and equations are addressed by Zeng [25] who worked together for this project.

### 3.4.1 Robot Dynamics

Consider the problem of manipulating a rigid object with N hydraulic robots as shown in Figure 3-5. The end-effectors of all robots are assumed to be rigidly connected to a common object, i.e., there is no relative motion between the object and any one of the end-effectors. Each robot exerts both force and moment on the object.

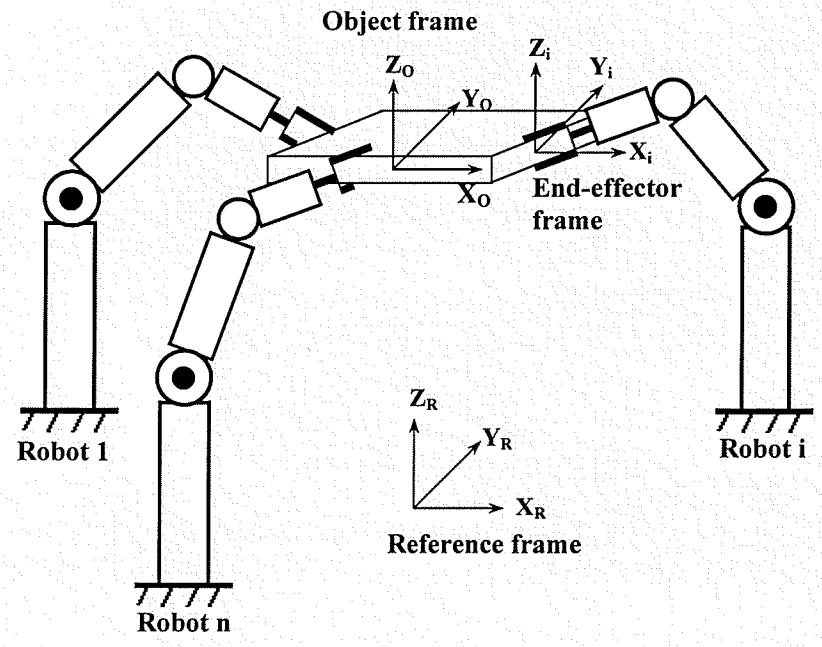


**Figure 3-5 Coordinate systems for cooperating manipulators and object.**

The dynamic equations of N cooperating robots are given as follows with respect to the joint coordinates [1, 10]

$$H(q)\ddot{q} + C(q,\dot{q})\dot{q} + G(q) = T - J^T F_c \tag{3.38}$$

where $H = diag\{H^1, H^2, ..., H^N\}$ , $C = diag\{C^1, C^2, ..., C^N\}$ , $G = [G^{1T}, G^{2T}, ..., G^{NT}]^T$ , $T = [T^{1T}, T^{2T}, ..., T^{NT}]^T$ , $F_c = [F_c^{1T}, F_c^{2T}, ..., F_c^{NT}]^T$. For each manipulator, $H^i$ denotes the robot inertia matrix, $C^i$ denotes the Coriolis/centrifugal effects and $G^i$ is the gravitational term. $T^i = [T_1^i, T_2^i, ..., T_6^i]^T$ where $T_j^i$ is the generalized joint torque originating from the $j^{th}$ hydraulic actuator of the $i^{th}$ manipulator. $F_c^i$ is the vector of contact force/moment on the object exerted by the $i^{th}$ end-effector. Note that $H(q)$ is a symmetric positive definite matrix, and $(\dot{H} - 2C)$ is a skew-symmetric matrix [17].

## 3.4.2 Object Dynamics

The object dynamics, expressed in Cartesian space, is given as:

$$\Lambda_o(X_o)\dot{v}_o + B_o(X_o, v_o)v_o + G_o(X_o) = F_{ext} \tag{3.39}$$

where $\Lambda_o(X_o) \in R^{6\times 6}$ , is the symmetric and positive definite inertia matrix of the object. $B_o(X_o, v_o)v_o \in R^{6\times 1}$ is the vector of Coriolis and centrifugal forces. $G_o(X_o) \in R^{6\times 1}$ is the vector of gravitational forces, and $F_{ext} \in R^{6\times 1}$ is the vector of resulting forces acting at the origin of the object frame. Note $\dot{\Lambda}_o(X_o) - 2B_o(X_o, v_o)$ is a skew-symmetric matrix.

In view of the duality between forces and velocities originating from the principle of virtual work, the mapping of the contact force vector, $F_c$, onto the external force vector, $F_{ext}$, is unique and is expressed as [1, 7, 10, 20]:

$$F_{ext} = WF_c \tag{3.40}$$

where $W$ is a grasp matrix [1, 20].

On the other hand, the reverse mapping is not unique and should take the internal force $F_{\text{int}}$ into account:

$$F_c = W^+ F_{ext} + V F_{\text{int}} \tag{3.41}$$

where $W^+$ is a pseudo-inverse (see Appendix 1) of $W$, $V$ is a full column rank matrix satisfying $WV = 0$. Rewriting $F_c$ in the following form:

$$F_c = W^+ W F_c + (I - W^+ W) F_c \tag{3.42}$$

and knowing $F_c = J^{-T} T_c$, a similar relation can be obtained for $T_c$,

$$T_c = J^T W^+ W J^{-T} T_c + J^T (I - W^+ W) J^{-T} T_c \tag{3.43}$$

Equation (3.43) indicates that any set of torques, which produces the end-effector object contact forces, can be decoupled into two parts. One contributes to the motion of the object while $J^T W^+ W J^{-T}$ in (3.43) acts as a filter to remove those torques corresponding to the internal forces. The other one makes no contribution to the motion of the object. For a rigid object the second part of the torque in (3.43) only corresponds to the internal forces; thus, the following property is true:

$$\dot{q}^T J^T (I - W^+ W) F_c = 0 \tag{3.44}$$

Since $F_c$ can have any value, one has

$$\dot{q}^T J^T (I - W^+ W) = 0 \tag{3.45}$$

It has been shown [20] that $W^+$ must be properly chosen, otherwise internal forces may arise even if $F_{\text{int}} = 0$. For manipulators that equally share the load, the pseudo-inverse of $W$ is chosen as

$$W^{+} = 1/N \begin{bmatrix} I & 0 \\ -R^1 & I \\ \vdots & \vdots \\ I & 0 \\ -R^N & I \end{bmatrix} \tag{3.46}$$

where $R^i = \begin{bmatrix} 0 & -r_{ez}^i & r_{ey}^i \\ r_{ez}^i & 0 & -r_{ex}^i \\ -r_{ey}^i & r_{ex}^i & 0 \end{bmatrix}$.

Vector $[r_{ex}^i, r_{ey}^i, r_{ez}^i]^T$ describes the position of the $i^{th}$ end-effector with respect to the object frame, expressed in Cartesian reference frame. Similarly, under the assumption that manipulators have almost the same performance, a solution is adopted, for $V$ :

$$V = \begin{bmatrix} a^1 I & 0 \\ -a^1 R^1 & a^1 I \\ \vdots & \vdots \\ a^N I & 0 \\ -a^N R^N & a^N I \end{bmatrix} \tag{3.47}$$

where $a^i = \dfrac{2(-1)^i}{N-(-1)^i(1-(-1)^N)/2}$, $i = 1,...,N$.

## 3.4.3 Actuator Dynamics

With reference to Figure 3-6, the governing equations that describe the nonlinear valve flow characteristics of the $j^{th}$ actuator of the $i^{th}$ manipulator given in [12, 16] are rewritten in compact forms as:

$$q_{I,j}^i = K_j^i x_{sp,j}^i Q_{I,j}^i \tag{3.48a}$$

$$q_{O,j}^i = K_j^i x_{sp,j}^i Q_{O,j}^i \tag{3.48b}$$

where $K_j^i = C_d \sqrt{\frac{2}{\rho}} w_j^i$ is the constant flow gain, and

$$Q_{I,j}^{i} = \sqrt{\frac{P_s - P_e}{2} + \mathrm{sgn}(x_{sp,j}^{i})(\frac{P_s + P_e}{2} - P_{I,j}^{i})}$$

$$Q_{O,j}^{i} = \sqrt{\frac{P_s - P_e}{2} + \mathrm{sgn}(x_{sp,j}^{i})(P_{O,j}^{i} - \frac{P_s + P_e}{2})}$$

$q_{I,j}^{i}$ and $q_{O,j}^{i}$ represent fluid flows into and out of the valve, respectively. $C_d$ and $\rho$ are the orifice coefficients of the discharge and the mass density of the fluid, respectively. $x_{sp,j}^{i}$ represents the spool displacement. $P_{I,j}^{i}$ and $P_{O,j}^{i}$ are the input and the output line pressures, respectively. $P_s$ and $P_e$ are the pump and exit pressures and $w_j^i$ is the orifice area gradient. Continuity equations for oil flow through the cylinder are [12, 16]

$$q_{I,j}^{i} = A_{I,j}^{i}\dot{x}_j^i + \frac{V_{I,j}^{i}(x_j^i)}{\beta}\dot{P}_{I,j}^{i} \tag{3.49a}$$

$$q_{O,j}^{i} = A_{O,j}^{i}\dot{x}_j^i - \frac{V_{O,j}^{i}(x_j^i)}{\beta}\dot{P}_{O,j}^{i} \tag{3.49b}$$

where $\beta$ is the effective bulk modulus of the hydraulic fluids. $x_j^i$ is the cylinder position. $V_{I,j}^{i}$ and $V_{O,j}^{i}$ are the fluid volumes trapped in each side of the actuator, respectively. They are expressed as

$$V_{I,j}^{i}(x_j^i) = \bar{V}_{I,j}^{i} + x_j^i A_{I,j}^{i} \tag{3.50a}$$

$$V_{O,j}^{i}(x_j^i) = \bar{V}_{O,j}^{i} - x_j^i A_{O,j}^{i} \tag{3.50b}$$

$\bar{V}_{I,j}^{i}$ and $\bar{V}_{O,j}^{i}$ are the initial volumes of the fluid trapped at the sides of the actuator. Due to very small rise time, the relation between the spool displacement, $x_{sp,j}^{i}$, and input voltage, $u_j^i$, to the proportional valve can be simply expressed as

$$u_j^i = \frac{1}{K_{sp,j}^{i}} x_{sp,j}^{i} \tag{3.51}$$

$K^i_{sp,j}$ in (3.51) is a gain. The hydraulic actuator force, $F^i_j$ is

$$F^i_j = (A^i_{I,j}P^i_{I,j} - A^i_{O,j}P^i_{O,j} - K^i_{damp,j}\dot{x}^i_j) \tag{3.52}$$

where $K^i_{damp,j}$ is the equivalent viscous damping coefficient. The cylinder speed is related to the joint angular velocity as

$$\dot{x}^i_j = \hat{J}^i_j(q^i_j)\dot{q}^i_j \tag{3.53}$$

Note that $\hat{J}^i_j(q^i_j)$ is the Jacobian from link joint space to the linear actuator coordinate. Similarly, the torque originating from the actuator, $T^i_j$ is

$$T^i_j = \hat{J}^i_j(q^i_j)F^i_j \tag{3.54}$$

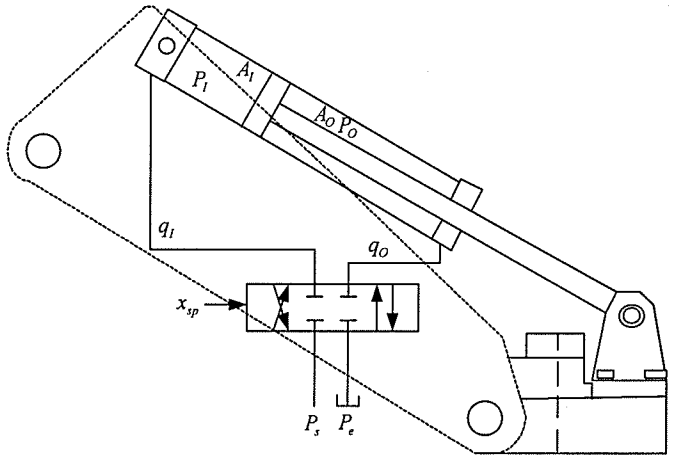


**Figure 3-6 Typical hydraulic actuator with its driven link.**

## 3.4.4 Complete System Dynamics

Combining equations (3.38) and (3.39), one arrives at the following equation:

$$(\Lambda_o + \Lambda)\dot{v}_o + (B_o + B)v_o + G_o + WJ^{-T}G = WJ^{-T}T \tag{3.55}$$

where

$$\Lambda = WJ^{-T}HJ^{-1}W^{-T};$$

$$B = WJ^{-T}HJ^{-1}(\dot{W}^T - \dot{J}J^{-1}W^T) + WJ^{-T}CJ^{-1}W^T;$$

$$T = \hat{J}F - K_{damp}\hat{J}^2\dot{q};$$

$$F = A_I P_I - A_O P_O;$$

$$P_I = [P_I^{1T}, P_I^{2T}, ..., P_I^{NT}]^T;\ P_I^i = [P_{I,1}^i, P_{I,2}^i, ..., P_{I,6}^i]^T;$$

$$P_O = [P_O^{1T}, P_O^{2T}, ..., P_O^{NT}]^T;\ P_O^i = [P_{O,1}^i, P_{O,2}^i, ..., P_{O,6}^i]^T;$$

$$A_I = diag(A_{I,j}^i);\quad A_O = diag(A_{O,j}^i);$$

$$\hat{J}(q) = diag(\hat{J}_j^i(q_j^i));$$

$$K_{damp} = diag(K_{damp,j}^i).$$

From equations (3.49a) to (3.50b), the following are obtained

$$\dot{P}_I = C_I\left[KK_{sp}UQ_I - A_I\hat{J}(q)\dot{q}\right] \tag{3.56a}$$

$$\dot{P}_O = C_O\left[-KK_{sp}UQ_O + A_O\hat{J}(q)\dot{q}\right] \tag{3.56b}$$

where

$$C_I = diag(C_{I,j}^i);\ C_{I,j}^i = \beta_j^i/(V_{I,j}^i + A_{I,j}^i x_j^i);$$

$$C_O = diag(C_{O,j}^i);\ C_{O,j}^i = \beta_j^i/(V_{O,j}^i - A_{O,j}^i x_j^i);$$

## 3.5 Manipulability of Magnum

Manipulability has been mentioned in chapter 2. In this chapter, the method of manipulability measure was employed for the Magnum subsea dual arms. Intuitively, manipulability can be defined as how easily and uniformly the end-effector is able to move in arbitrary directions. To analyze a manipulability of the mechanism, the manipulability ellipsoid is the most intuitive and useful measure. The manipulability ellipsoid can be made by mapping a unit sphere in the joint input space to the output space through the Jacobian matrix (see Figure 3-7).

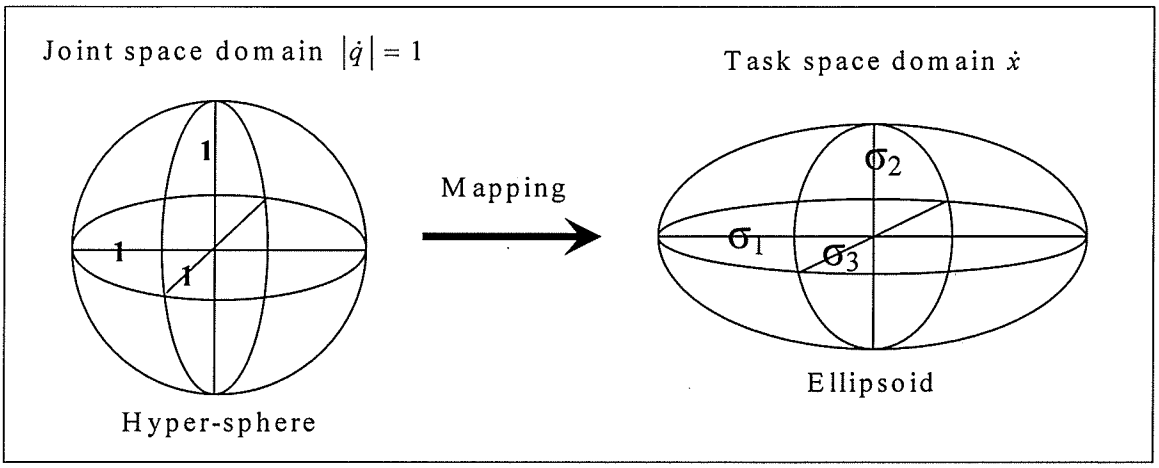


**Figure 3-7 Manipulability ellipsoid II [14].**

The major and minor axes of the ellipsoid indicate the directions in which the end-effector can move most and least easily and the ease is proportional to the principal axes length. Also, the magnitude and direction of the major and minor axes can be obtained from the singular value decomposition as described in chapter 3. If the ellipsoid is larger and more circular, then the end-effector has faster and more uniform motion.

### 3.5.1 Translational Manipulability

From these physical insights, Yoshikawa [23, 24] defined the manipulability of a mechanism as

$$w = \sqrt{\det J(q)J^T(q)}. \tag{3.57}$$

In (3.57), translational and rotational manipulability are not distinguishable [3, 5, 9]. Magnum subsea manipulator has 6 dimensional space, 3 translational and 3 rotational. Therefore (3.57) may not be suitable for the Magnum subsea dual arms. To define the translational and rotational manipulability, workspace velocity can be rewritten (3.58) as linear (3.59) and angular velocity (3.60).

$$V = [V_x, V_y, V_z, \omega_x, \omega_y, \omega_z]^T \tag{3.58}$$

$$V_T = [V_x, V_y, V_z]^T = J_T \dot{q} \tag{3.59}$$

$$V_R = [\omega_x, \omega_y, \omega_z]^T = J_\omega \dot{q} \tag{3.60}$$

and Jacobian matrix $J$ can be rewritten in (3.61).

$$J = \begin{bmatrix} J_T \\ J_\omega \end{bmatrix} \tag{3.61}$$

The following are defined as individual manipulability measures [9].

$$w_T = \sqrt{\det J_T(q) J_T^T(q)} : \text{translational velocity manipulability.} \tag{3.62}$$

$$w_R = \sqrt{\det J_\omega(q) J_\omega^T(q)} : \text{rotational velocity manipulability.} \tag{3.63}$$

Translational velocity manipulability was employed in this thesis to measure the manipulability of Magnum subsea dual arms.

## 3.5.2 Dual Arms Manipulability Ellipsoid

### 3.5.2.1 Model of Two Cooperating Robots

The model of the two robot arms and the object is shown in Figure 3-8, where the end-effectors of the robots are grabbing an object. $x_i$ is the position and orientation vector of the end-effector of robot $i$ in the reference frame. For convenience, the subscripts $i = 1, 2$ are used to indicate the two robots. The end-effectors of the robots are imaginarily extended and the reference position of the object is viewed as the end-effector positions of the two robots. The following assumptions are made.

(i) The object is held rigidly by the grippers so that no relative motion is allowed the robot grippers and the object.

(ii) Two robots do not pass through singular positions, so that the Jacobian matrix always has full ranks.

(iii) Two robots have the same number of degrees of freedom.

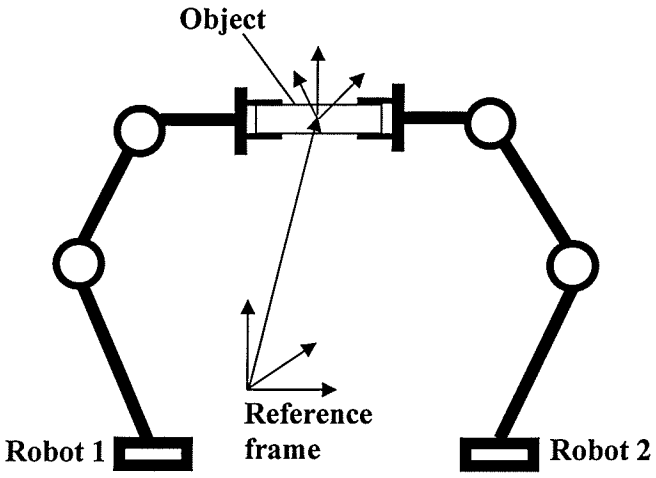


**Figure 3-8 Robots handling a common object.**

Assumption (i) is required to model the object and the grippers as a rigid body. Hence, slipping between the object and grippers is not considered [1, 15, 21].

### 3.5.2.2 Manipulability Ellipsoid of Magnum Dual Arms

Next, the equation of the dual arms manipulability ellipsoid is developed. Let $\dot{x}_1$ and $\dot{x}_2$ denote the end-effector velocities of the robots and, respectively:

$$\dot{x}_1 = J_1(q_1)\dot{q}_1$$
$$\dot{x}_2 = J_2(q_2)\dot{q}_2 . \qquad (3.64)$$

Since the object is held rigidly by the end-effectors and $\dot{x}_2$ and $\dot{x}_2$ are in fact the same as the velocity of the object reference point, the constraint below is obtained [1, 15].

$$\dot{x}_1 = \dot{x}_2 . \tag{3.65}$$

Using this constraint, the expression for the dual arms manipulability ellipsoid is developed as follows.

$$v = [\dot{x}_1^T \dot{x}_2^T]^T \ , \ q = [\dot{q}_1^T \dot{q}_2^T]^T \quad and \quad J = diag\{J_1, J_2\} \ .$$

Then,

$$v = J\dot{q} . \tag{3.66}$$

The unit sphere in $R^{2n}$ and described by $\|q\|^2 = 1$ can be transformed into $R^{2m}$ through $J$ as follows.

$$\begin{aligned} \|\dot{q}\|^2 &= \dot{q}^T \dot{q} \\ &= v^T (J^+)^T J^+ v \\ &= v^T (JJ^T)^+ v \\ &= [\dot{x}_1^T \dot{x}_2^T] diag\{(J_1 J_1^T)^{-1}, (J_2 J_2^T)^{-1}\} [\dot{x}_1^T \dot{x}_2^T]^T \\ &= 1 . \end{aligned} \tag{3.67}$$

Since the end velocities of the two arms must be equal as expressed in (3.65). Equation (3.67) can be rewritten as below.

$$\dot{x}^T [(J_1 J_1^T)^{-1} + (J_2 J_2^T)^{-1}] \dot{x} = 1 . \tag{3.68}$$

# 4 Case studies and Results

## 4.1 Kinematic Simulations

Kinematic simulations are done for monitoring arms movement and testing other functions in the simulator. Movement of arm links can be commanded directly by giving target joint angle values or changing the position of end-effectors. This simulator is for training a robot operator. First of all, graphic user interface (GUI) was focused on the user friendly. Figure 4-1 shows the graphic user interface of the Magnum subsea dual arms simulator.

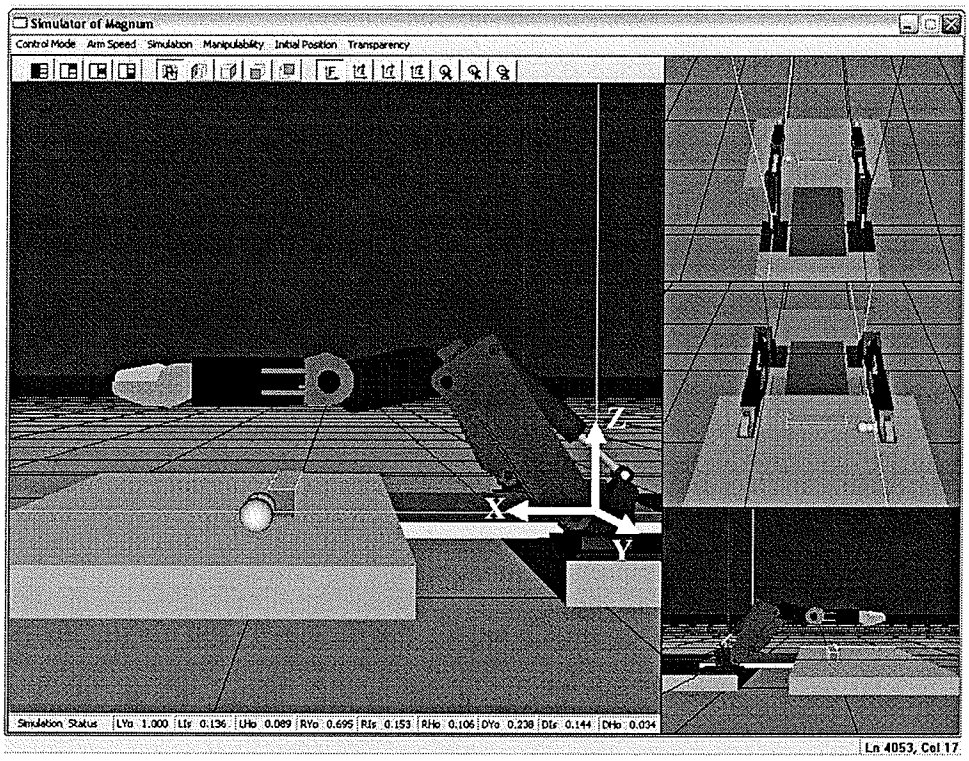


**Figure 4-1 Snapshot of GUI of Magnum simulator.**

As shown in Figure 4-1, the GUI has 4 windows that help an operator observe the movement of robot arms easily. Each window's view port can be controlled by using the following icon

bar menu. A user can control the view port by using the icon menu bar so it is possible to make the expected working viewpoint. Figure 4-2 shows the changed viewpoint.

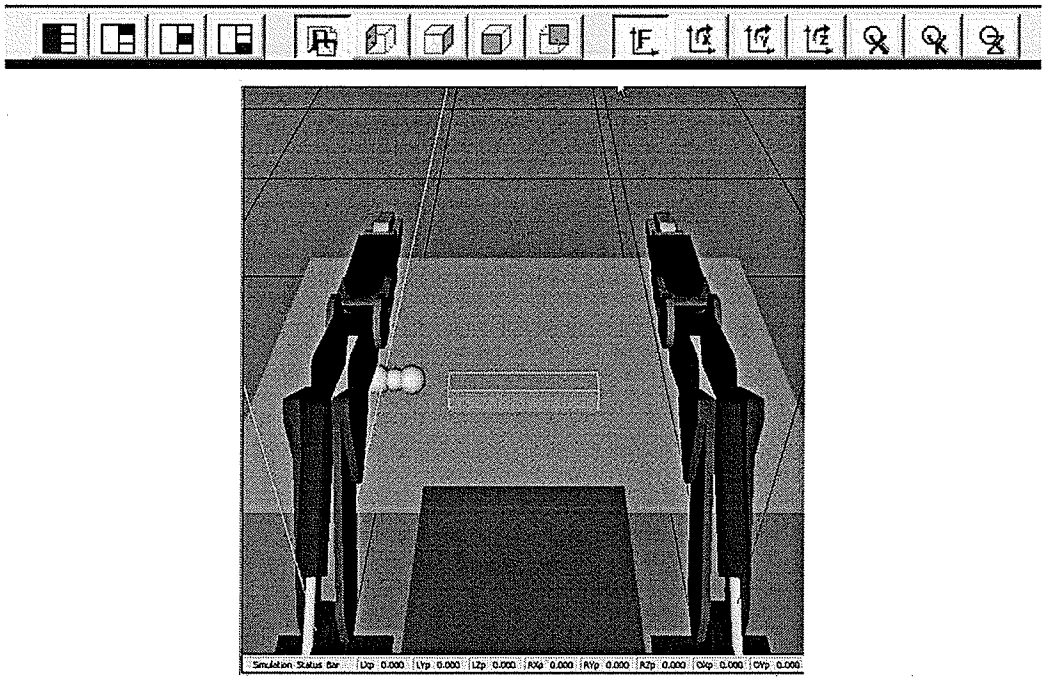

**Figure 4-2 Icon bar menu and snapshot of Magnum simulator from a different viewpoint.**

There are several dropdown menu bars. First of all, the control mode bar is for choosing the type of movement of robot arms according to kinematics simulation. Arm speed can be controlled by using the Arm Speed dropdown menu bar. The Initial Position menu bar is to reset the position of objects and robot arms. When an operator is done the task, the operator can try again the task without rebooting the application.

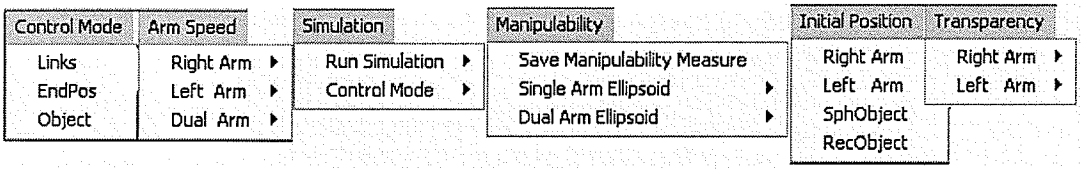


**Figure 4-3 Dropdown menu bars.**

As shown in Figure 4-4, the color of the object was changed when the robot arm contacted

the object. The purpose of the color change is to help the operator know whether the robot arms are contacting with the object or not. The color black(a) means a robot arm was grabbing the object and the object was still on a surface. Light blue(b) means one robot arm was holding the object without contacting with a surface. When an operator is controlling both arms to grab an object, the operator should know whether the robot arms are contacting the object or not through sound or tension on the master in the real world. This simulator doesn't provide sound, so the changing color of the object is employed. When an arm was holding the object, and the other arm was contacting to the object later, the color was changed from light blue(b) to red(c). According to indicating color, the operator could stop the other arm or move it to the better position to grab the object.

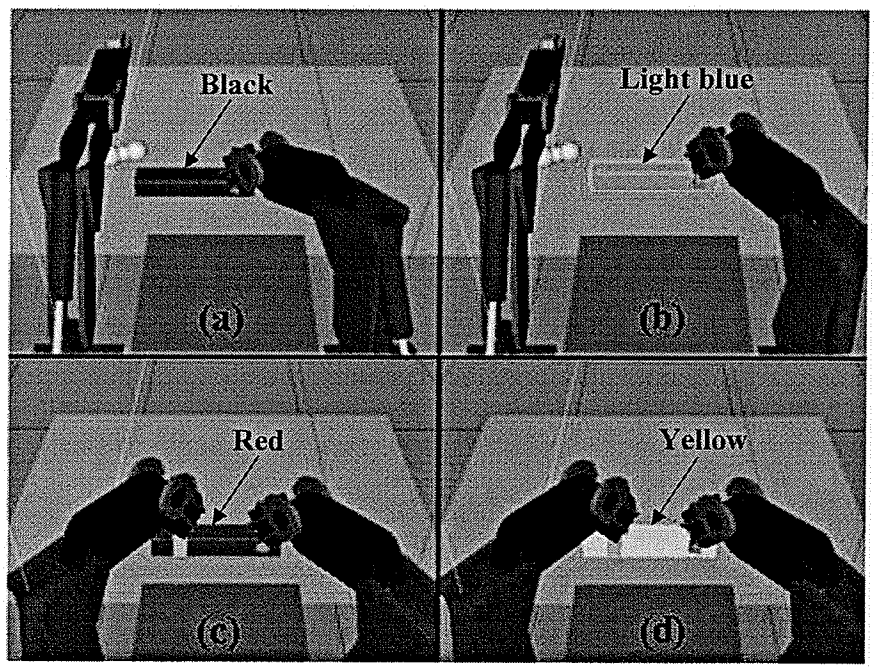


**Figure 4-4 Snapshots of two Magnum arms are lifting an object and cooperatively handling it: (a)the right arm grabbing an object;(b)the right arm lifting an object;(c)the right arm grabbing an object and the left arm contacting with it;(d)both arms grabbing an object and lifting it.**

Finally, the color was changed to yellow(d). It means that both arms were holding the object. Collision and detection algorithm was used to grab and to carry the object in this simulator.

## 4.2 Dynamic Simulations

The dynamic model is obtained from the kinematics model by adding dynamics properties to the robot model such as mass, inertia moments, and by extending the virtual environment. When the robot arms are being simulated, dynamics data of both arms, like contact forces and joints torque, are saved to files for post processing and analysis. This simulator uses an integration step size of 0.001second for the following studies and updates the graphical display every 0.017second (60 fps) of simulated time. When running on 3.2 GHz Pentium 4 under Windows XP, the simulation updates all joints at a real time speed.

### 4.2.1 Case study 1

The purpose of this study is to show that the simulation is working properly when a single arm is moving without object in the end-effector. In the case of this study, the each joint of the left arm was moved by an individual signal. Figure 4-5 shows time chart for test.

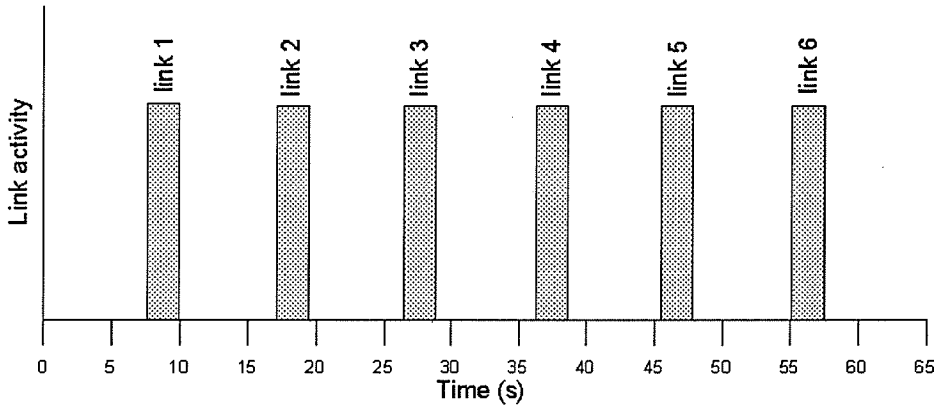


**Figure 4-5 Time chart for test in Case study 1.**

Each link, from link 1 to link 6, tested as shown in the above time chart. Based on the saved data, the following results are shown about link 1, link 2, and link 5. First, the angle of the link will be shown. Line pressures will be followed. Figure 4-6 shows the angle of link 1 when a control signal was input by using a joystick. According to the signal, the line pressures of link 1 were changed. The signal was not given, in Figure 4-7, the arm was stopped and continued to vibrate slightly because of arm's inertia. It means that piston 1 was working based on actuator dynamics suggested in this thesis. As shown in Figure 4-7, 4-9,

and 4-11, the value range of $P_I$ and $P_O$ is between 0 $kPa$ and 6,890 $kPa$. It is reasonable value because the input pressure value is 6,890 $kPa$ in this simulator. Also, the shape of graph is proper.

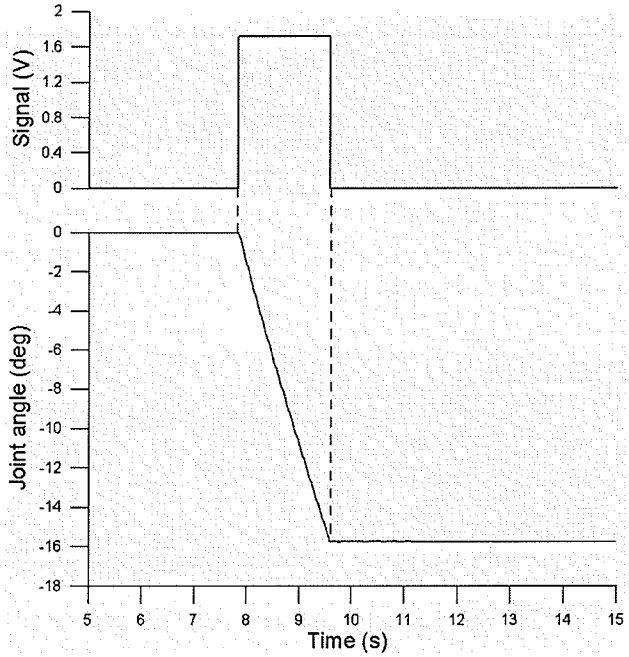


**Figure 4-6 Input signal and joint rotation of link 1.**

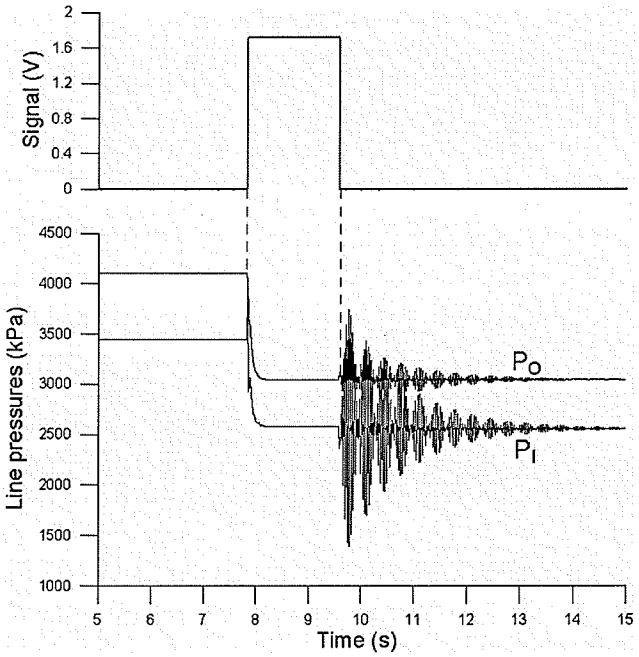


**Figure 4-7 Input signal and line pressures of link 1 actuator.**

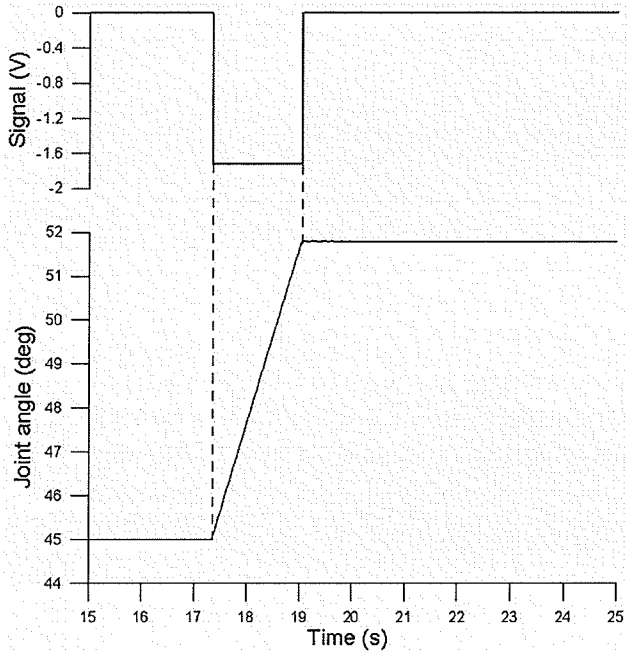


**Figure 4-8 Input signal and joint rotation of link 2.**

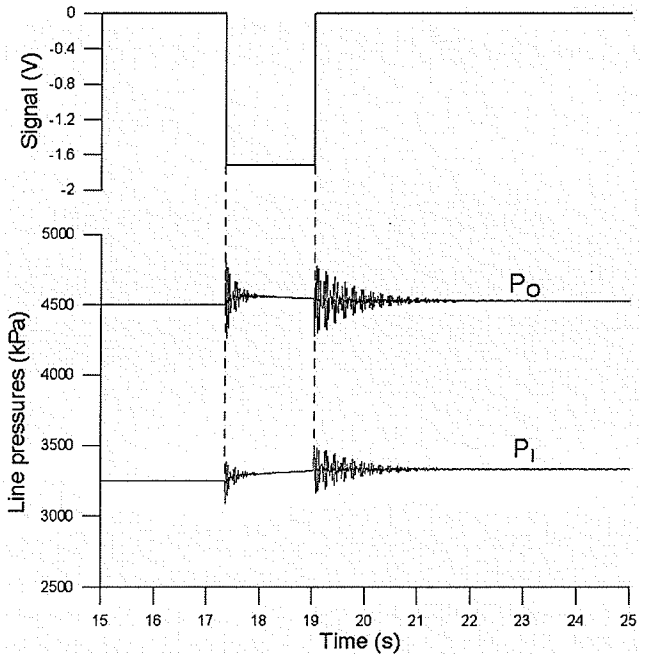


**Figure 4-9 Input signal and line pressures of link 2 actuator.**

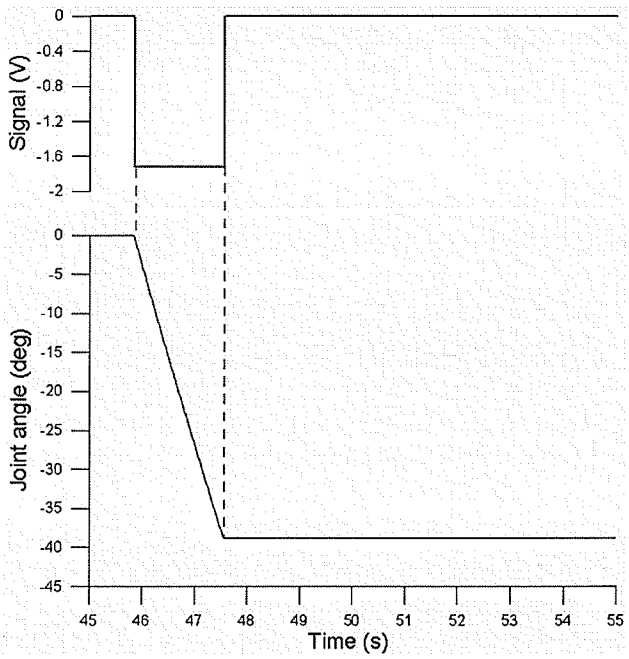


**Figure 4-10 Input signal and joint rotation of link 5.**

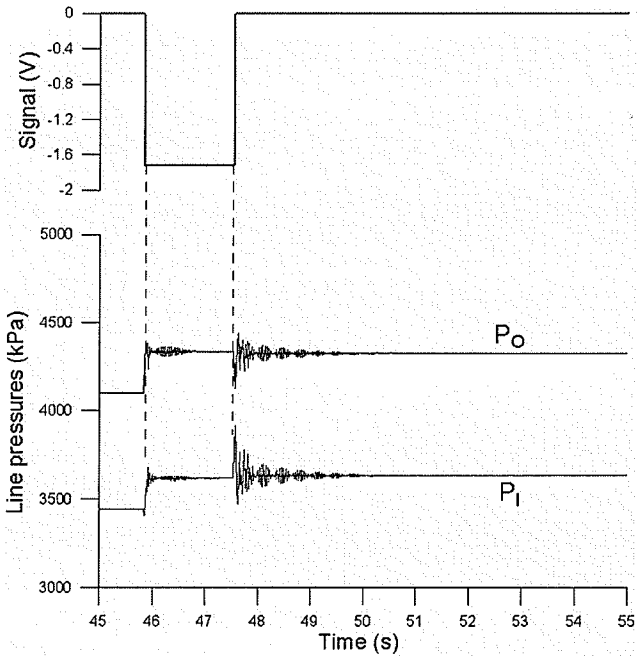


**Figure 4-11 Input signal and line pressures of link 5 actuator.**

### 4.2.2 Case study 2

The purpose of this study is to show that the simulation results are reasonable when a single arm was loaded. First, the left arm was located at the initial position, and it was moved to grab an object which is 50 kg. Second, the arm grabbed the object and stayed for several seconds with no signal. Third, the object was lifted vertically and stayed for several seconds. Finally, the arm dropped the object and stayed for several seconds with no signal also. Figure 4-12 shows the time chart for this test.

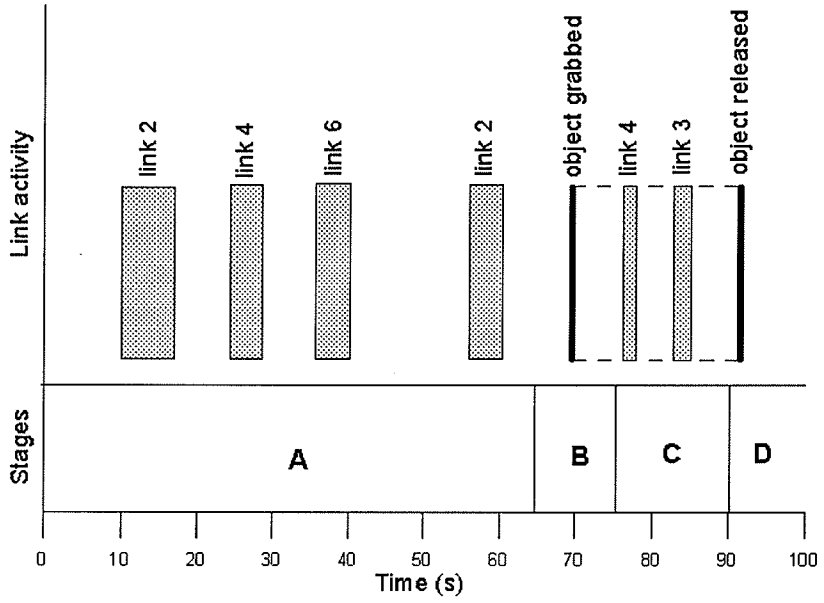


**Figure 4-12 Time chart for test in Case study 2: (A)Links were activated to grab an object;(B)The object were grabbed;(C)Links were activated to carry the object;(D)The object was released.**

Figure 4-13 and 14 shows results in stage A which was defined in Figure 4-12. As shown in Figure 4-13, three signals were used to move the end-effector to reach to an object. Each link was rotated by its own signal. Figure 4-14 shows the line pressure of link 2. Signal 2 changed the line pressures although vibration was occurred when signal 4 was given.

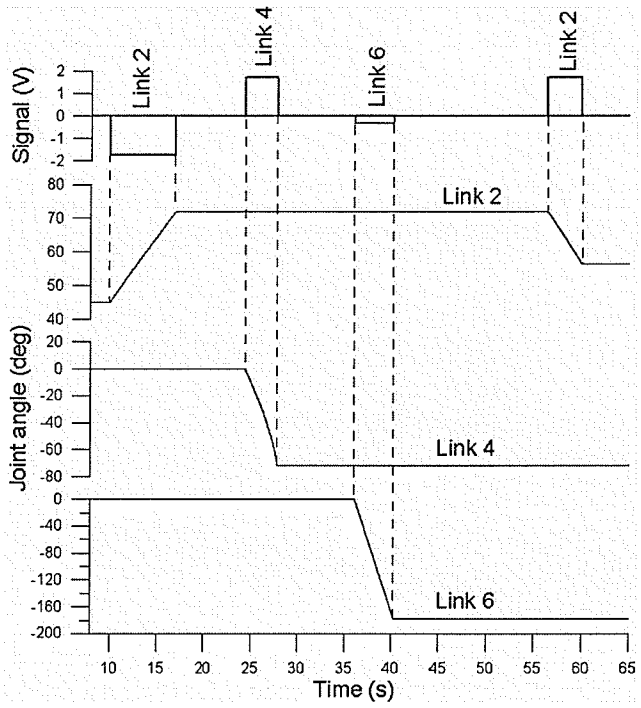


**Figure 4-13 Input signal and joint rotation of link 2, 4, and 6 (Stage A).**

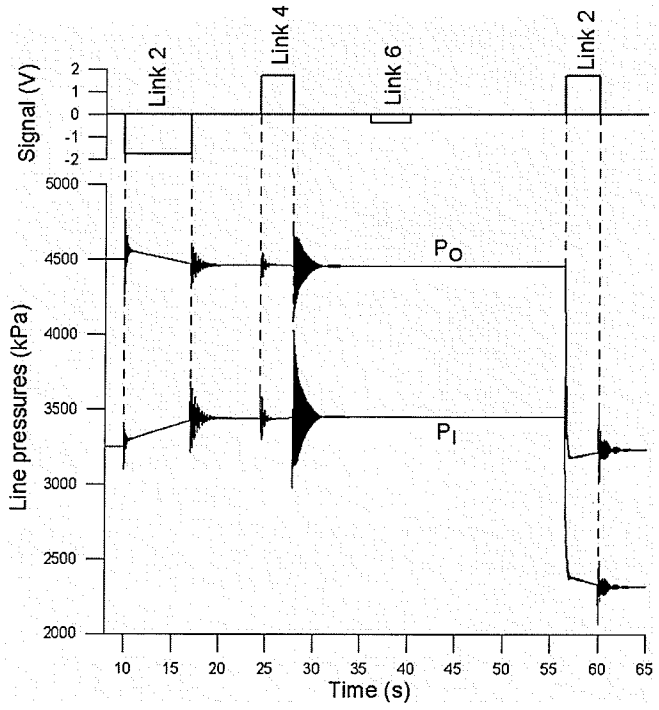


**Figure 4-14 Input signal and line pressures of link 2 actuator (Stage A).**

Figure 4-15 shows the changing of the line pressures when the arm grabbed an object in stage B of Case study 2. It means that the arm's weight was changed. The line pressures of cylinders were changed to keep the posture of arm when the arm was loaded.

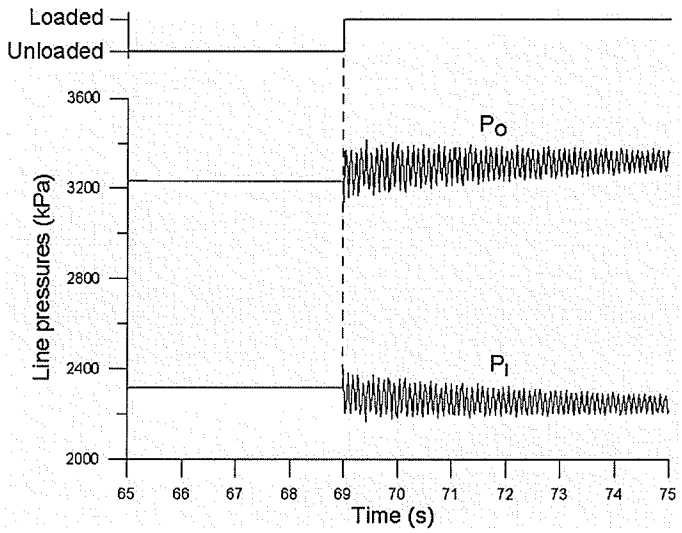


**Figure 4-15 Line pressures of link 2 actuator (Stage B).**

The line pressures of cylinders were also changed when the arm was unloaded in stage D of this case study. Figure 4-16 shows result.

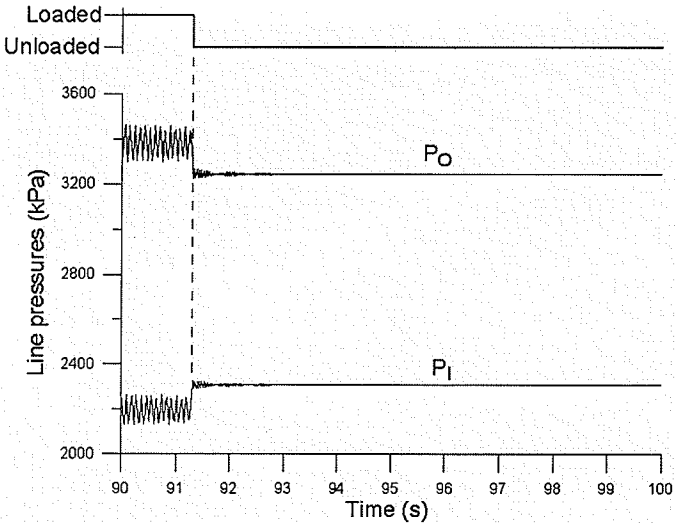


**Figure 4-16 Line pressures of link 2 actuator (Stage D).**

### 4.2.3 Case study 3

The purpose of this study is to show simulation results of dual arms when grabbing an object and carrying it with open-loop control. First, both arms were located at the initial position, and they were moved to grab an object which was 50 kg. The right arm then grabbed the object and stayed several seconds with no signal. Next, the left arm also grabbed the object and stayed several seconds. The object was then lifted vertically with open-loop control. An attempt was then made to move the object to left with open-loop control. Finally, the arms dropped the object. Figure 4-17 shows time chart for test.

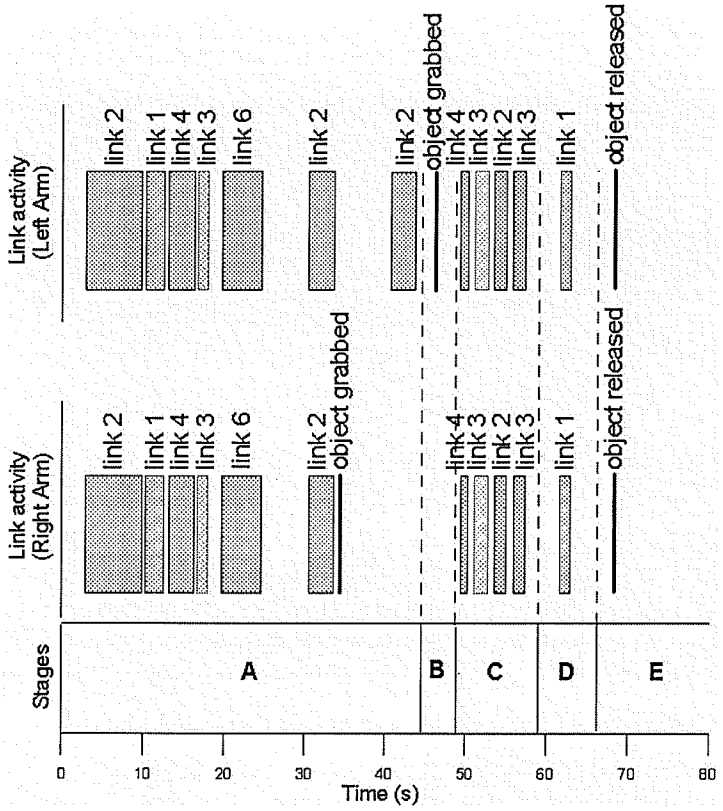


**Figure 4-17 Time chart for test in Case study 3: (A)Links were activated to grab an object and the right arm grabbed it;(B)The left arm grabbed the object also;(C)Links were activated to carry the object vertically;(D)Links were activated to carry the object to the left;(E)The object was released.**

Figure 4-18 to 4-19 show results of stage B in Case study 3. These figures show that $P_I$ and $P_o$ of cylinders were not much changed when the left arm grabbed an object comparison to stage B and D of Case study 2 (see Figure 4-15 and 4-16). The reason why the values of $P_I$

and $P_o$ had not changed significantly was related to control mode. Open-loop control was employed for this case study. While the right arm was holding the object the left arm grabbed it later. This means that both arms were not sharing the object equally in open-loop control.

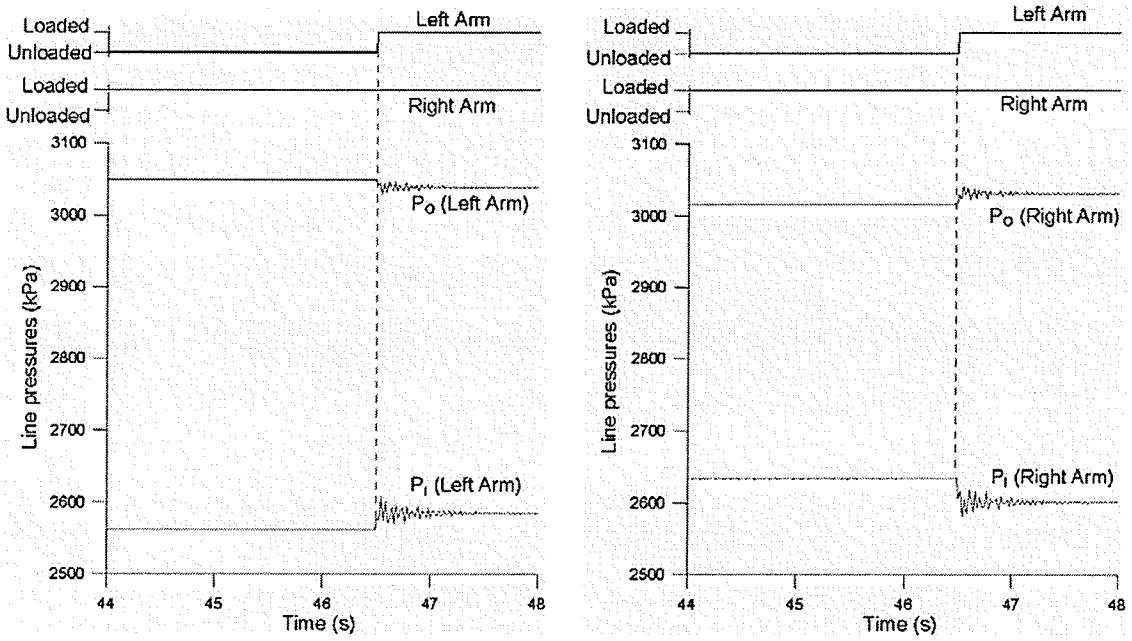


**Figure 4-18 Line pressures of link 1 actuator (Stage B).**

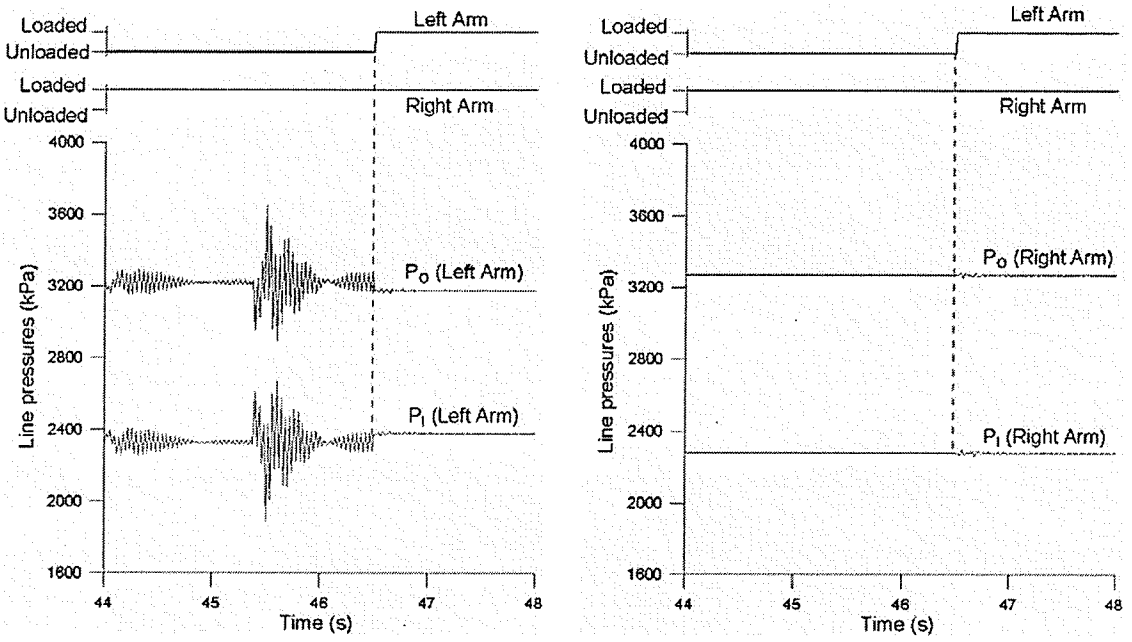


**Figure 4-19 Line pressures of link 2 actuator (Stage B).**

In stage C of Case study 3, dual arms lifted an object with open-loop control. As shown in Figure 4-20, the object was lifted in Z direction of the reference frame and stopped even though signal 3 of both arms was given. This implies that the line pressures of the cylinder 3 were already at maximum input pressures (pump pressures). Each cylinder's line pressures can be influenced by other link's movement. As shown in Figure 4-20, the line pressures of cylinder 2 were influenced by rotating of link 3 and 4.

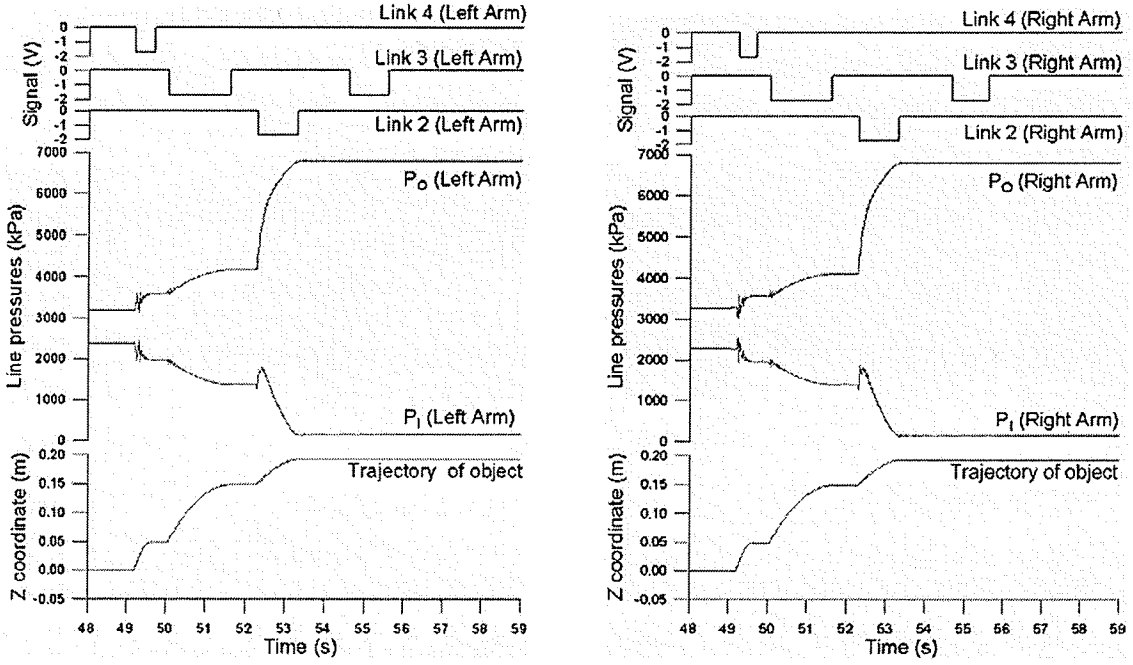


**Figure 4-20 Line pressures of link 2 actuator (Stage C).**

The object was moved with open-loop control and the results are showed up in the following figures. As shown in Figure 4-21, line pressure value of cylinder 4 of both arms was reached to 12,000 $kPa$. It never happens in the real Magnum manipulator because there are relief valves to avoid over line pressures. However, this simulator did not employ the relief valves. This means that the links can be overloaded when both arms are being cooperated through open-loop control. According to (2.67a) and (2.67b), if the line pressures reach maximum value, but the cylinder is still moving, $P_I$ and $P_o$ satisfy the following.

$$P_I = -C_I A_I \dot{x} < 0$$

$$P_O = C_O A_O \dot{x} > 0 \qquad (if \;\; Q_I = Q_O = 0)$$

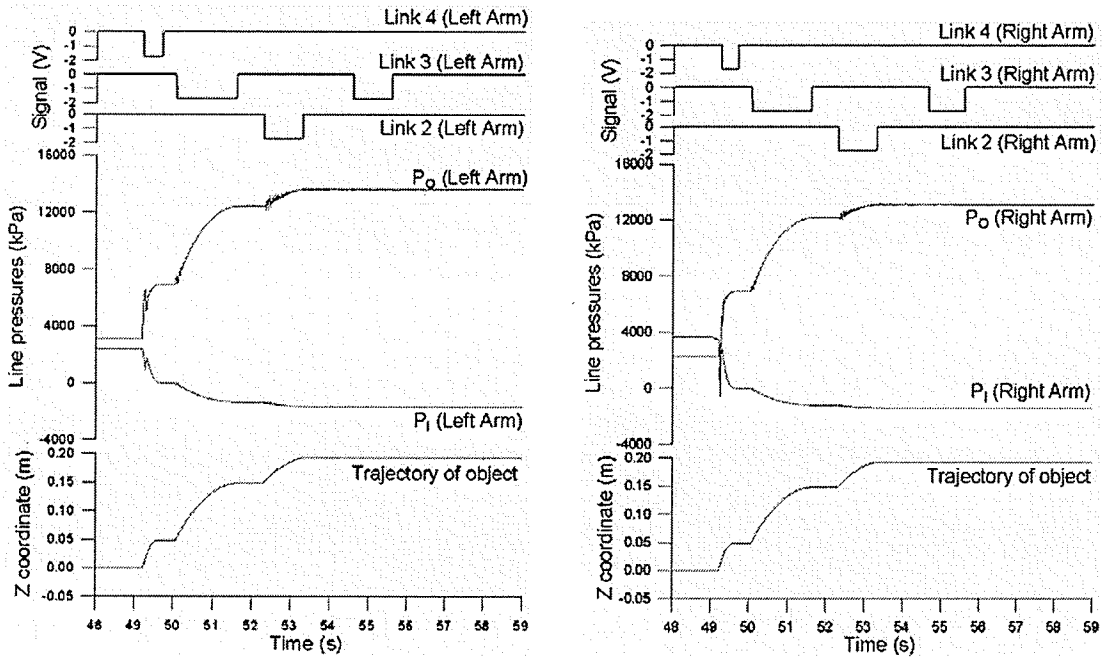


**Figure 4-21 Line pressures of link 4 actuator (Stage C).**

The object was influenced by the overload. Figure 4-22 to 4-24 show contact forces and torques. The contact force and torque were too big. This implies that the object also was under overload.

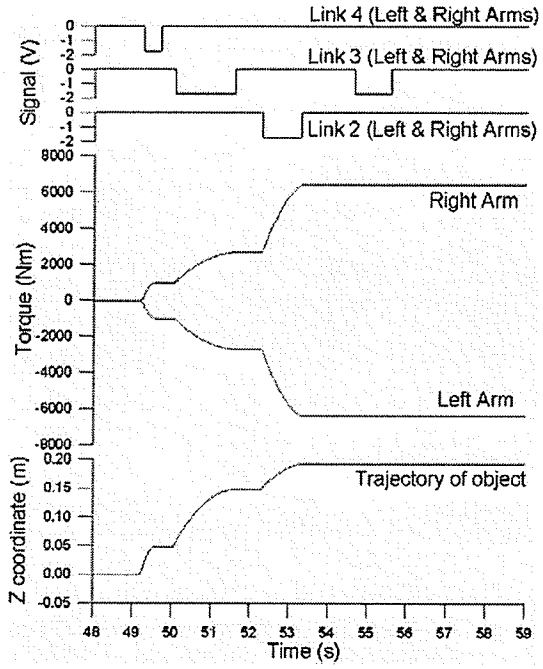


**Figure 4-22 Contact torque in X direction and the trajectory of object in Z direction of reference frame in Figure 3-5 (Stage C).**

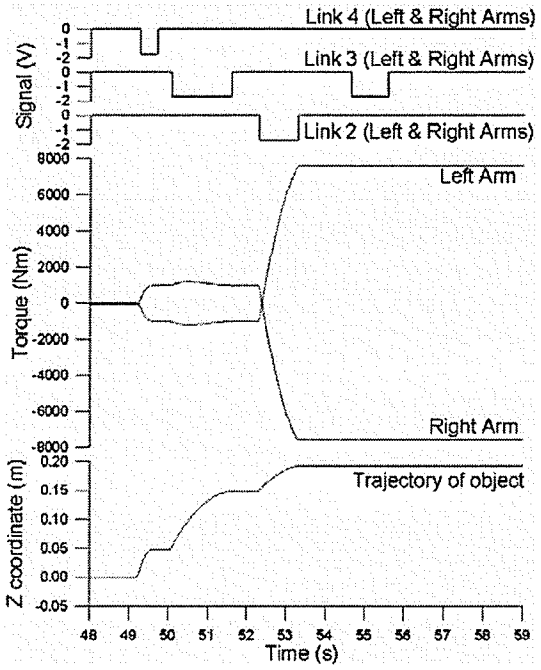


**Figure 4-23 Contact force in Y direction and the trajectory of object in Z direction of reference frame in Figure 3-5 (Stage C).**

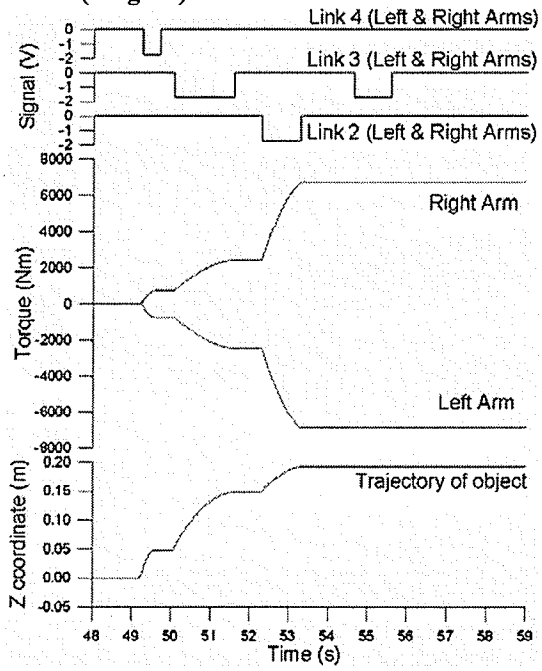


**Figure 4-24 Contact torque in Z direction and the trajectory of object in Z direction of reference frame in Figure 3-5 (Stage C).**

The object was moved in Y direction of the reference frame in stage D. As shown in Figure 4-25, the object was moved and stopped because the cylinders were already at maximum input value.

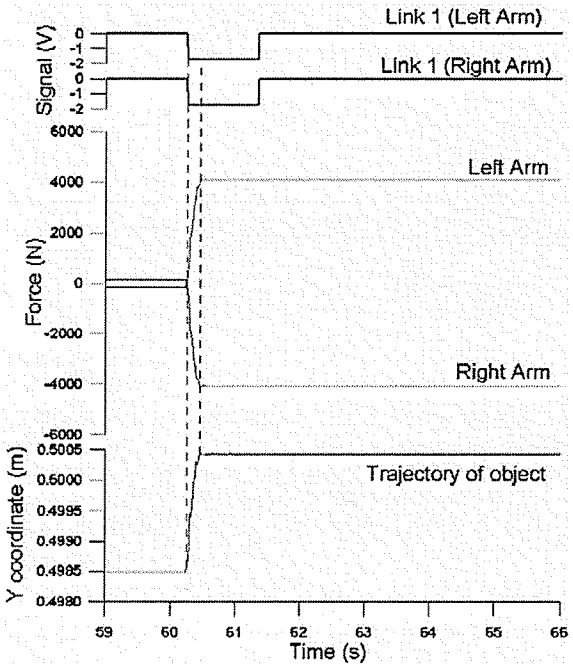


**Figure 4-25 Contact force in X direction and the trajectory of object in Y direction of reference frame in Figure 3-5 (Stage D).**

The object was translated with cooperating in stage C and D of Case study 3. Figure 4-26 shows the trajectory of object. Figure 4-27 shows internal force and torque in stage C and D. Control signals are also shown in Figure 4-28.

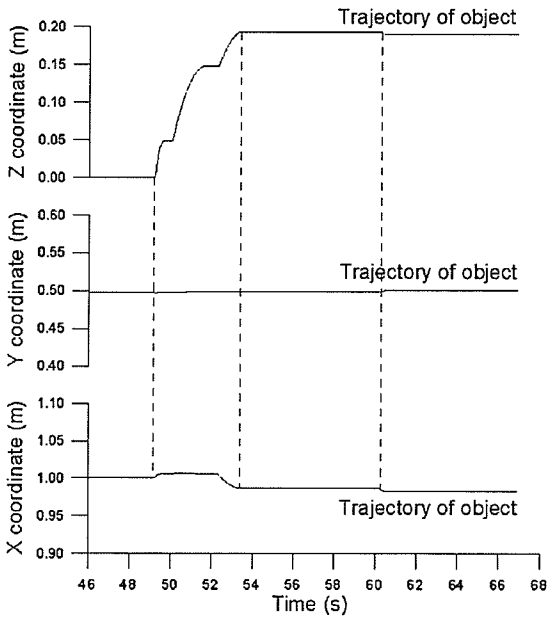


**Figure 4-26 Trajectory of object in X, Y, and Z direction of reference frame in Figure 3-5 (Stages C and D).**

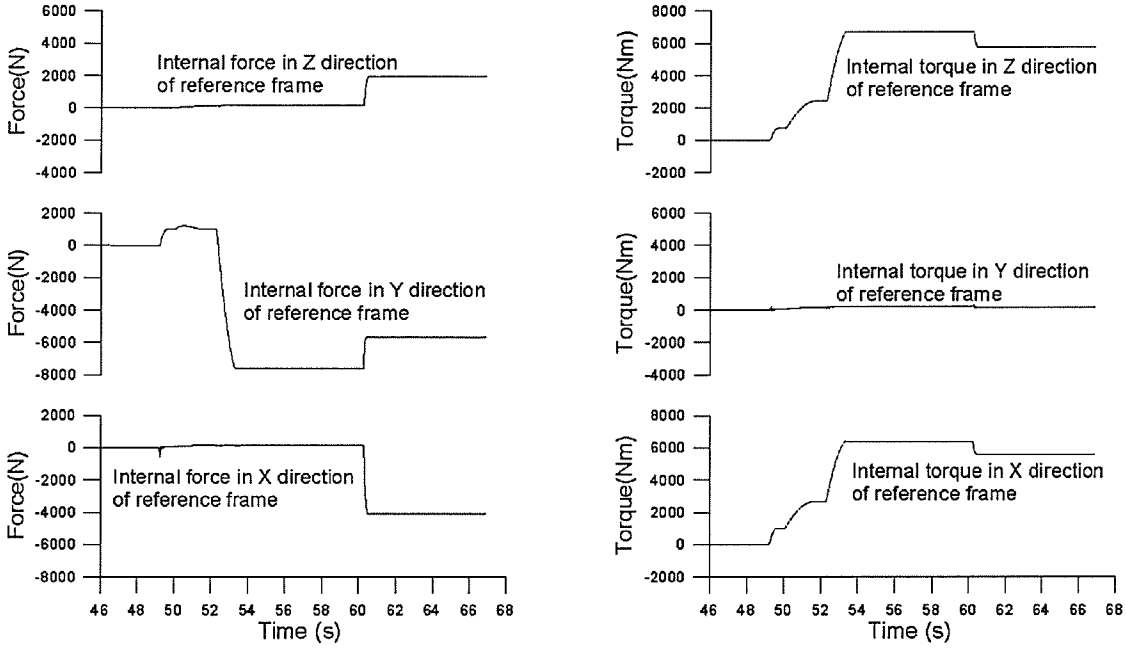


**Figure 4-27 Internal force and torque (Stages C and D).**

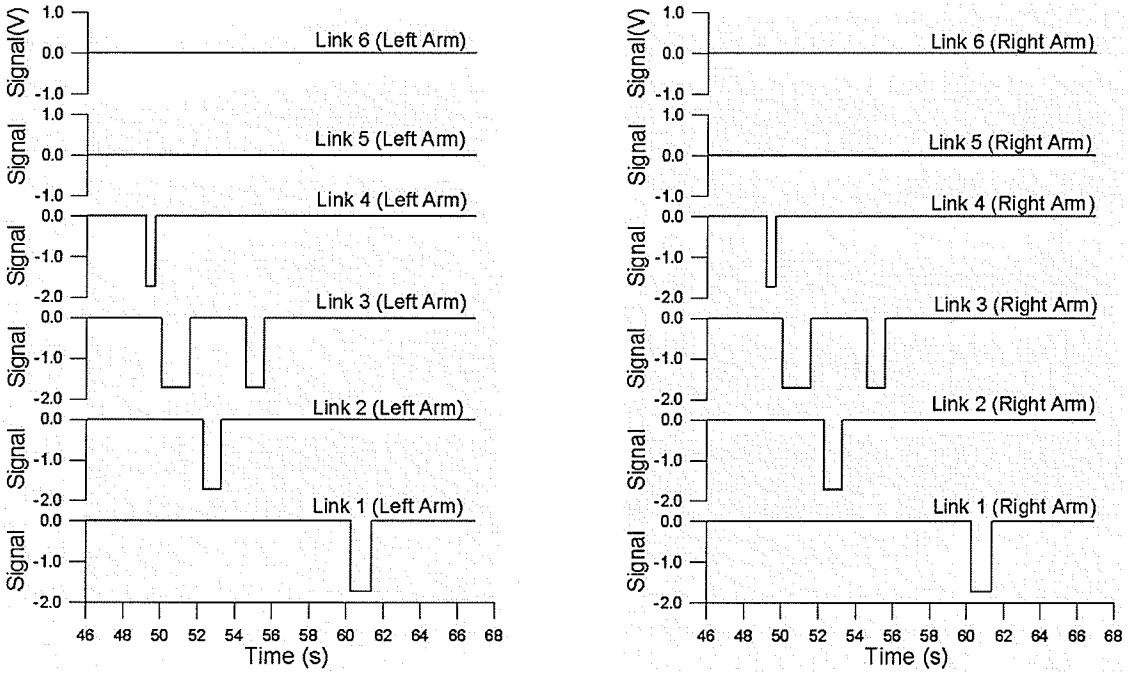


**Figure 4-28 Control signals (Stages C and D).**

### 4.2.4 Case study 4

The purpose of this study is to compare open-loop control and closed-loop control. Based on the following steps, performance was tested and results will be shown. First, both arms were located at the initial position, and they were moved to grab an object which is 50 kg. The right arm grabbed the object and stayed several seconds with no signal. Second, the left arm also grabbed the object and stayed for several seconds while the control mode was changed from open-loop control to closed-loop control. Third, the object was lifted vertically with closed-loop control. Fourth, an attempt was made to move the object to the left with closed-loop control. Finally, the arms dropped the object and stayed several seconds with no signal. Figure 4-29 shows time chart for test.

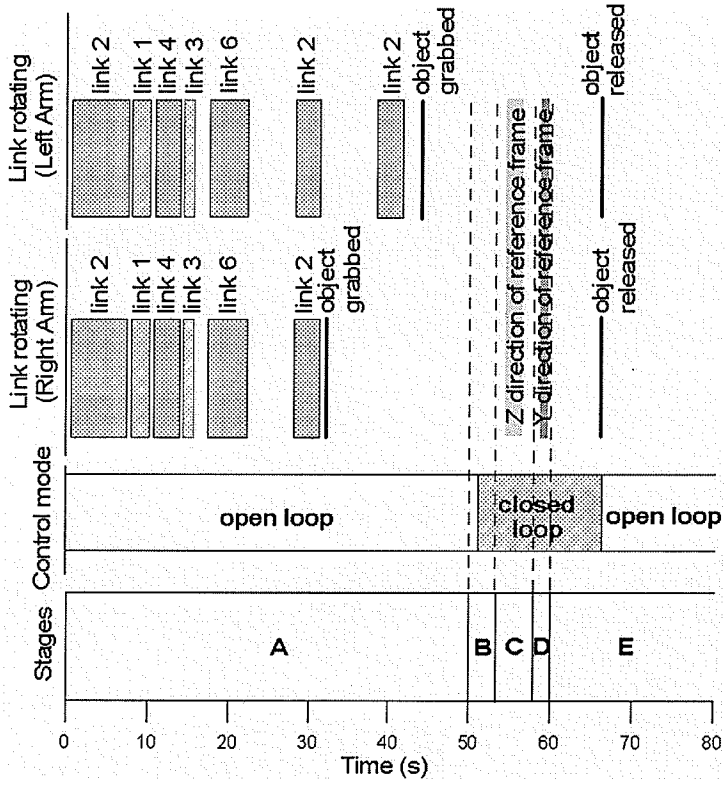


**Figure 4-29 Time chart for test in Case study 4: (A)Links were activated to grab an object and the right arm grabbed it. The left arm grabbed the object later;(B)The control method was changed from open-loop to closed-loop;(C)The object was translated in Z direction of the reference frame;(D)The object was translated in Z direction of the reference frame;(E)the object was released.**

In stage B of this case study, when the control mode was changed from open-loop control to closed-loop control, the object was then shared by both arms. Results were different in comparing stage B of Case study 3 (see Figure 4-18 and 4-19). As shown in Figure 4-30 and 4-31, the line pressures value of cylinders became similar, yet it was not exactly same, because the posture of each arm varied slightly.

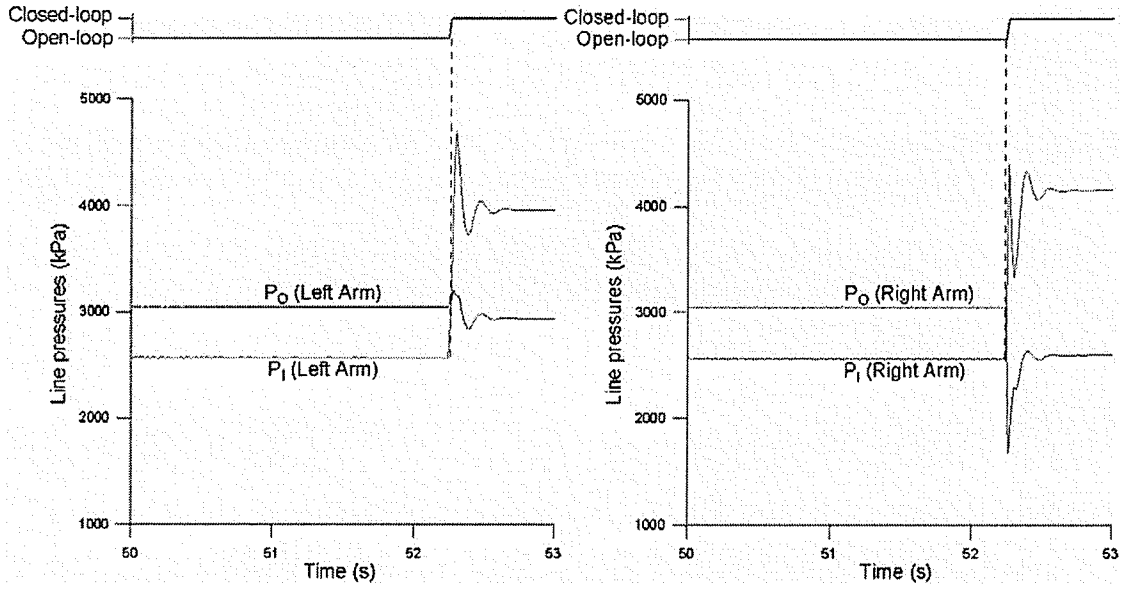


**Figure 4-30 Line pressures of link 1 actuator (Stage B)**

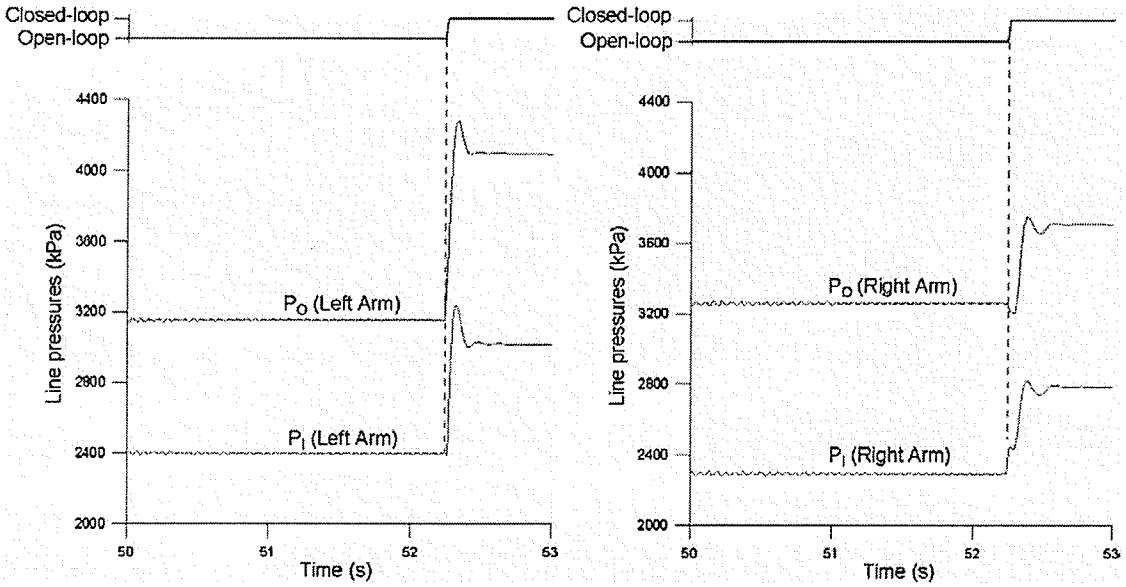


**Figure 4-31 Line pressures of link 2 actuator (Stage B)**

As the results of Case study 3, it was difficult to move the object by cooperating arms with open-loop control. Over-loading occurred to the robot arms as well. Figure 4-32 and 4-33 show the results of stage C of Case study 4. The figures show that closed-loop control did not occur with over-loading to both arms during the process of cooperating arms.

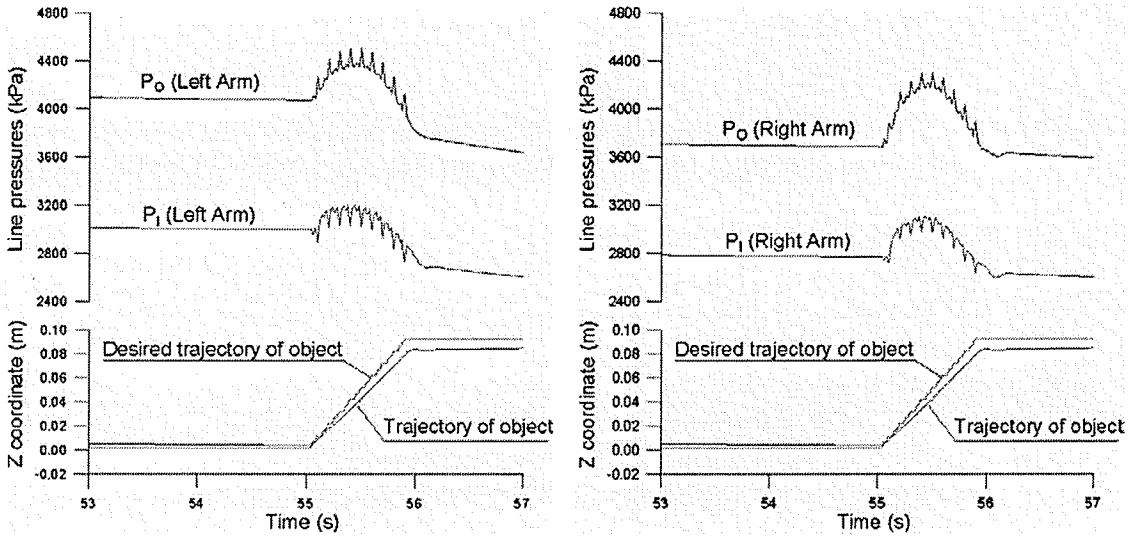


**Figure 4-32 Line pressures of link 2 actuator (Stage C)**

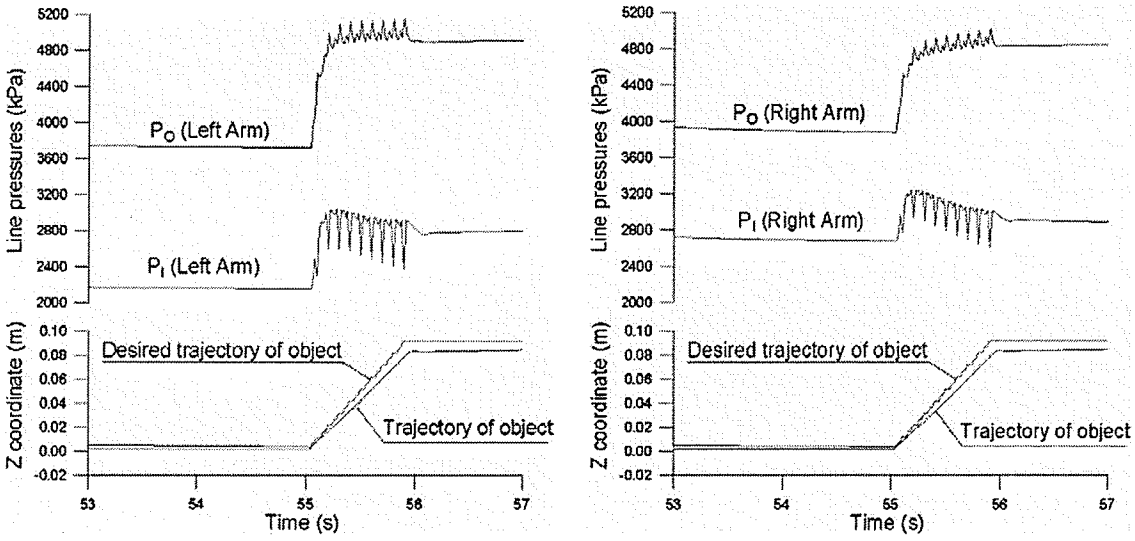


**Figure 4-33 Line pressures of link 4 actuator (Stage C)**

Contact force and torque were also in the normal value range in stage C and D of Case study 4. Results are shown in Figure 4-34 to 4-37.

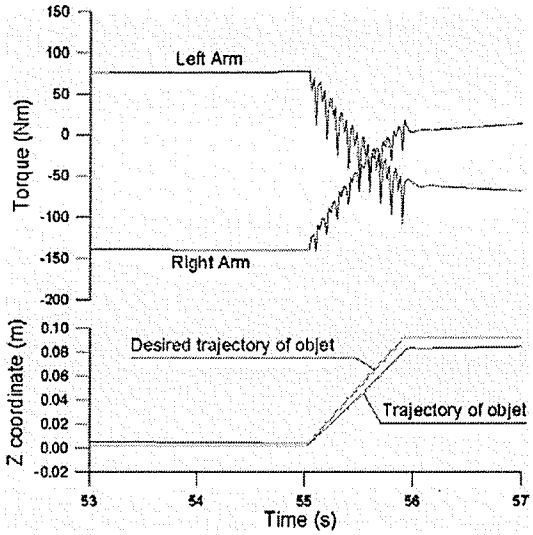


**Figure 4-34 Contact torque in X direction and the trajectory of object in Z direction of reference frame in Figure 3-5 (Stage C).**

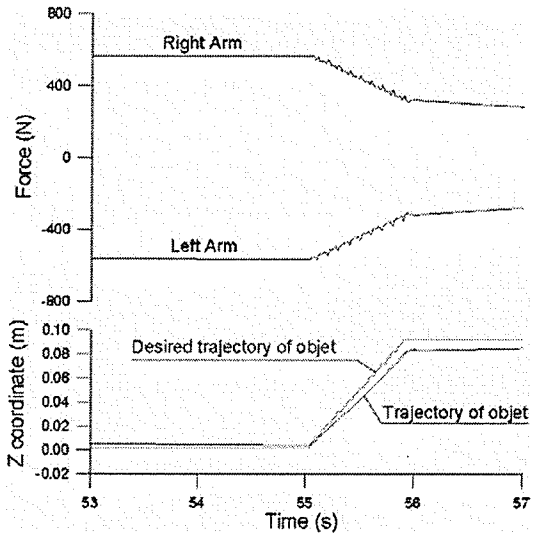


**Figure 4-35 Contact force in Y direction and the trajectory of object in Z direction of reference frame in Figure 3-5 (Stage C).**

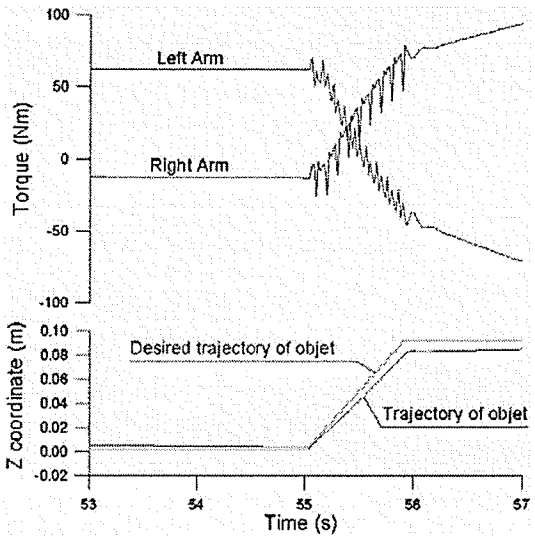


**Figure 4-36 Contact torque in Z direction and the trajectory of object in Z direction of reference frame in Figure 3-5 (Stage C).**

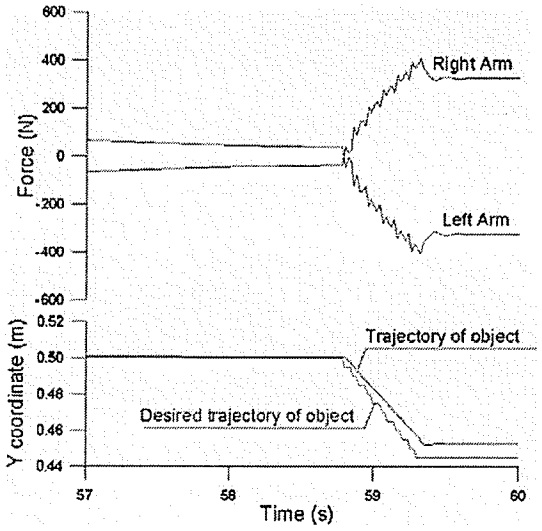


**Figure 4-37 Contact force in X direction and the trajectory of object in Y direction of reference frame in Figure 3-5 (Stage D).**

The object was translated by cooperating with closed-loop control. Figure 4-38 indicates the trajectory of object. Figure 4-39 shows internal force and torque while the arms were cooperated in closed-loop control. Control signals are also shown in Figure 4-40.

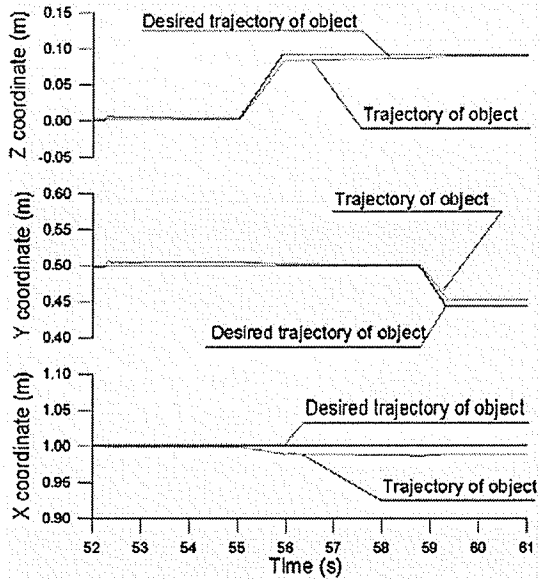


**Figure 4-38 Trajectory of object in X, Y, and Z direction of reference frame in Figure 3-5 during closed-loop control.**

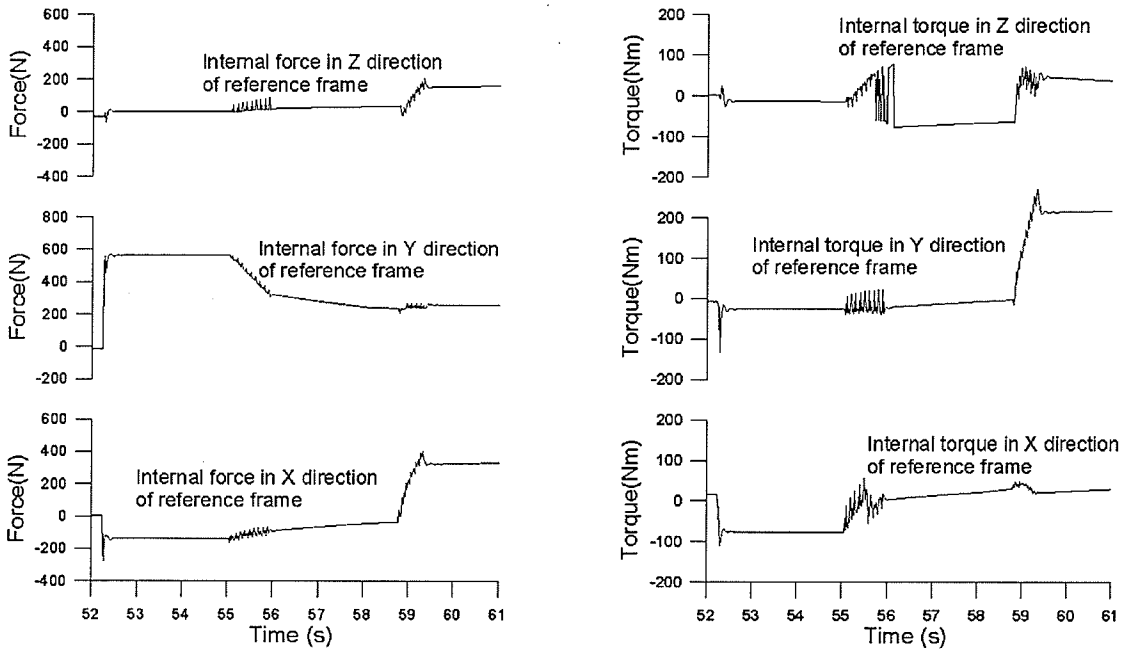


**Figure 4-39 Internal force and torque during closed-loop control.**

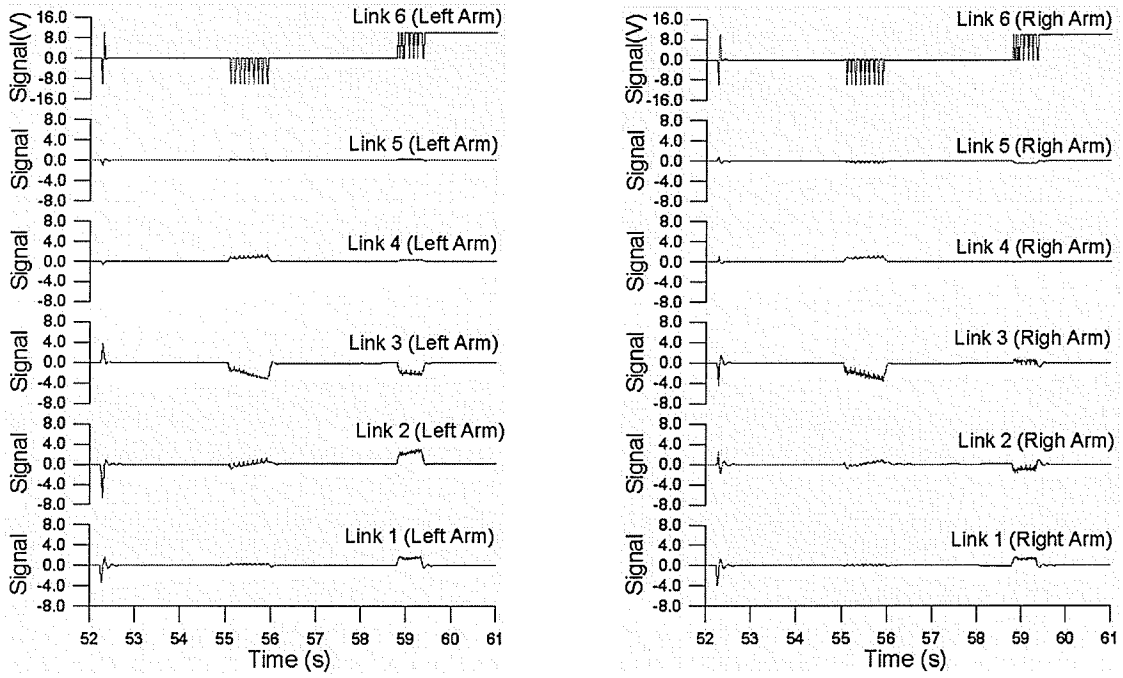


**Figure 4-40 Control signals during closed-loop control.**

## 4.2.5 Summary

Through case studies, it was proved that dynamic simulation is working properly. According to Case study 3 and 4, the following conclusions are obtained. First, it is very hard to move an object by using dual arms cooperating with open-loop control. In Case study 3, the results showed that line pressures of each cylinder were easily reached to the maximum input value (6,890kPa). The links therefore could not be moved. This could damage the robot arms or the object when the dual arms are being cooperated with open control in this simulator. According to Figure 4-27 and Figure 4-39, the internal force and torque of Case study 4 were much smaller than Case study 3. The figures of Case study 4 showed that closed-loop control did not occur over-loading of the robot arms. The second conclusion is that closed-loop control was a solution for over-loading problems even though it was not yet applied to the real Magnum subsea dual arms. Based on these case studies, this thesis shows the dynamic conditions of Magnum subsea dual arms. Through these studies, a robot operator who is being trained will understand the robot arm's performance form the view point of dynamics.

## 4.3 Manipulability Case Studies

### 4.3.1 Single Arm Manipulability Measure

This thesis analyzes the kinematics manipulability measure. In chapter 3 three manipulability indices were introduced such as Yoshikawa's Measure of manipulability, Condition Number, and Isotropy Index. Isotropy Index, Yoshikawa's method and Hong's [5] method to be introduced next were employed to measure the manipulability of Magnum subsea dual arms in this thesis.

#### 4.3.1.1 Case Study 1

The purpose of this study is to show the manipulability of a single arm when the end-effector moves to the boundary of the workspace in X direction of the reference frame. As shown in Figure 4-41, the end-effector was elevated from Z=0.0*m* to Z=0.5*m* at approximately 0.2*m* step size and without any changing to the Y coordinate. When the Z coordinates were determined, the end-effector was moved to the boundary of the workspace through the X axis. The Y and Z coordinates were not changed. Values for pitch, yaw, and roll were not changed as well.

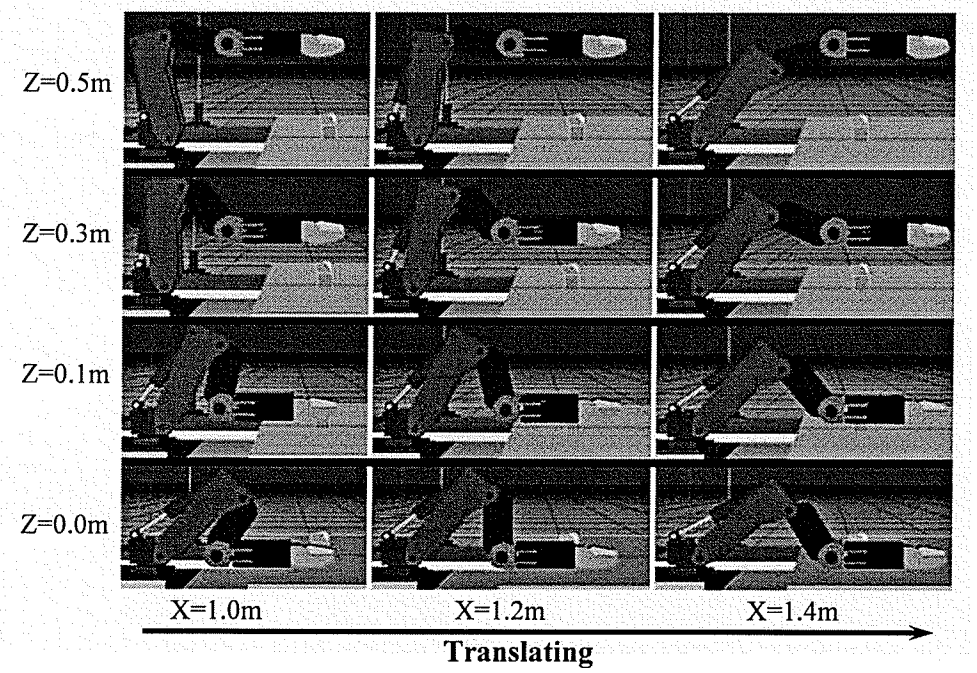


**Figure 4-41 Captured images describing Case study 1 (Single arm).**

Figure 4-42 shows translational ellipsoids captured during test for Z=0.3*m*. In Figure 4-43, when the end-effector reaches the workspace boundary, the minor axes of the ellipsoids lessen and the major axes of the ellipsoids expanded. This implies that the manipulator isotropy is decreased when the end-effector reaches the workspace boundary.

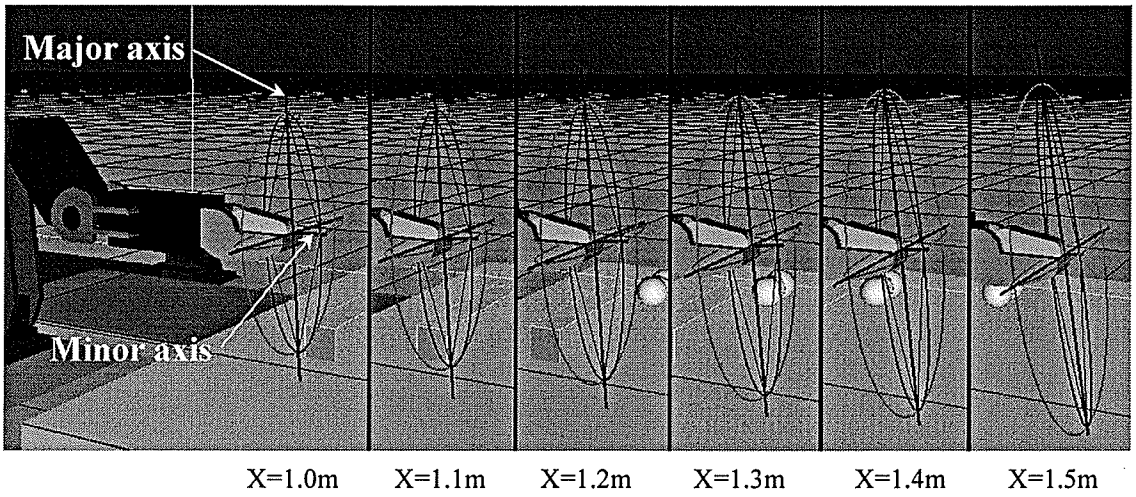


**Figure 4-42 Ellipsoids according to Case study 1 (Single arm).**

The following figures show the results of manipulability according to Case study 1. Figure 4-43 and 4-44 explain the different results, when the manipulability measure methods are different.

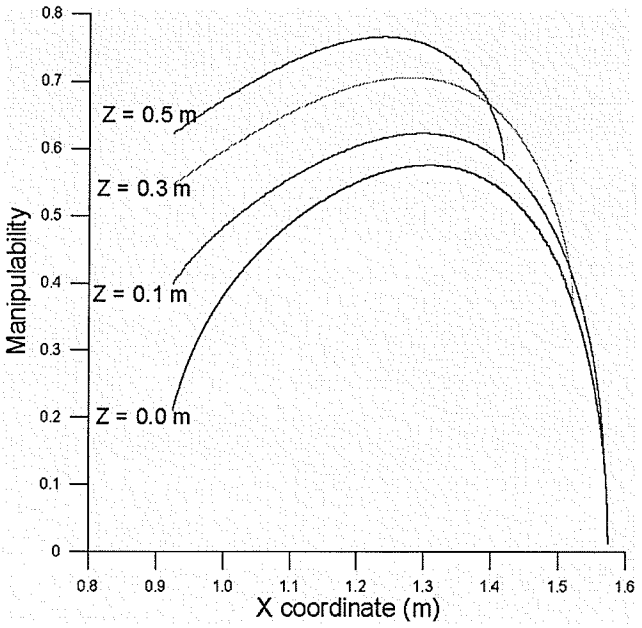


**Figure 4-43 Manipulability measure based on Yoshikawa's method (Case study 1)**

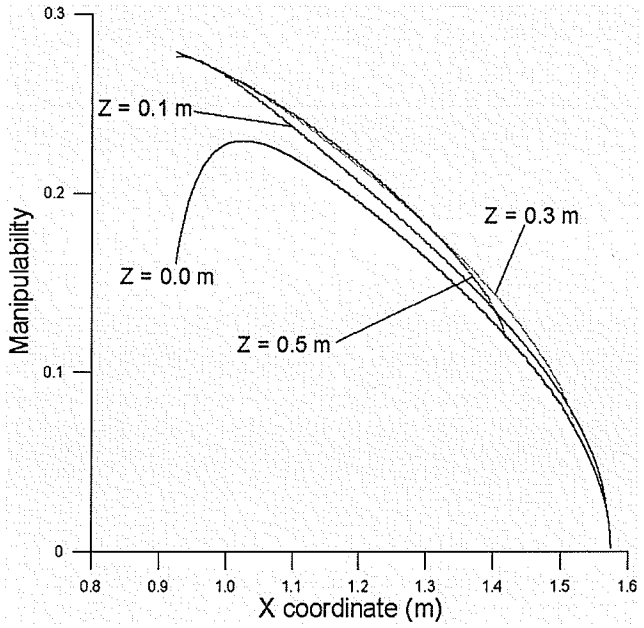


**Figure 4-44 Manipulability measure based on Isotropy Index (Case study 1)**

Yoshikawa's method defined manipulability as the volume of the manipulability ellipsoid. Larger the volume of the manipulability ellipsoid is, the greater the total output is for a given input [5, 24]. This means that the larger the ellipsoid is, the faster the end-effector can move. Isotropy Index is the ratio of the minimum and maximum radii of the ellipsoid. The closer to 1 this index implies that the manipulator's isotropy is preeminent. Therefore, it is desirable to have a high value of Isotropy Index and a large volume of ellipsoid. Hong [5] suggested a method (4.1) as followed.

$$w_n = w_1 \times w_2 \quad \left( w_1 = \sigma_1\sigma_2...\sigma_m \;,\; w_2 = \frac{\sigma_m}{\sigma_1} \right) \qquad (4.1)$$

The results are shown in Figure 4-45.

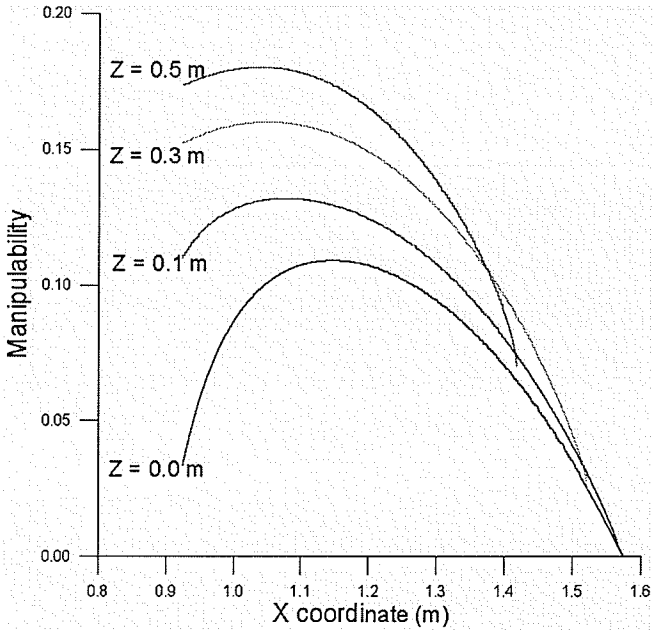


**Figure 4-45 Manipulability measure based on Hong's method (Case study 1).**

As results of Case study 1, the Magnum subsea manipulator has highest manipulability based on Yoshikawa's method at approximately 1.3*m* on the X coordinate. As the Z coordinate was increased, the manipulability increased correspondingly. Hong's method, in Figure 4-45, shows that the Magnum subsea manipulator has highest manipulability between 1.0*m* and 1.2*m* on the X coordinate it dependent on the positioning on the Z coordinates.

### 4.3.1.2 Case Study 2

The purpose of this study is to show the manipulability of a single arm when the end-effector moves to the boundary of the workspace in Z direction of the reference frame. As shown in Figure 4-46, the end-effector was moved from X=0.9*m* to X=1.4*m* at approximately 0.2*m* step size and without any changing to the Y coordinate. The X coordinates were determined, the end-effector was translated to the boundary of the workspace through the Z axis. The X and Y coordinates were not changed. Values for pitch, yaw, and roll were not changed as well.

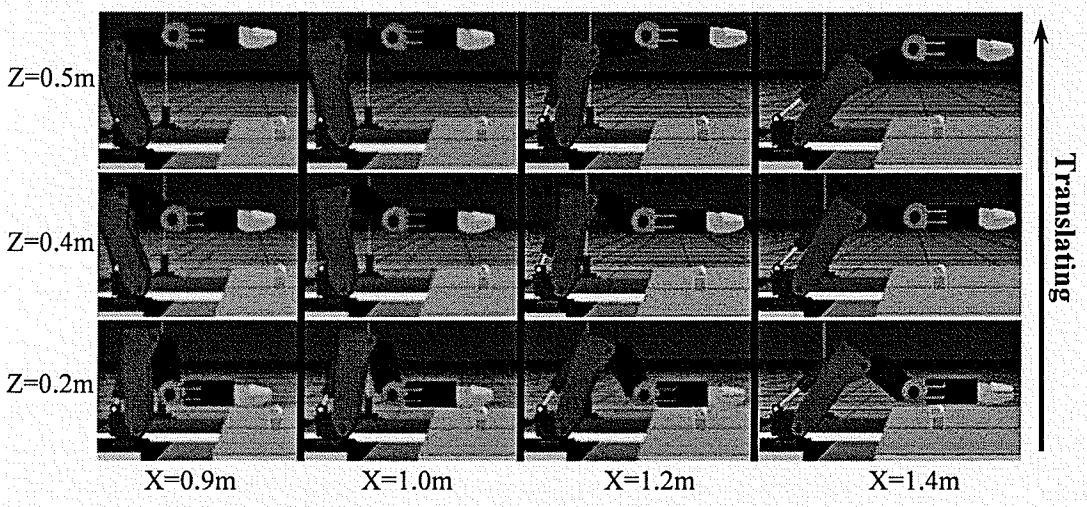


**Figure 4-46 Captured images describing Case study 2 (Single arm).**

Figure 4-47 shows translational ellipsoids captured during test for X=1.2*m*. In Figure 4-47, when the end-effector was elevated, the minor and the major axes of the ellipsoids did not much lessen and expanded comparison to Case study 1. This implies that the Magnum subsea manipulator isotropy is not much changed when the end-effector is elevated through Z axis (see Figure 4-49).

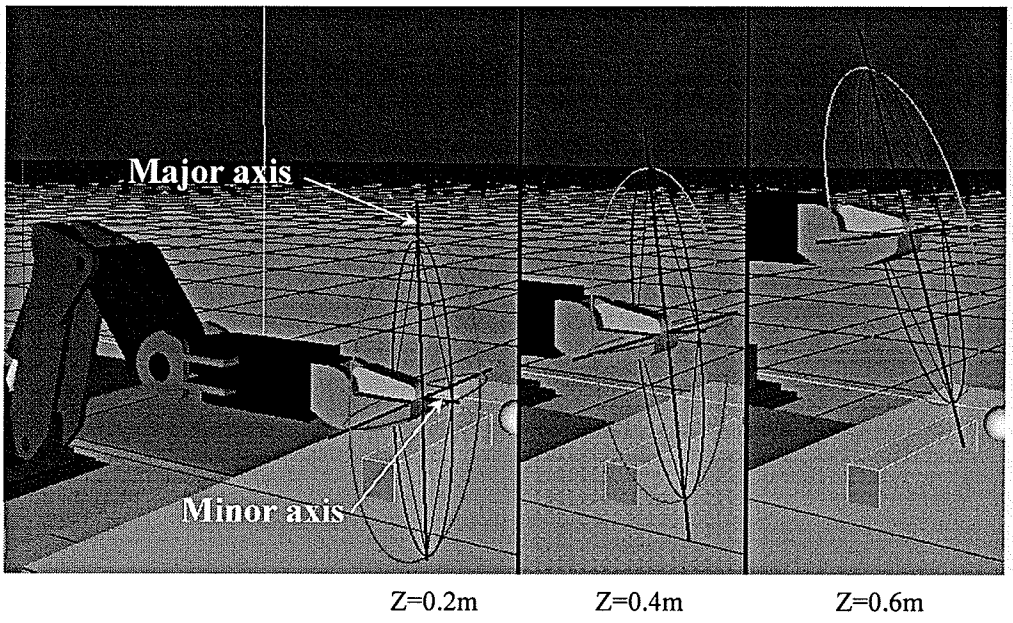


**Figure 4-47 Ellipsoids according to Case study 2 (Single arm).**

The following figures, Figure 4-48, 4-49, and 4-50, show results of manipulability according to Case study 2.

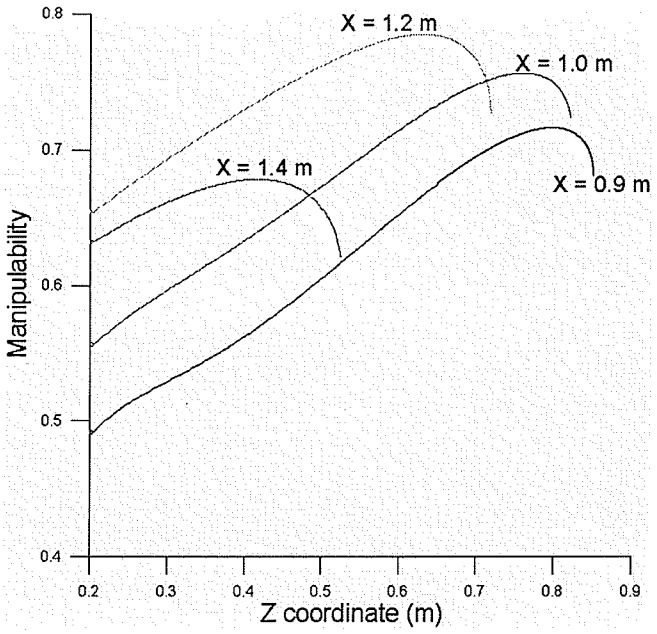


**Figure 4-48 Manipulability measure based on Yoshikawa's method (Case study 2).**

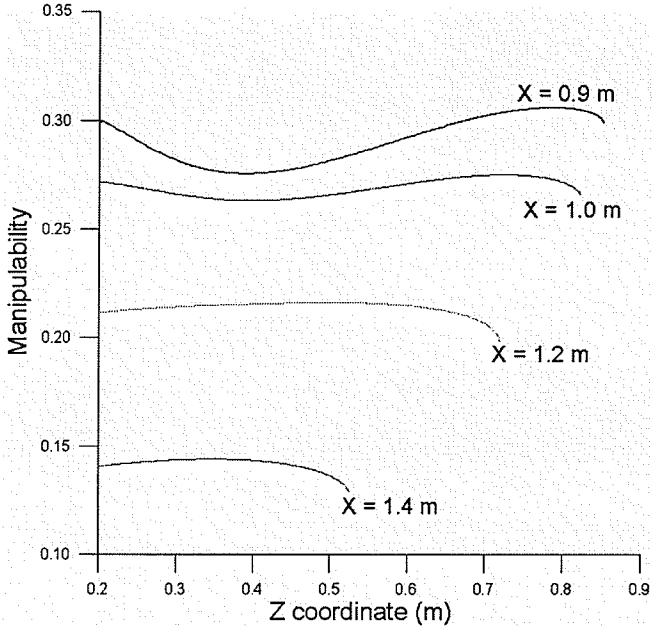


**Figure 4-49 Manipulability measure based on Isotropy Index (Case study 2).**

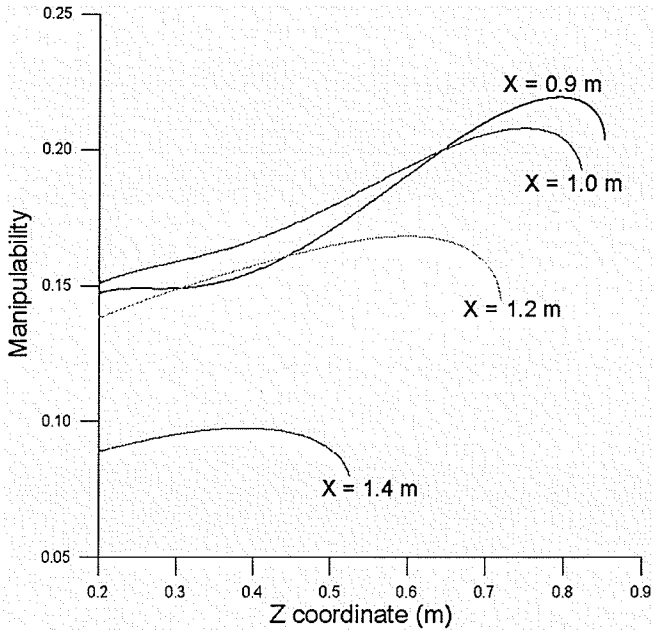


**Figure 4-50 Manipulability measure based on Hong's method (Case study 2).**

As results of Case study 2, the Magnum subsea manipulator manipulability based on Yoshikawa's method increased and decreased as the Z coordinate increased. The Z coordinates for the highest manipulability was varied. It dependent on the positioning on the Z coordinates in Figure 4-48.

### 4.3.1.3 Case Study 3

The purpose of this study is to know the manipulability when the posture of the Magnum manipulator is changed with changing pitch or yaw. First of all, as shown in Figure 4-51, the six points located in workspace were selected for this study. Those coordinates were based on the base coordinate on showing in Figure 4-1. The end-effector was translated to each point without changing pitch (90°) and yaw (90°). First, only the pitch from 75° to 135° was changed as shown in Figure 4-52(a). After measuring manipulability, the arm was returned to its initial posture and translated to the next point. This measuring processing was completed at point F and applied to yaw also.

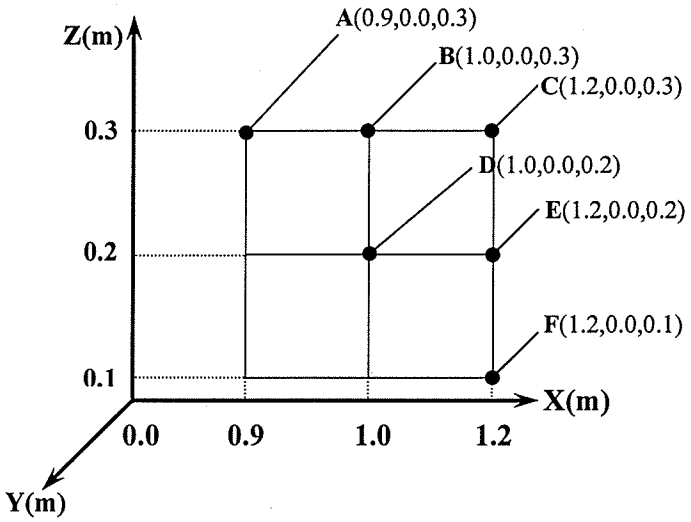


**Figure 4-51 Six points for Case study 3.**

As results of this case study, changing pitch increased the manipulability based on Yoshikawa's method, changing yaw can decrease the manipulability based on Yoshikawa's method (see Figure 4-53 to 4-57). From the results of using the Isotropy Index, the manipulability of the Magnum was increased regardless of the changing pitch or yaw.

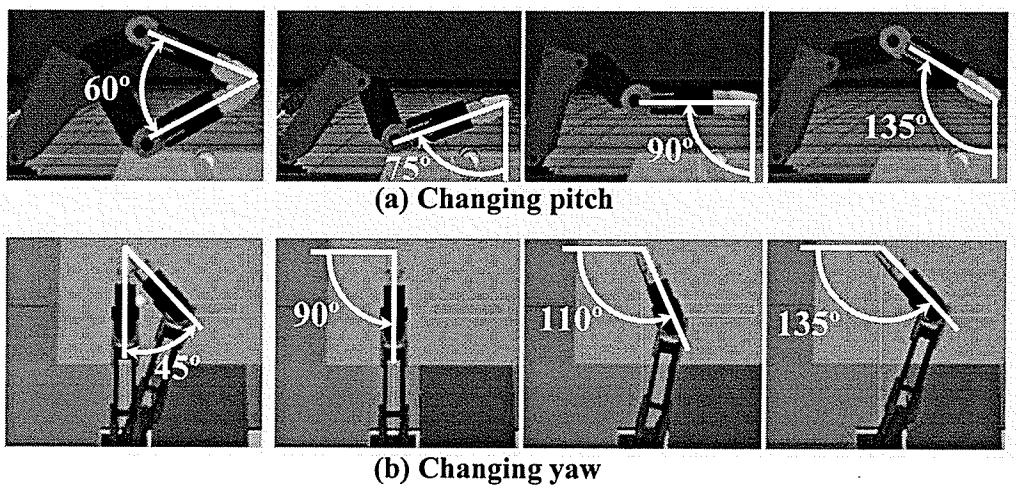


**(a) Changing pitch**

**(b) Changing yaw**

**Figure 4-52 Captured images describing Case study 3 (Single arm)**

The following figures show results of Case study 3.

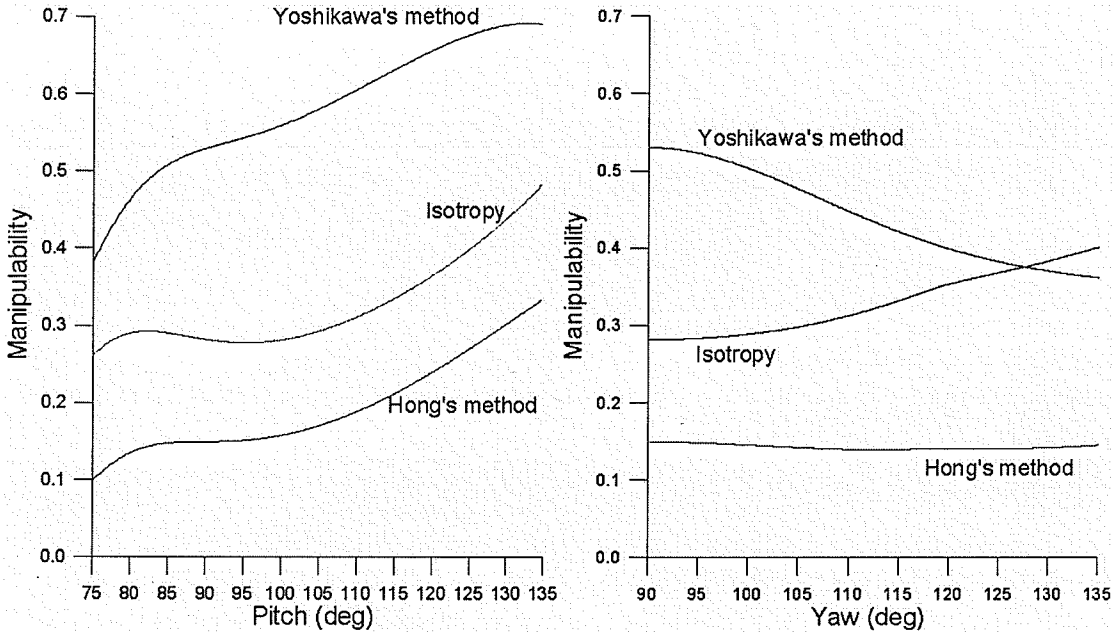


**Figure 4-53 Manipulability at point A according to changing pitch and yaw.**

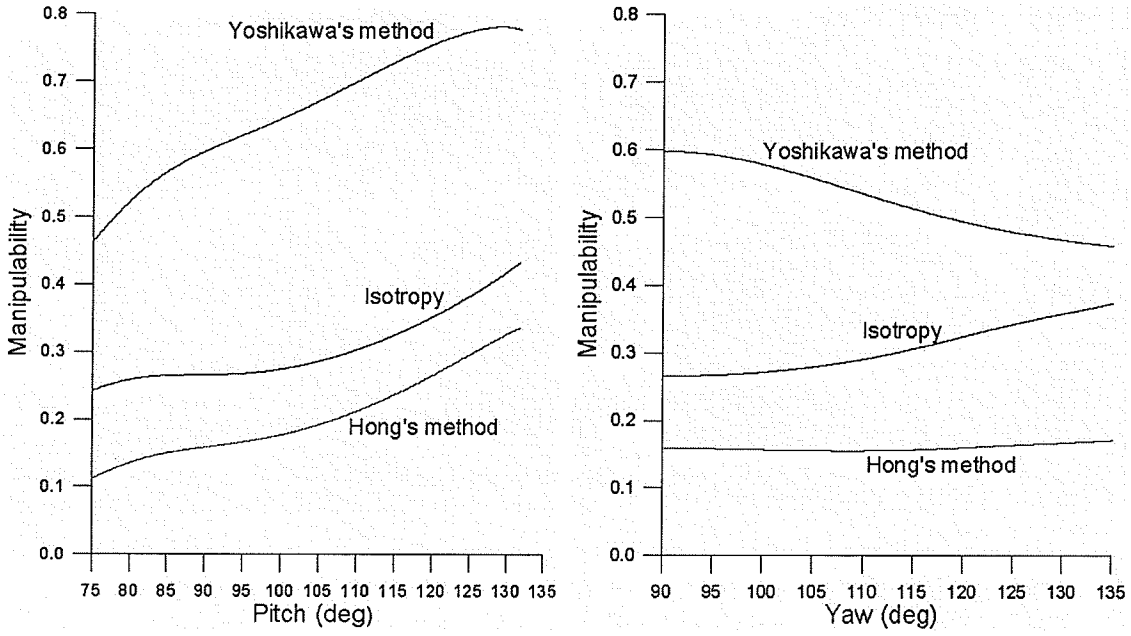


**Figure 4-54 Manipulability at point B according to changing pitch and yaw.**

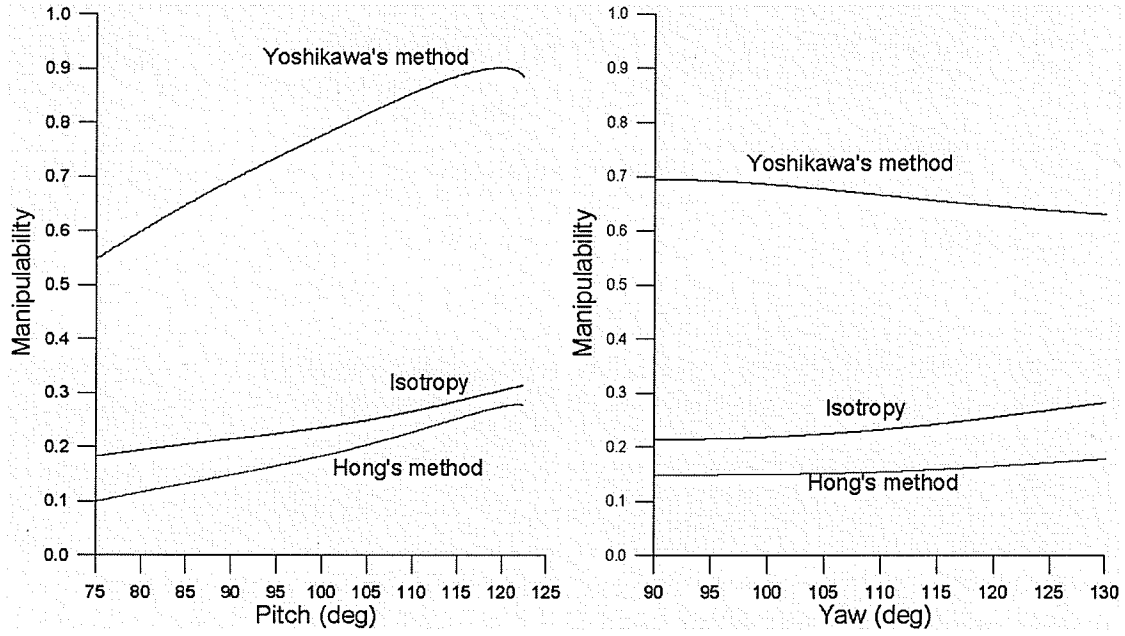


**Figure 4-55 Manipulability at point C according to changing pitch and yaw.**

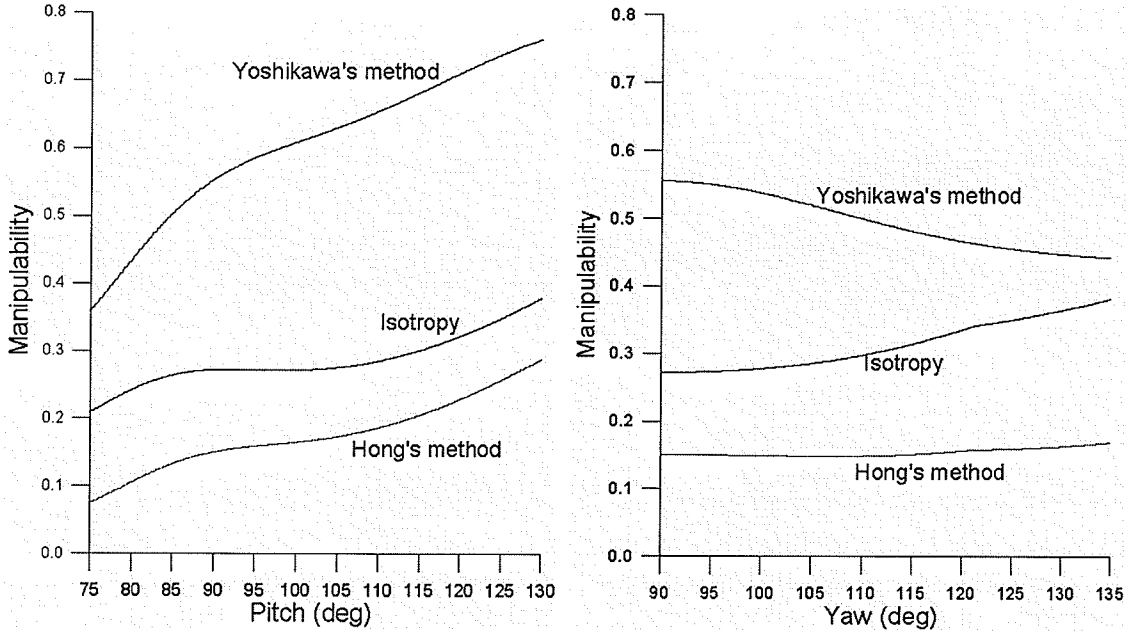


**Figure 4-56 Manipulability at point D according to changing pitch and yaw.**

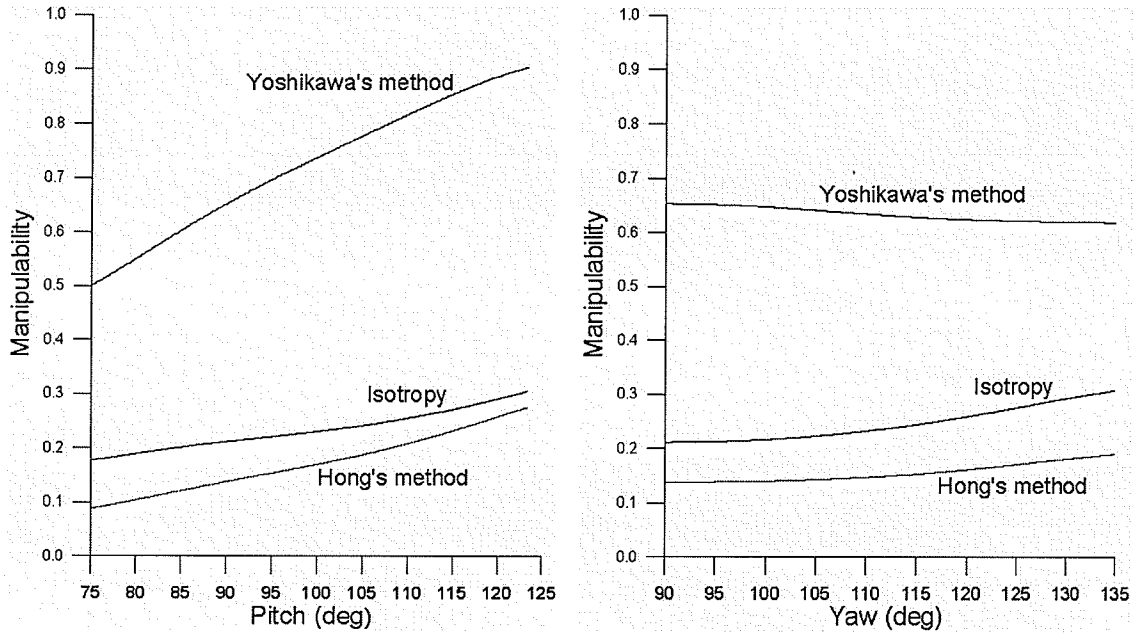


**Figure 4-57 Manipulability at point E according to changing pitch and yaw.**

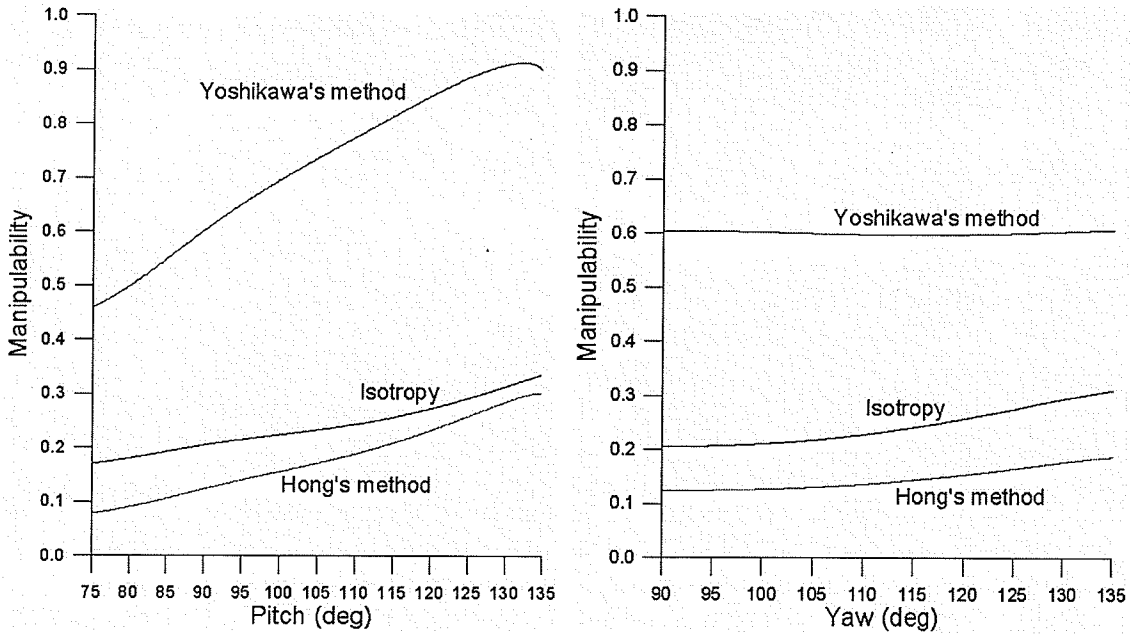


**Figure 4-58 Manipulability at point F according to changing pitch and yaw.**

### 4.3.2 Dual Arms Manipulability Measure

The purpose of this thesis is to find desirable manipulability of the Magnum subsea dual arms and to give suggestions to improve training for the robot operator using this simulator. The desirable manipulability of dual arms will be obtained through the following studies.

#### 4.3.2.1 Case study 1

To compare the manipulability of single arm and dual arms, this study was based on Case study 1 of the single arm. Movement both arms under the same condition as in Case study 1 of the single arm. Figure 4-59 shows translational ellipsoids captured during test for Z=0.3*m* in this case study. The ellipsoids were smaller than the single arm's (see Figure 4-42). This means that the manipulability of single arm was better than the manipulability of the dual arms based on Yoshikawa's method. As shown in Figure 4-60, the manipulability of dual arms was lower than single arm, but the behavior of manipulability was similar. In Figure 4-61, isotropy of the dual arms was almost same as the single arm. This implies that if both arms are same posture and parallel, the isotropy of the dual arms is almost same as the single arm, but the ellipsoid volume of the dual arms are smaller than the single arm at all times.

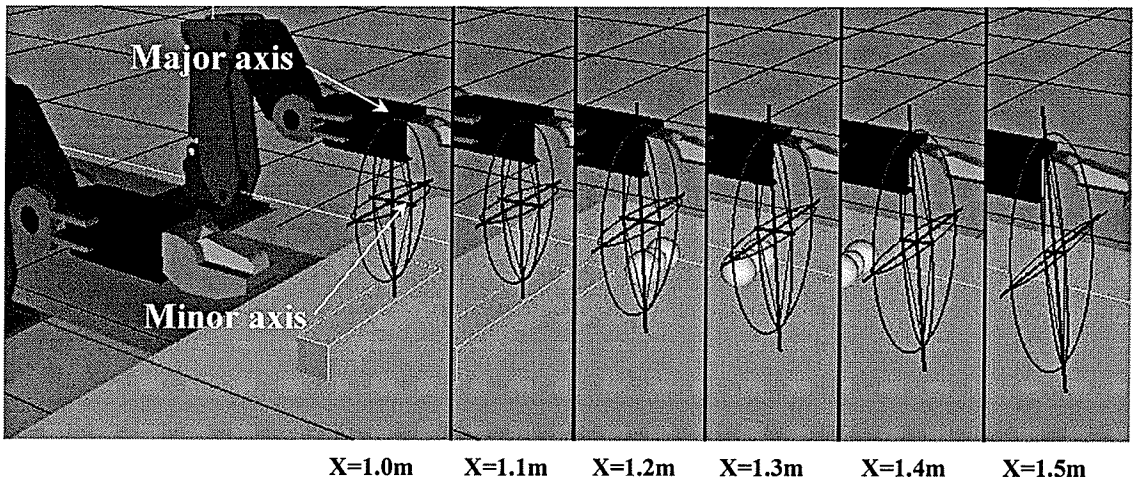


**Figure 4-59 Ellipsoids according to Case study 1 (Dual arms).**

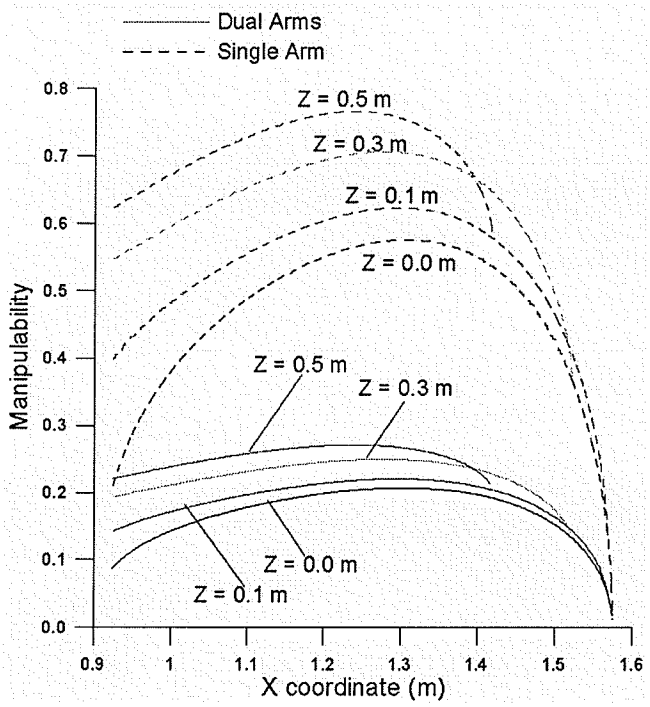


**Figure 4-60 Manipulability measure based on Yoshikawa's method (Case study 1).**

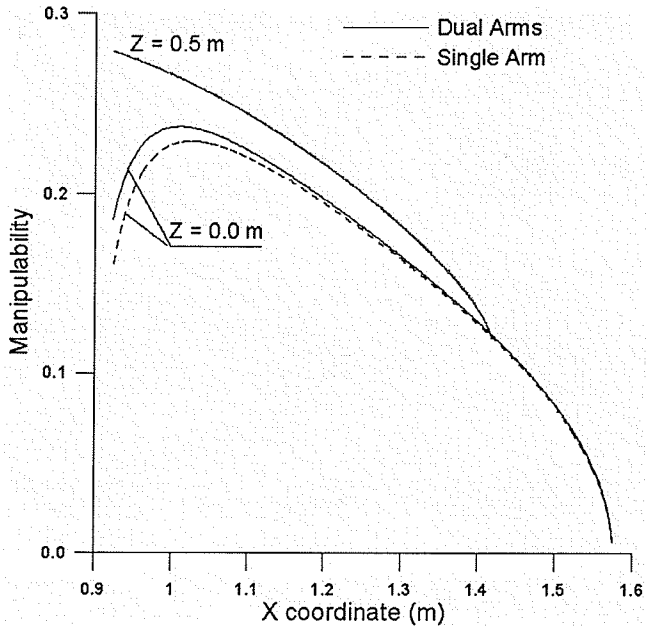


**Figure 4-61 Manipulability measure based on Isotropy Index (Case study 1).**

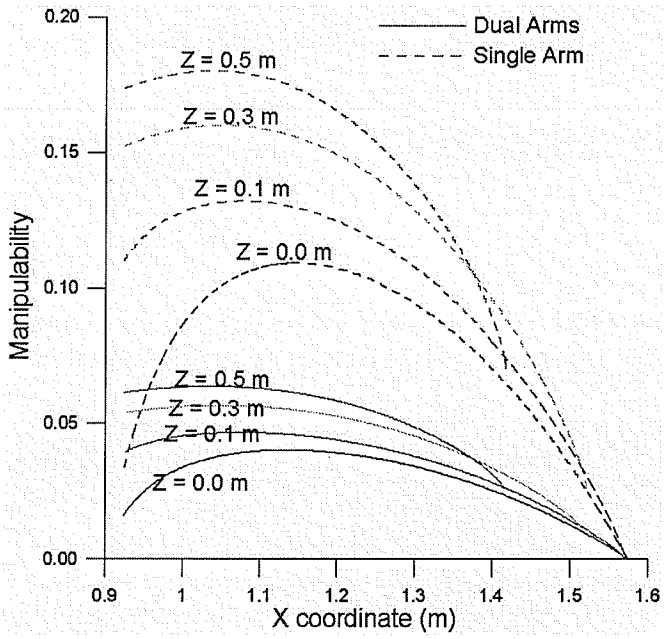


**Figure 4-62 Manipulability measure based on Hong's method (Case study 1).**

### 4.3.2.2 Case study 2

The purpose of this study is to know the relation between manipulability of dual arms and the posture of the arms. Case study 3 of the single arm was adopted for this study. Both arms were moved to point A (the Y coordinate of the right arm was $0.0m$ and the left arm was $1.0m$). The pitch of the right arm was changed based on the process of case study 3 of the single arm. The left arm was not changed. After changing the pitch, the yaw was changed. Both were tested at the six points which were shown in Figure 4-51. As shown in Figure 4-63 and 4-64, the manipulability of dual arms was influenced by the changing of the arm posture. According to these figures, if the manipulability of the single arm was increased, the dual arms manipulability was also increased. The same results occur when the manipulability of the single arm was decreased. This implies that good manipulability of each arm can be the cause of good manipulability of dual arms. The following results are according to point A and F.

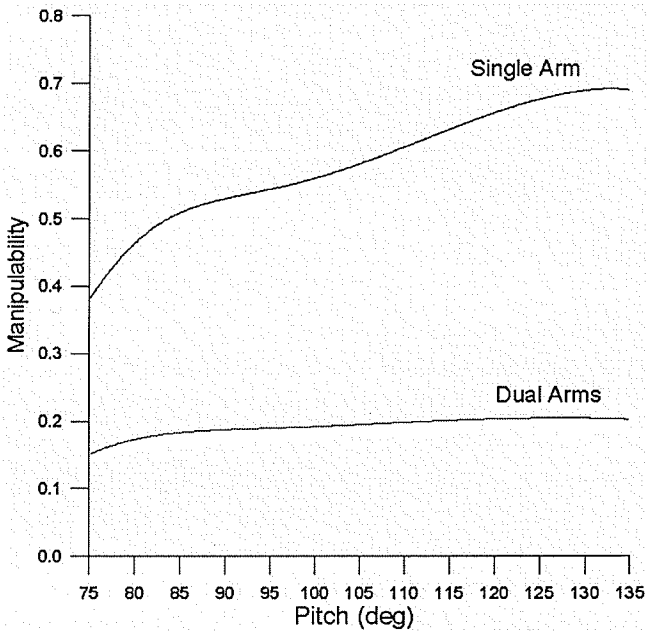


**Figure 4-63 Yoshikawa's method at point A according to changing pitch of right arm.**

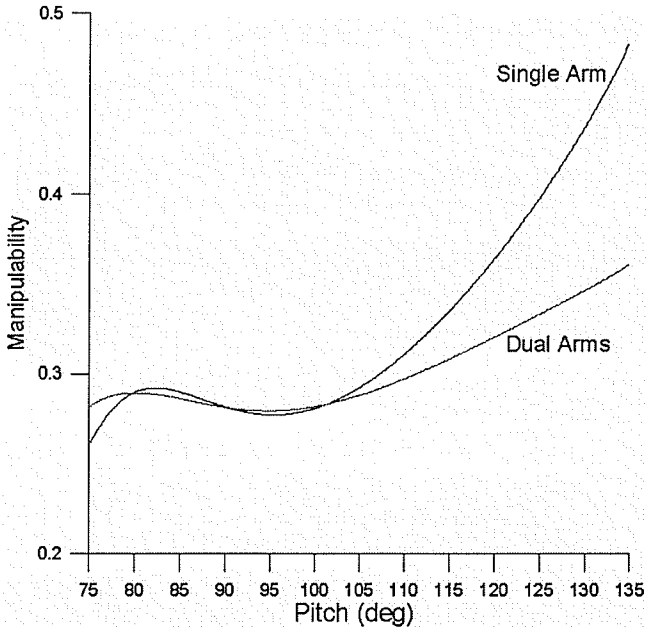


**Figure 4-64 Isotropy Index at point A according to changing pitch of right arm.**

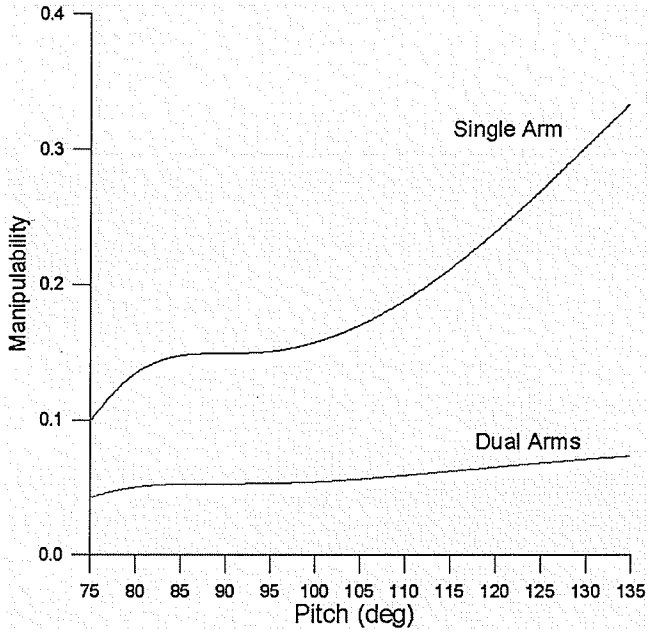


**Figure 4-65 Hong's method at point A according to changing pitch of right arm.**

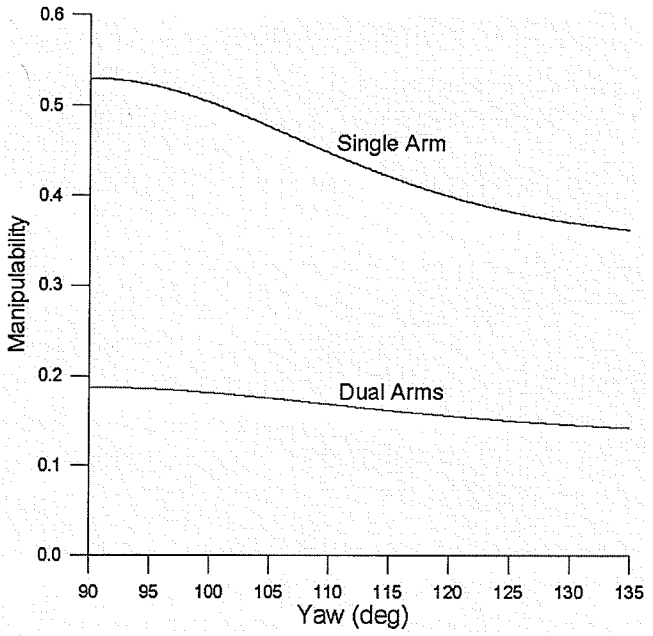


**Figure 4-66 Yoshikawa's method at point A according to changing yaw of right arm.**

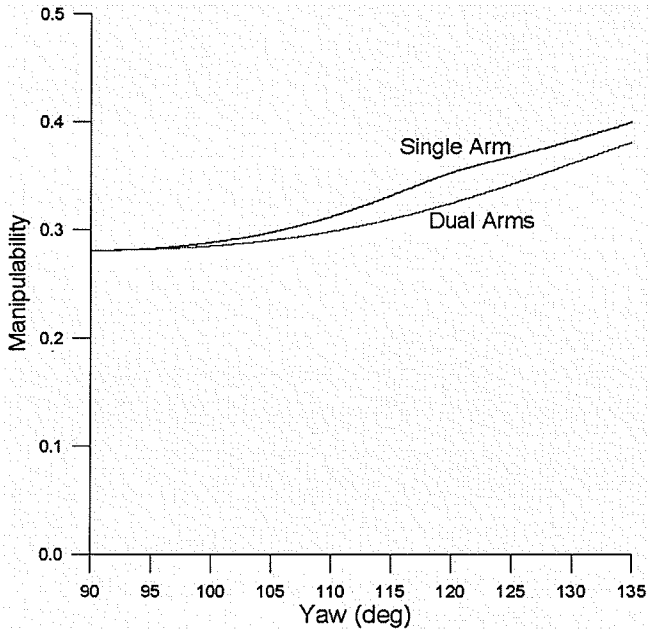


**Figure 4-67 Isotropy at point A according to changing yaw of right arm.**

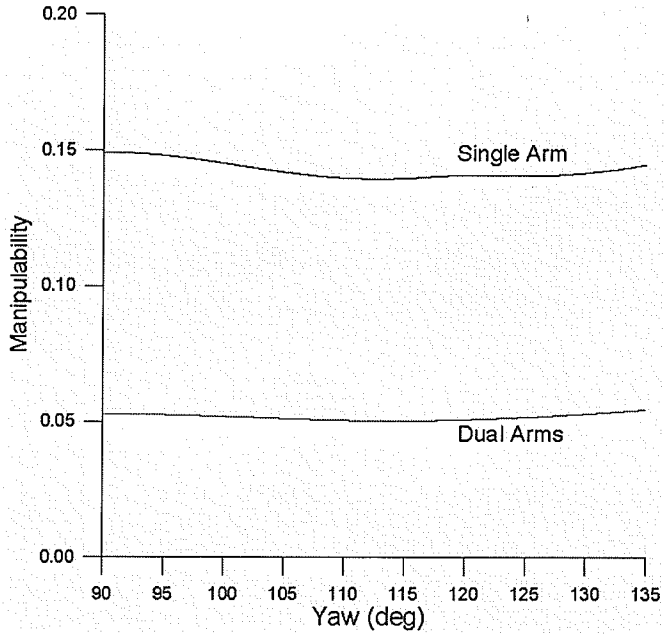


**Figure 4-68 Hong's method at point A according to changing yaw of right arm.**

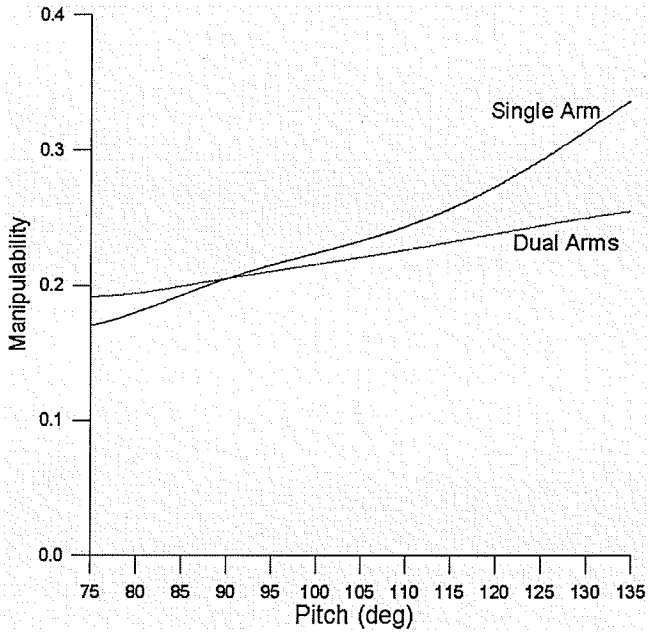


**Figure 4-69 Yoshikawa's method at point F according to changing pitch of right arm.**

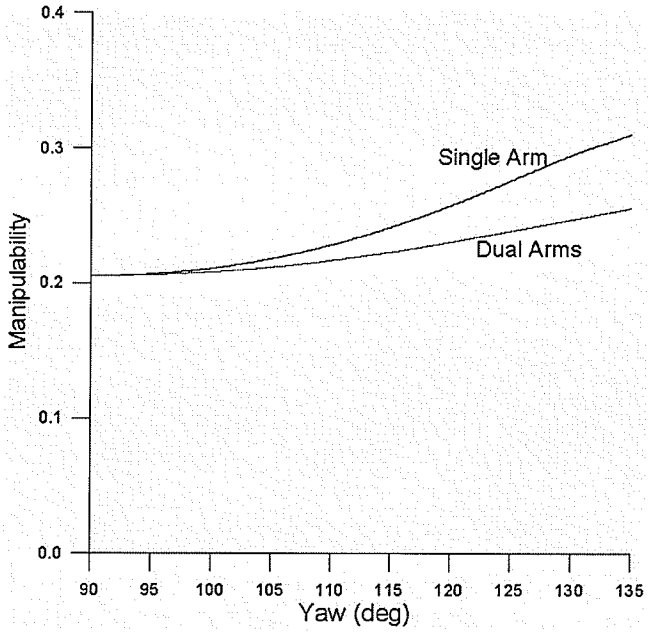


**Figure 4-70 Isotropy at point F according to changing pitch of right arm.**

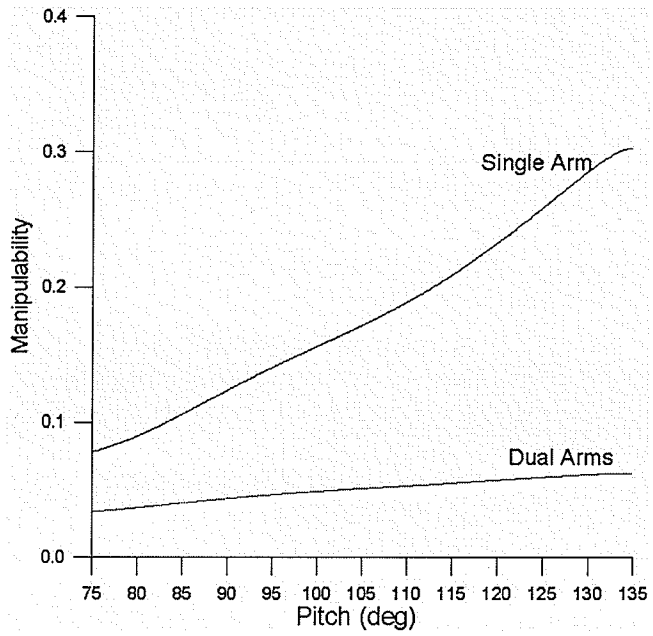


**Figure 4-71 Hong's method at point F according to changing pitch of right arm.**

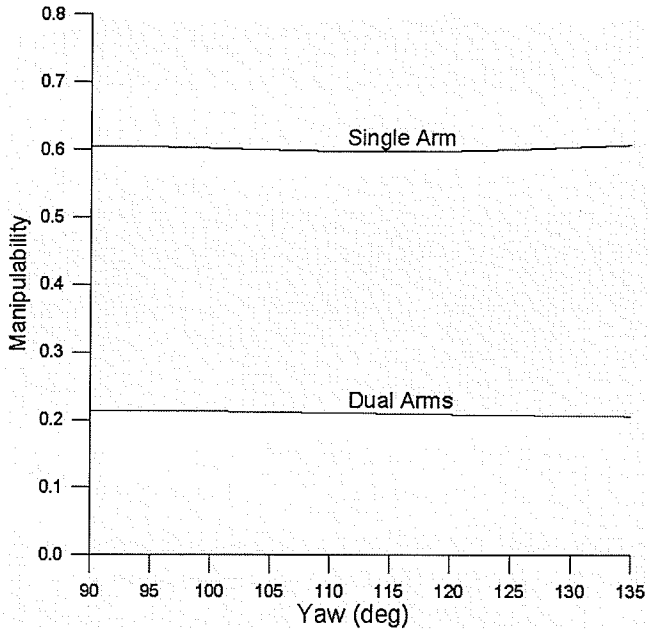


**Figure 4-72 Yoshikawa's method at point F according to changing yaw of right arm.**

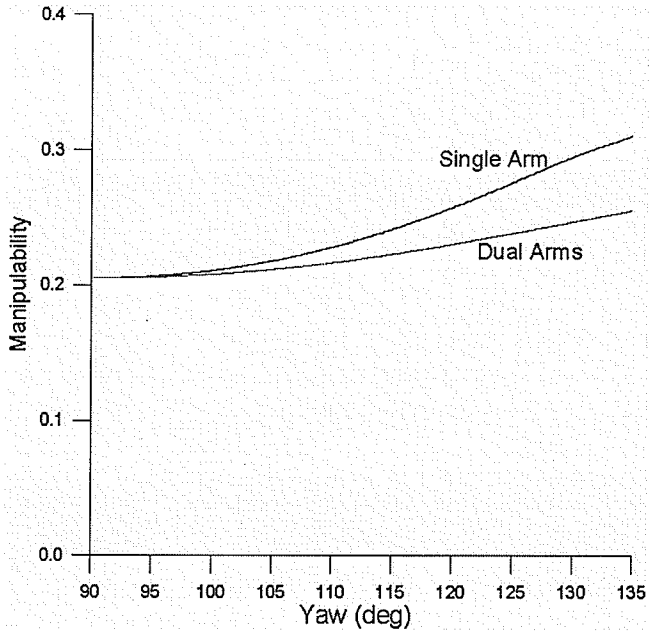


**Figure 4-73 Isotropy at point F according to changing yaw of right arm.**

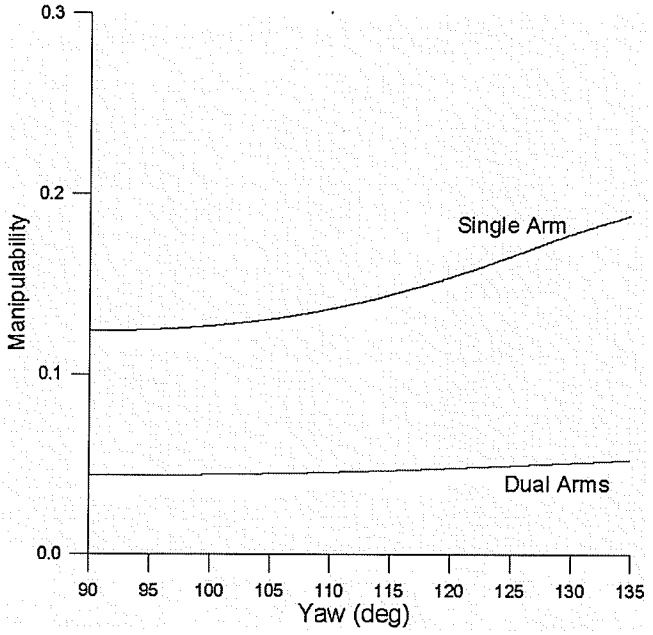


**Figure 4-74 Hong's method at point F according to changing yaw of right arm.**

### 4.3.2.3 Case study 3

Many tasks involving manipulation require cooperation between robots. Meanwhile, it is necessary to determine the adequate values for the robot parameters to obtain a good performance. The purpose of this study is to show the relationship between distance A shown in Figure 4-75 and manipulability of the Magnum subsea dual arms.

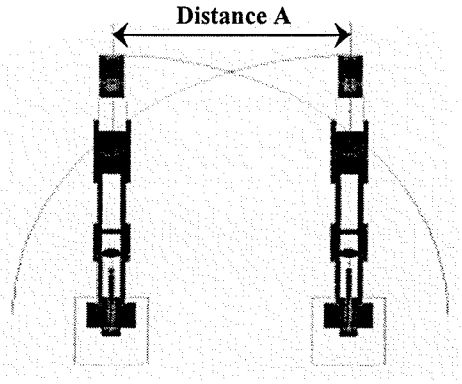


**Figure 4-75 Distance between end-effectors.**

Both arms were moved to X=1.4*m* which was shown in Figure 4-76(a), and both arms were swung as shown in Figure 4-76(a) by using link 1. This process was repeated at X=1.2*m* and X=1.0*m* as shown in Figure 4-76(b) and 4-76(c).

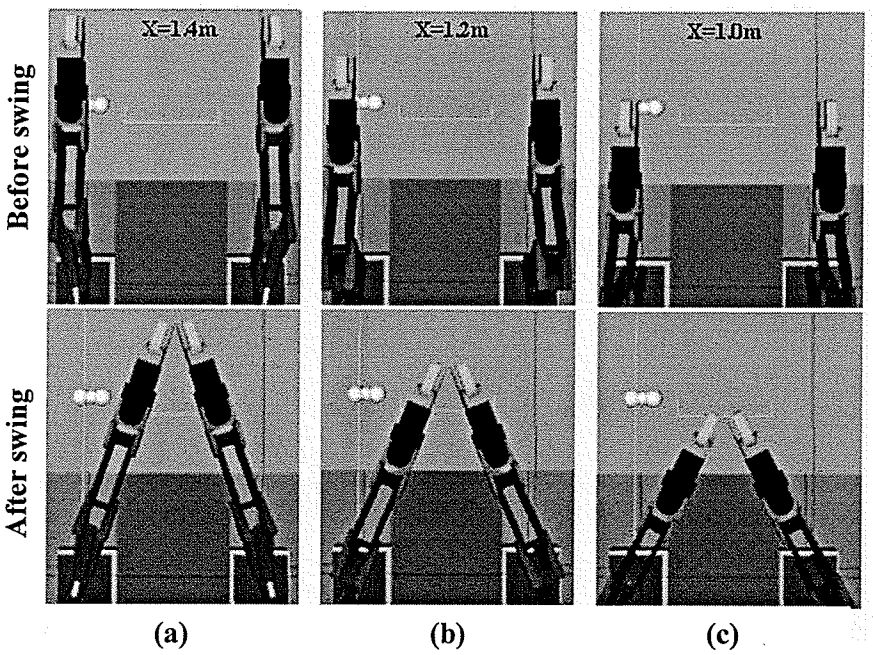


**Figure 4-76 Captured images describing Case study 3 (Dual arms).**

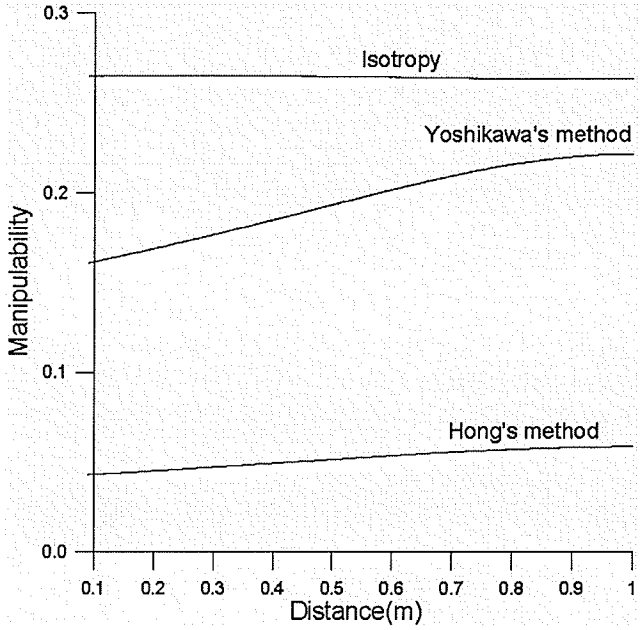


**Figure 4-77 Manipulability at X = 1.0m (Case study 3).**

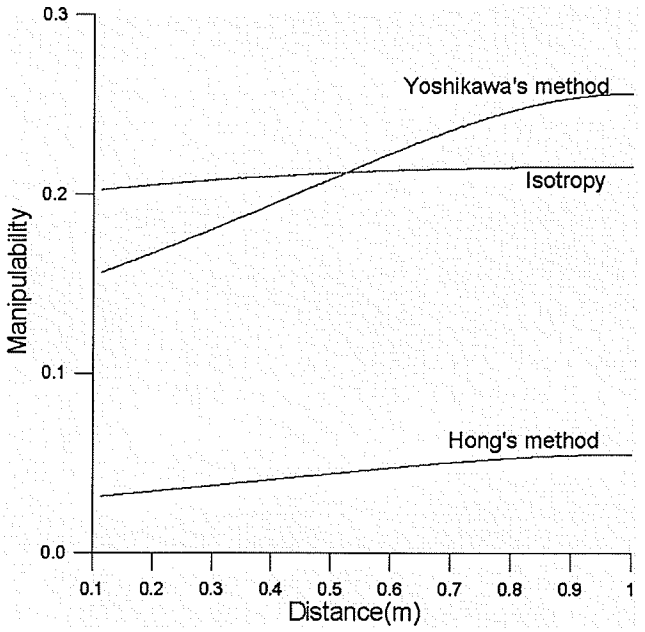


**Figure 4-78 Manipulability at X = 1.2m (Case study 3).**

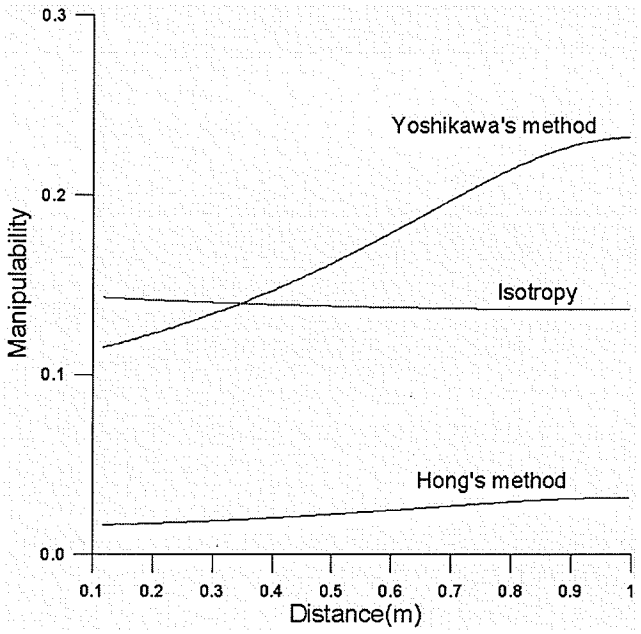


**Figure 4-79 Manipulability at X = 1.4m (Case study 3).**

As results of this study, the manipulability of Magnum dual arms was decreased when the distance A was diminished based on Yoshikawa's method as shown in Figure 4-77, 4-78, and 4-79. Isotropy Index is not much influenced when distance A is getting small. It implies that the highest manipulability based on Yoshikawa's method can be obtained when the robot arms are parallel (when the end-effectors of both arms are located at same X and Z coordinate).

## 4.3.3 Summary

As results of Case study 1 of the single arm, manipulability of the single arm based on Yoshikawa's method was getting high when the end-effector was elevating. (see Figure 4-43). However, as results of Case study 2 of the single arm, the manipulability was decreased from some points, for example, Z coordinate $0.42m$ when X coordinate was $1.4m$ as shown in Figure 4-48. According to the results of Case study 1 of the single arm, based on Yoshikawa's method, the Magnum subsea manipulator has high manipulability when the end-effector was located at the higher coordinate of Z and between $1.1m$ and $1.3m$, on the X coordinate, but it will be decreased from some points and influenced by changing the pitch of

the end-effector. From the results of using the Isotropy Index, the isotropy of the Magnum is a high value when the end-effector is passing near $0.9m$, on the X coordinate.

As results of Case study 3 of the single arm, changing pitch increased the manipulability based on Yoshikawa's method, changing yaw can decrease the manipulability based on Yoshikawa's method (see Figure 4-53 to 4-58). From the results of using the Isotropy Index, the manipulability of the Magnum was increased regardless of the changing pitch or yaw.

According to the studies of dual arms, the manipulability of dual arms was decided by each arm's manipulability. This means that to get high manipulability of dual arms, the high manipulability of each arm is needed. Distance A shown in Figure 4-75 is considered to get high manipulability of Magnum subsea dual arms. Thus, a robot operator who is trained by using this simulator has to keep a desirable posture of each arm to get high performance of dual arms from the viewpoints of kinematics. Several suggestions will be followed. First, to get high manipulability of a single arm, the operator has to understand when the single arm has high manipulability as seen in the case studies of single arm and monitoring manipulability value that are shown in the status bar at the bottom of the simulator (see Figure 4-80). Second, to get high manipulability of dual arms, the operator has to keep the high manipulability of each arm and understand the distance A. Third, this simulator provides manipulability ellipsoids on the screen. Manipulability measure dose not indicate the direction. To know the direction of manipulability, the operator has to monitor the ellipsoids. The desirable kinematics posture of the Magnum subsea dual arms can be obtained by these suggestions.

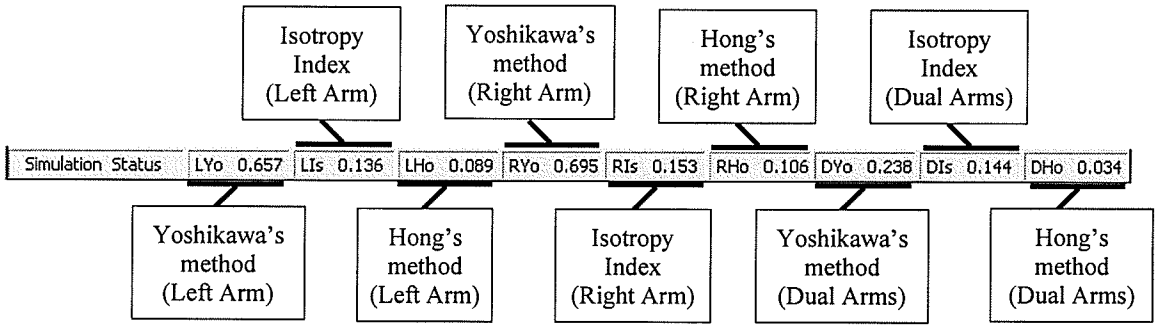


**Figure 4-80 Status bar of Magnum subsea dual arms simulator.**

# 5 Conclusions

## 5.1 Contribution of this thesis

Through case studies of dynamics, it was shown that dynamic simulation is working properly. Understanding of the performance of the Magnum subsea dual arms from the viewpoints of dynamics was obtained. The studies showed that over-loading could occur to the robot arms and the object while the dual arms cooperate with open-loop control as taking place. Closed-loop control can solve this problem, but it has not been employed to real Magnum subsea dual arms. Thus, the case studies inform the dynamic conditions of the Magnum subsea dual arms and the capabilities from the viewpoints of dynamics.

The assessment based on the manipulability is defined to evaluate the performance of the Magnum subsea dual arms. The goal of the assessment was to determine optimal posture of the Magnum subsea dual arms that has faster end-effector motion and isotropy status of performance. Through case studies of manipulability, several suggestions were given. First, to achieve high manipulability of a single arm, the operator has to understand when the single arm has high manipulability as seen in the case studies of single arm and monitoring manipulability value that are shown in the status bar at the bottom of the simulator. Second, to achieve high manipulability of dual arms, the operator has to keep the high manipulability of each arm and understand the distance A shown in Figure 4-75. Third, this simulator provides manipulability ellipsoids on the graphic user interface. Manipulability measure dose not indicate the direction. To know the direction of manipulability, the operator has to monitor the major axes and the minor axes of the ellipsoids. The desirable kinematics posture of the Magnum subsea dual arms can be obtained by these suggestions. In the future, other solutions may be applied to solve optimizations for force and dynamic manipulability.

The developed simulator can help the robot operator become more skilled without extra cost and any risk. The results of case studies also help a trainer understand the performance of the Magnum subsea dual arms from the viewpoints of both dynamics and kinematics.

## 5.2 Future work

a. Force Manipulability – Several authors have extended methods to determine and analyze the force transmission capability of manipulators. For a serial chain manipulator, the Jacobian also features in the relationship between the joint torques and the task space forces. One could also extend the kinematics manipulability analysis in this thesis in a similar manner to examine the force transmission characteristic.

b. Dynamic Manipulability – The manipulability discussed in this thesis is based on kinematics; the manipulator dynamics are completely ignored. Therefore, although one can apply it to the conceptual design of arm mechanisms and to the avoidance of singularities without considering complicate dynamics of arm, it may not be suitable for the detailed design of arms or for high-speed, high-precision motion control. So, dynamic manipulability is one of future works.

c. Collision Response – In a physically-based dynamic simulation, there are two major components to a successful and realistic system display: collision detection and collision response. Given that the problem of collision detection is reasonably understood for the rigid objects, another related problem is to resolve the difficulty of simulating the physics of real world objects: Contact forces must be calculated and applied until separation finally occurs; in addition, objects' velocities must be adjusted during the contact course in response to the impacts. All these processes are considered as a part of the dynamics response to the collision following the basic laws of physics. The advanced collision response algorithms can be studied for the future work.

# References

[1] Caccavale, F., Chiacchio, P., and Chiaverini, S., "Stability Analysis of a Joint Space Control Law for a Two-Manipulator System", IEEE Transactions on Automatic Control, 44, pp. 85-88, 1999

[2] Choi, M. H., "The Optimal Load Distribution for Two Cooperating Robots Using Force Ellipsoid ", Seoul National University in Seoul, a thesis of master of science, 1992

[3] Ferreira, N. Fonseca, M., Machado, J., Tenreiro, A., "Manipulation Analysis of Two Cooperating Arms", ICAR'01-10th International Conference on Advanced Robotics, pp. 125-130, 2001

[4] Hawkins, K., Astle, D., and LaMothe, A., "OpenGL Game Programming", Prima Tech, 1999

[5] Hong, K. S. and Kim, J. G., "Manipulability Analysis of a Parallel Machine Tool: Application to Optimal Link Parameter Design", Journal of Robotics Systems, Vol. 17, No. 8, pp.403-415 2000

[6] Kemény, Z., "Mapping, detection and handling of singularities for kinematically redundant serial manipulators", Periodica Polytechnica Ser. el. eng. vol. 46, no. 1, pp. 29–45 2002

[7] Khatib, O., 1988, "Object Manipulation in a Multi-Effector Robot System", Robotics Research, the Fourth International Symposium, pp. 137-144.

[8] Kwon, W., "Geometrical approach to optimal load distribution of two cooperating robots considering internal force", Seoul National University in Seoul, a thesis of Master of Science , 1993

[9] Lee, J., "A study on the manipulability measures for robot manipulators", in Proc. IEEE/RSJ Int. Conf. Intell. Robots, System, pp.1458–1465, 1997

[10] Liu, Y.H., and Arimoto, S., "Distributively Controlling two Robots Handling an Object in the Task Space without any Communication", IEEE Transactions on Automatic Control, 41, pp. 1193-1198 , 1996

[11] Mulle, N., Magai, L. and Herbst, B.M., "Singular Value Decomposition, Eigenfaces, and 3D Reconstructions", Society for Industrial and Applied Mathematics Review, Vol. 46, No. 3, pp. 518–545, 2004

[12] Niksefat, N., and Sepehri, N., "Design and Experimental Evaluation of a Robust Force Controller for an Electro-Hydraulic Actuator via Quantitative Feedback Theory", Control Engineering Practice, pp.1335–1345, 2000.

[13] Paul, R. P., "Mathematics, programming, and control : the computer control of robot manipulators", Cambridge, Mass. : MIT Press,1981.

[14] Salisbury, J. K. and Craig, J. J., "Articulated Hands: Force Control and Kinematic Issues", The International Journal of Robotics Research, pp. 4-17, 1982.

[15] Seo, C. W., "An application of the force ellipsoid to the optimal load distribution of cooperating robots", Seoul National University in Seoul, a thesis of master of science , 1992

[16] Sirouspour, M.R., and Salcudean, S.E., "Nonlinear Control of Hydraulic Robots", IEEE Transactions on Robotics and Automation, 17, pp. 173–182, 2001

[17] Slotine, J.-J. E., and Li, W., Applied Nonlinear Control, Prentice-Hall, Engliwood Cliffs, NJ. , 1991

[18] Tang, C. P., "Manipulability-Based Analysis of Cooperative Payload Transport by Robot Collectives", University of New York at Buffalo, a thesis of master of science, 2004

[19] Togai, M., "An application of the singular value decomposition to manipulability and sensitivity of industrial robots", SIAM J. ALG. DISC. METH. Vol. 7, No. 2, pp. 315-320 April 1986

[20] Walker, I.D., Freeman, R.A., and Marcus, S.I., "Analysis of Motion and Internal Loading of Objects Grasped by Multiple Cooperating Manipulators", International Journal of Robotics Research, 10, pp. 396–409, 1991

[21] Wen, J. T. Y. Senior Member, IEEE, and Wilfinger, Lee S., "Kinematic Manipulability of General Constrained Rigid Multibody Systems", IEEE Transactions on Robotics and Automation, Vol. 15, No. 3, pp. 1020-1025, June1999

[22] Wright Jr., R. S. and Sweet, M. R., "OpenGL SuperBible, Second Edition", Waite Group Press, 1999

[23] Yoshikawa, T., "Manipulability of Robotic Mechanisms", The International Journal of Robotics Research, vol. 4, pp. 3-9, 1985

[24] Yoshikawa, T., "Foundations of Robotics: Analysis and Control", Corona Publishing Co. Ltd., p127-p137, 1988

[25] Zeng, H., and Sepehri, N., "Design of a Nonlinear Position Regulator for Cooperating Hydraulic Manipulators Handling a Rigid Object", ASME International Mechanical Engineering Congress and RD&D Expo, 2004

[26] International Submarine Engineering Ltd. Vancouver, B.C.
http://www.ise.bc.ca/

[27] Silicon Graphics Inc., California, U.S.A.
http://www.sgi.com/products/software/opengl/

# Appendix 1. Pseudo-Inverses Matrix

For every finite $m \times n$ real matrix $A$, there is a unique $n \times m$ real matrix $A^+$ satisfying the following four conditions:

$$AA^+A = A, \tag{A1.1}$$

$$A^+AA^+ = A^+, \tag{A1.2}$$

$$(AA^+)^T = AA^+, \tag{A1.3}$$

$$(A^+A)^T = A^+A. \tag{A1.4}$$

This $A^+$ is called the pseudo-inverse of $A$. First, it will show that the existence of $A^+$ satisfying equations (A1.1) to (A1.4). If $A = 0$, then the obvious solution $A^+ = 0$ satisfies these conditions. If it is assumed that $A \neq 0$ and let $r = rankA$, then $A$ can be expressed as the product of an $m \times r$ matrix $B$ and an $r \times n$ matrix $C$:

$$A = BC \tag{A1.5}$$

Using the above $B$ and $C$, we define an $n \times m$ matrix $D$ by

$$D = C^T(CC^T)^{-1}(B^TB)^{-1}B^T. \tag{A1.6}$$

Then it is easy to show that $A^+ = D$ satisfies equations (A1.1) to (A1.4). This completes the proof of the existence of $A^+$.

Next, the uniqueness of the $A^+$ will be shown. Let any two matrices satisfying equations (A1.1) to (A1.4) be $A_1^+$ and $A_2^+$. Then

$$\begin{aligned} A_1^+ - A_2^+ &= A_1^+AA_1^+ - A_2^+AA_2^+ \\ &= A^TA_1^{+T}A_1^+ - A_2^+A_2^{+T}A^T \\ &= (AA_2^+A)^TA_1^{+T}A_1^+ - A_2^+A_2^{+T}(AA_1^+A)^T \\ &= A^TA_2^+A^TA_1^{+T}A_1^+ - A_2^+A_2^{+T}A^TA_1^{+T}A^T \\ &= A^TA_2^+A_1^+ - A_2^+A_2^{+T}A^T \\ &= A_2^+AA_1^+ - A_2^+AA_1^+ = 0, \end{aligned} \tag{A1.7}$$

proving the uniqueness of $A^+$. The pseudo-inverse has the following properties:

(i) $(A^+)^+ = A$ (A1.8)

(ii) $(A^T)^+ = (A^+)^T$ , $(AA^T)^+ = (A^+)^T A^+$. (A1.9)

(iii) Let $A$ be an $m \times n$ matrix and $B$ be an $n \times p$ matrix. Then generally $(AB)^+$ is not equal to $B^+A^+$. If, however, rankA = rankB = n, then$(A^+)^+ = (AB)^+ = B^+A^+$. (A1.10)

(iv) $A^+ = (A^TA)^+A^T = A^T(AA^T)^+$ (A1.11)

(v) If an $m \times n$ matrix $A$ satisfies rank$A = m$, then $A^+ = A^T(AA^T)^{-1}$. Also, if rank$A = n$, then $A^+ = (A^TA)^{-1}A^T$. (A1.12,13)

(vi) Let $r$ = rank$A$, and let the singular - value decomposition of $A$ be $A = U\Sigma V^T$, (A1.14)

where $U$ and $V$ are orthogonal matrices and $\Sigma$ is the following $m \times n$ matrix:

$$\Sigma^+ = \begin{bmatrix} \sigma_1 & & & \\ & \sigma_2 & 0 & \\ & & \ddots & \\ & & & 0 \\ & 0 & & \sigma_r \\ & & 0 & 0 \end{bmatrix} \begin{matrix} \} r \\ \\ \\ \\ \} n-r \end{matrix} \quad \begin{matrix} \\ \\ \\ \\ \\ m-r \end{matrix} \qquad \text{(A1.15)}$$

$$\underbrace{\qquad\qquad}_{r}$$

with

$$\sigma_1 \geq \sigma_2 \geq \cdots \geq \sigma_r > 0.$$

Then $A^+$ is given by

$$A^+ = V\Sigma^+U^T, \qquad \text{(A1.16)}$$

where $\Sigma^+$ is the $n \times m$ matrix defined by

$$\Sigma^{+} = \underbrace{\begin{bmatrix} \sigma_1^{-1} & & & & \\ & \sigma_2^{-1} & & 0 & \\ & & \ddots & & \\ & & & \sigma_r^{-1} & \\ & 0 & & 0 & \end{bmatrix}}_{r} \begin{matrix} \left.\begin{matrix} \\ \\ \\ \\ \end{matrix}\right\} r \\ \left.\begin{matrix} \\ \end{matrix}\right\} n-r \end{matrix} \qquad \begin{matrix} \\ \\ \\ \\ \\ m-r \end{matrix} \tag{A1.17}$$

Note that $\Sigma^{+}$ is the pseudo-inverse of $\Sigma$.

(vii) Consider a system of simultaneous linear equations given by

$$Ax = b, \tag{A1.18}$$

where $A$ is known as $m \times n$ matrix, $b$ is a known $m$-dimensional vector, and $x$ is an unknown $n$-dimensional vector. When is square ($m = n$) and nonsingular, the solution to equation (A1.18) is, as is well known, given by

$$x = A^{-1}b\,. \tag{A1.19}$$

When $A$ is not nonsingular, i.e. when $A$ and $b$ satisfy

$$b \in R(A), \tag{A1.20}$$

then equation (A1.18) is not unique. Taking this into account, now consider a more general problem of minimizing the Euclidean norm of the error $(Ax - b)$:

$$\|Ax - b\| = \sqrt{(Ax - b)^T (Ax - b)}. \tag{A1.21}$$

As is proved below, the general solution to this problem is

$$x = A^{+}b + (I - A^{+}A)k, \tag{A1.22}$$

where $k$ is an arbitrary n-dimensional vector. If equation (A1.18) has a solution, equation (A1.22) is its general solution; if equation (A1.18) has no solution, then equation (A1.22) is the general form of its best approximate solution in a sense that it minimizes the norm (A1.21). Furthermore, if the best approximate solution is not unique, the one that minimizes its own norm $\|x\|$ is given by

$$x = A^{+}b \tag{A1.23}$$

It will be proven that equation (A1.22) is the general solution to the problem of minimizing $\|Ax - b\|$. From equations (A1.8) to (A1.11), we have

$$A^{T}AA^{+} = A^{T}. \tag{A1.24}$$

Using this relation, it can be shown that

$$\begin{aligned} & b^{T}\left[I - (AA^{+})^{T}AA^{+}\right]B + \left[x - A^{+}b - (I - A^{+}A)k\right]^{T} A^{T}A\left[x - A^{+}b - (I - A^{+}A)k\right] \\ & = x^{T}A^{T}Ax - 2x^{T}A^{T}b + b^{T}b \\ & = \|Ax - b\|^{2} \end{aligned} \tag{A1.25}$$

Since the first term on the left-hand side of equation (A1.25) is independent of $x$, $\|Ax - b\|$ becomes minimum if and only if the second term is equal to zero, that is, if and only if

$$A\left[x - A^{+}b - (I - A^{+}A)k\right] = 0 \tag{A1.26}$$

Hence, equation (A1.22) is a solution to the problem for any k. On the other hand, since equation (A1.26) is equivalent to

$$A\left[x - A^{+}b\right] = 0 \tag{A1.27}$$

by equation (A1.1), any solution $x^{*}$ to the problem must satisfy

$$Ax^{*} = AA^{+}b. \tag{A1.28}$$

Thus,

$$\begin{aligned} x^* &= A^+b + x^* - A^+b \\ &= A^+b + x^* - A^+AA^+b \\ &= A^+b + (I - A^+A)x^*. \end{aligned} \tag{A1.29}$$

Therefore, $x^*$ can be expressed in the form of equation (A1.22). This completes the proof.

# Appendix 2. Singular-Value Decomposition

Suppose that a $m \times n$ real matrix is given. Then $A^T A$ is a nonnegative matrix whose eigenvalues, i.e., the solutions $\det(\lambda I_n - A^T A) = 0$, are nonnegative real numbers. Let the eigenvalues be $\lambda_1, \lambda_2, ..., \lambda_n (\lambda_1 \geq \lambda_2 \geq ... \geq \lambda_n \geq 0)$. Let also

$$\sigma_i = \sqrt{\lambda_i}, \qquad i = 1, 2, ..., \min(m, n). \tag{A2.1}$$

$\sigma_1 \geq \sigma_2 \geq \cdots \geq \sigma_{\min(m,n)} \geq 0$. Now express the matrix $A$ as the product of three matrices:

$$A = U \Sigma V^T, \tag{A2.2}$$

Where $U$ is a $m \times m$ orthogonal matrix, $V$ is a $n \times n$ orthogonal matrix, and $\Sigma$ is an $m \times n$ matrix defined by

$$\Sigma = \begin{cases} \begin{bmatrix} \sigma_1 & & 0 \\ & \ddots & \\ 0 & & \sigma n \\ & 0 & \end{bmatrix} & if \quad m \geq n \\ \left[\begin{array}{ccc:c} \sigma_1 & & 0 & \\ & \ddots & & 0 \\ 0 & & \sigma_m & \end{array}\right] & if \quad m < n \end{cases} \tag{A2.3}$$

The right-hand side of equation (A2.2) is called the singular-value decomposition, and $\sigma_i (i = 1, 2, ..., \min(m, n))$ are called singular values. The number of nonzero singular value is

$$r = rank A. \tag{A2.4}$$

Since $U$ and $V$ are orthogonal, they satisfy

$$UU^T = U^TU = I_m, \qquad VV^T = V^TV = I_n. \tag{A2.5}$$

Consider the meaning of the singular-value decomposition of $A$ in relation to the linear transformation $y=Ax$. Let $y_U = U^T y$ and $x_v = V^T x$, from (A2.2)

$$y_U = \Sigma x_V \tag{A2.6}$$

This implies that the transformation from $x$ to $y$ can be decomposed into three consecutive transformations: the orthogonal transformation from $x$ to $x_V$ by $V^T$, which does not change length; the one from $x_V$ to $y_U$, in which the $i^{th}$ element of $x_V$ is multiplied by $\sigma_i$ and becomes the $i^{th}$ element of $y_U$ without changing its direction; and the orthogonal transform from $y_U$ to $y$ by $U$, which does not change length. Therefore, the singular-value decomposition highlights a basic property of linear transformation.

A scheme to obtain the singular-value decomposition follows. First, the singular values are calculated by equation (A2.1). Since the numbers of nonzero eigenvalues for $A^TA$ and $AA^T$ are the same, it is computationally more efficient to find the singular values using the eigenvalus of $AA^T$ when $m < n$ and those of $A^TA$ when $m > n$.

Next we obtain $U$ and $V$. We define a diagonal matrix $\Sigma_r$ using $r$ nonzero singular values by

$$\Sigma_r = \begin{bmatrix} \sigma_1 & & 0 \\ & \ddots & \\ 0 & & \sigma_r \end{bmatrix} \tag{A2.7}$$

This is the $r \times r$ principal minor of $\Sigma$. We let the $i^{th}$ row vectors of $U$ and $V$ be $u_i$ and $v_i$, respectively, and let

$$U_r = \left[u_1, u_2, \ldots, u_r\right]$$

and

$$V_r = \left[v_1, v_2, \ldots, v_r\right]$$

Then, from equation (A2.2),

$$A = U_r \Sigma_r V_r^T$$

Also, from equation (A2.5),

$$U_r^T U_r = I_r$$

and

$$V_r^T V_r = I_r .$$

Hence,

$$A^T A V_r = V_r \Sigma_r^2, \qquad \text{(A2.8)}$$

$$U_r = A V_r \Sigma_r^{-1} \qquad \text{(A2.9)}$$

Since equation (A2.8) can be decomposed into

$$A^T A v_i = v_i \sigma_i^2, \qquad i = 1,2,....r \qquad \text{(A2.10)}$$

see that $v_i$ is the eigenvector of unit length for eigenvalue $\lambda_i$ of $A^T A$. Thus it can determine $V_r$ from the eigenvectors of $A^T A$ for eigenvalues $\lambda_1, \lambda_2, ..., \lambda_r$. The part of $V$ other than $V_r$, which consists of vectors $v_{r+1}$, obtained it can $V$ determine $U_r$ by equation (A2.9) and the other part of $U$ by equation (A2.5). Instead of equations (A2.8) and (A2.9), it can be also used

$$A^T A U_r = U_r \Sigma_r^2, \qquad \text{(A2.8')}$$

and

$$V_r = A^T U_r \Sigma_r^{-1} \qquad \text{(A2.9')}$$